NASA CR-134500
R-9125

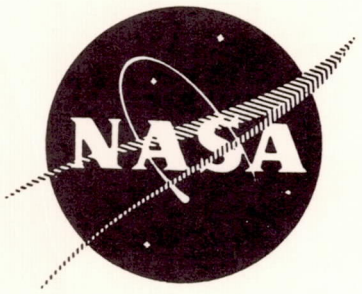

POGO INSTABILITIES SUPPRESSION EVALUATION

by E. C. Farrel and J. R. Fenwick

ROCKETDYNE DIVISION
ROCKWELL INTERNATIONAL

prepared for
NATIONAL AERONAUTICS AND SPACE ADMINISTRATION

NASA Lewis Research Center
Contract NAS 3-14382

1. Report No.	2. Government Accession No.	3. Recipient's Catalog No.
NASA CR-134500		

4. Title and Subtitle	5. Report Date
POGO INSTABILITIES SUPPRESSION EVALUATION	November 1973
	6. Performing Organization Code

7. Author(s)	8. Performing Organization Report No.
E. C. Farrel and J. R. Fenwick	R-9125
	10. Work Unit No.

9. Performing Organization Name and Address	11. Contract or Grant No.
Rocketdyne Division Rockwell International Canoga Park, California	NAS 3-14382
	13. Type of Report and Period Covered
12. Sponsoring Agency Name and Address	Contractor Report
National Aeronautics and Space Administration Washington, D.C. 20546	14. Sponsoring Agency Code

15. Supplementary Notes

Project Manager W.A. Rostafinski, Chemical Rocket Division,
NASA Lewis Research Center, Cleveland, Ohio

16. Abstract

A dynamic (frequency response) analysis was made of a liquid oxygen feed system consisting of a low-speed inducer, a high-speed main pump and a positive displacement pulser utilized for simulating POGO induced pressure oscillations. Based on the results of the analysis, an active control system for suppression of pulser generated pressure oscillations was designed, fabricated and tested. The test results verified that the suppressor was effective in attenuating the generated pressure oscillations over the frequency range from 10 to 30 Hz.

17. Key Words (Suggested by Author(s))	18. Distribution Statement
Active control; analysis, design and test Suppression of feed system pressure oscillations Frequency response characteristics in 2- to 50-Hz range Pump-fed liquid oxygen feed system High and low pump net positive suction pressure	Unclassified

19. Security Classif. (of this report)	20. Security Classif. (of this page)	21. No. of Pages	22. Price*
Unclassified	Unclassified	133	

* For sale by the National Technical Information Service, Springfield, Virginia 22151

FOREWORD

The research described herein was done at Rocketdyne Division, Rockwell International, under NASA Contract NAS3-14382 with Mr. W. A. Rostafinski, Chemical Rocket Division, NASA Lewis Research Center, as Project Manager, and Mr. Carl F. Lorenzo, Technical Advisor.

Acknowledgement is made to Mr. H. G. Diem, Rocketdyne Program Manager, Mr. J. A. King, Rocketdyne Principal Engineer, Mr. D. Heister and his test technicians for conducting a successful test program, Mr. R. H. Peterson and his instrumentation techniques for their data acquisition, and Mr. F. R. Fishburn for his engineering-test coordination efforts. Acknowledgement is also made to the members of the Spectral Dynamics Unit for their data reduction work.

CONTENTS

ILLUSTRATIONS

TABLES

SUMMARY

This report covers analytical studies leading to design and experimental verification of an active pressure oscillation suppression system and to determination of the frequency response characteristics of a low-speed inducer, high-speed pump system operating in a liquid oxygen feed system. The design requirements of the oscillation suppressor controller were defined by a frequency response analysis of the test stand feed system, and were based on estimated servovalve-actuator characteristics and a determination of the controller requirements to attenuate or eliminate generated flow-pressure oscillations in the range of 2 to 50 Hz.

Based on the analytical results, an electronic controller was designed and built. The control system, consisting of the controller, electro-hydraulic servovalve, and hydraulic driven piston, was tested in a liquid oxygen feed system. The tests consisted of introducing a variable frequency flow disturbance into the system upstream of the inducer. The effectiveness of the control is determined by its ability to attenuate the resulting pressure oscillations. Tests were run for two hardware configurations, two inducer inlet pressures, and with and without the control active.

From the test results, the major conclusions are:

1. The low-frequency dynamics of the low-speed inducer can be represented by an inlet compliance and resistance; there is negligible fluid inertia associated with an axial flow inducer.

2. For operation at high (non-cavitating) inducer NPSP's, the control attenuated the pressure oscillations by at least 8 db from about 10 to 25 Hz. This was true when the control was located upstream of the inducer as well as between the inducer and main pump.

3. Above 35 Hz, the phase shift through the control system caused the control to reinforce the oscillations. After testing, the problem was found to be due partially to the electronics and partially to the servovalve. This can be corrected by revising the electronics.

4. For operation at low inducer NPSP's, the control showed little, if any, attenuation when the control was upstream of the inducer. Placing the control between the inducer and pump, however, resulted in about 8-db attenuation in the range of 10 to 25 Hz.

5. Electrically setting the low frequency break at 12 rads/second resulted in an effective control above about 8 Hz. To lower the effective frequency to 2 Hz, the break frequency should be set for about 0.5 Hz.

6. The theoretically established feasibility of an active control for suppressing POGO induced pressure oscillation was verified by testing with simulated POGO induced pressure oscillations.

INTRODUCTION

All vehicles using pump-fed rocket engines are susceptible to in-flight longitudinal oscillations referred to as POGO. This is a closed loop problem of resonant tuning of the fluid feed system pressure oscillation and vehicle structural motion. The closed loop can be visualized by tracing the response of the system to a perturbation in vehicle acceleration. The acceleration oscillations cause pump inlet flow oscillations that result in pump inlet pressure oscillations that are dependent on the feed line and pump inlet dynamics. The pump inlet pressure (flow) oscillations are transmitted through the engine and produce thrust oscillations. The thrust oscillations then feed back through the structure, producing acceleration oscillations. This system will be unstable if the closed loop gain becomes greater than one and the net loop phase shift approaches zero.

To eliminate these oscillations, the loop gain and/or phase shift must be altered in the critical oscillation frequency ranges. Flight data from Thor, Titan, and Saturn vehicles indicate that the oscillations occur at a structural resonant frequency and are caused by coupling of the engine and structure through the pump feed lines. The critical feed line frequency is the lumped parameter resonant frequency defined by $[1/CL]^{1/2}$, where C is the effective line termination capacitance and L is the fluid inertia.

Vehicle oscillation corrective devices used to date have been passive, changing the feed line resonant frequency by the addition of capacitance. The capacitance has been added by the addition of trapped gas or gas filled accumulators. This fix has been used on the Saturn SIC and SII stages, Titan, and is being implemented on Thor vehicles. One main disadvantage to this approach is that final sizing of the accumulators must be delayed until late in the program when empirical data are available to define the vehicle and feed line frequencies. The resultant vehicle modifications could result in significant expense.

Rocketdyne studies of Space Shuttle POGO suppression systems (Ref. 1) have shown that an active control that suppresses the pump inlet pressure oscillation and is located near the pump inlet appears to be the most advantageous solution for POGO in any projected vehicle. The advantages are small size and weight, ease of activation without causing system transients, and the ability to suppress POGO over a wide frequency range. Areas of concern with an active device, include coupling and possible limit cycling between the pump and control system, the effect of pump-generated noise on control system operation, optimum location of the device, and proper sensing parameters.

To evaluate the concept and provide answers in the areas of concern, an active control pressure oscillation suppression system was analyzed, built, and tested.

SYSTEM ANALYSIS - NO CONTROL

The pressure oscillation suppression system that was studied consisted of a hydraulically actuated piston, hydraulic servovalve, piston position feedback transducer, pressure sensing for control, and the required electronics for system frequency response compensation. To determine the required electronic compensation, the frequency response characteristics of the test system, as installed in test stand CTL-I, Cell 2A, were estimated analytically.

Details, schematics, and a block diagram of the test system are given in Appendix A. The test system consisted of a liquid oxygen run tank, 16.5 feet of ducting from the tank to the test section, the test section, and ducting from the test section outlet to the liquid oxygen catch tank. The test section components consisted of an electro-hydraulic servovalve controlled disturbance piston, a low-speed hydraulic turbine driven inducer, the controller, and a high-speed, high head motor generator driven pump. To determine the frequency response characteristics, a set of linearized equations describing the dynamic performance of the system were written. The equations were solved in the frequency domain, using a digital computer program, for gain (in decibels) and phase (in degrees) of various system pressures with respect to distrubance pulser flowrate. Figures 1 and 2 show the predicted response of main pump inlet pressure to pulser flowrate, P_s/W_{p1}, for a close coupled inducer at high and low inducer inlet NPSH. For the inducer operating at high inlet NPSH, Fig. 1, the model predicts a fluid resonance at about 8 Hz followed by an anti-resonance at about 11 Hz and a double resonance in the range of 18 to 20 Hz. The main pump inlet pressure response for a close coupled inducer operation at low inducer NPSH is presented in Fig. 2 and shows a reduction of the 8-Hz resonance to about 3.5 Hz. Both of the higher resonances appear to move down (one of them cancelling the 11-Hz anti-resonance), leaving a single significant resonance at about 12 Hz.

Frequency response characteristics were also determined for the configuration where the inducer was remote-coupled to the main pump. Figures 3 and 4 show the high and low inducer inlet NPSH results. The high NPSH condition produces a 6- to 7-Hz resonance, an anti-resonance about 12 Hz, and a double resonance in the range of 17 to 22 Hz. The low NPSH condition shows a lowering of the 17- to 22-Hz resonances into the 12-Hz range.

The results of this part of the study were used to establish the design requirements of the suppression system controller and provide a basis for estimating the effectiveness of the controller. For further system analysis details see Appendix A.

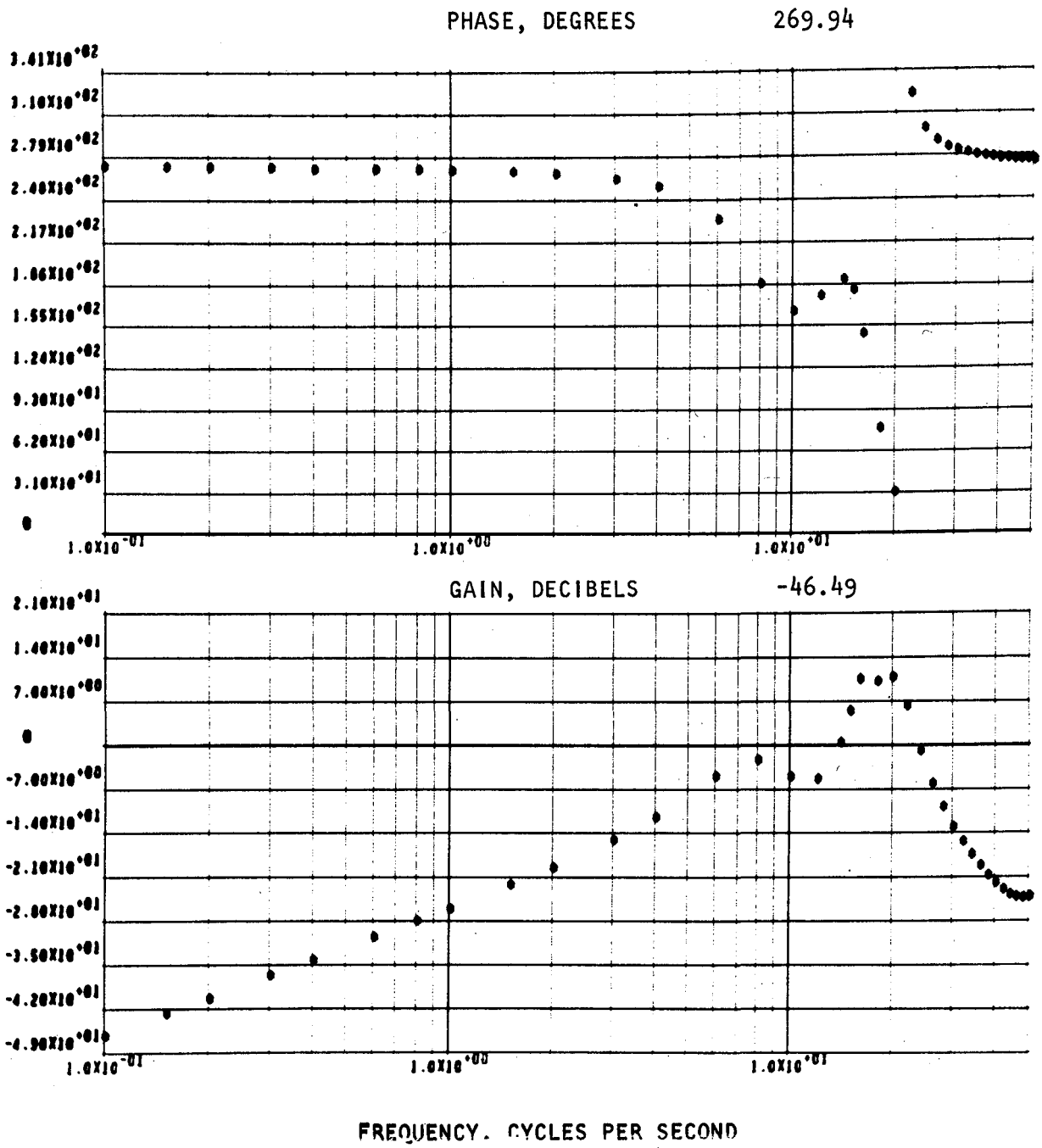

Figure 1. Response of Pump Inlet Pressure (P_s) to Disturbance Pulser Flowrate ($\tilde{W}_{P1}$) With Inducer Close-Coupled to the Pump Inlet and NPSH = 12.2 Meters (40 ft)

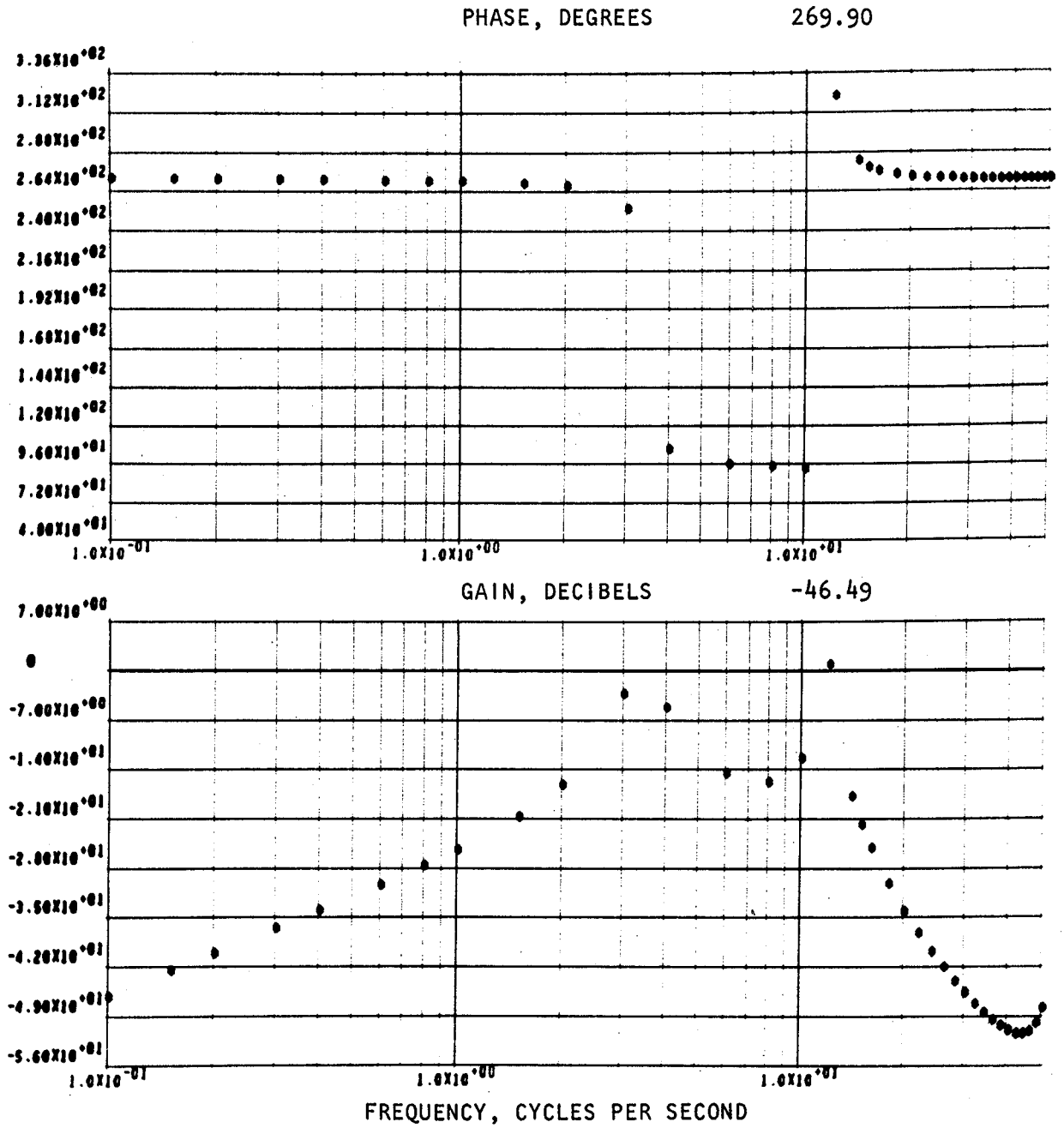

Figure 2. Response of Pump Inlet Pressure (P_s) to Disturbance Pulser Flowrate ($\dot{W}_{Pl}$) With Inducer Close-Coupled to Pump and NPSH = 6.1 Meters (20 ft)

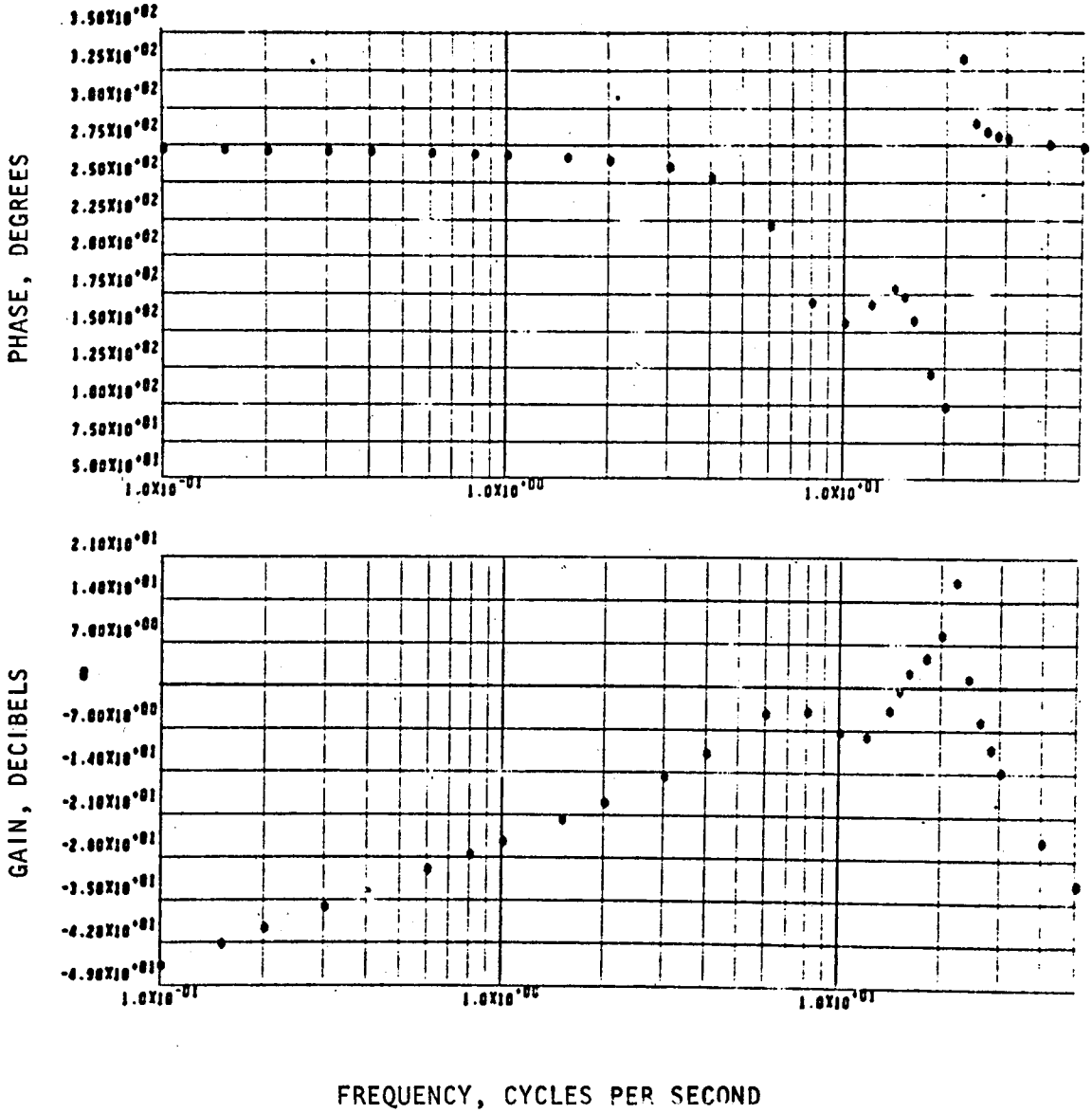

Figure 3. Response of Pump Inlet Pressure (P_s) to Disturbance Flowrate ($\hat{W}_{p1}$) With Inducer Remote-Coupled to the Pump Inlet and NPSH = 12.2 Meters (40 ft) Pulser Upstream of Inducer

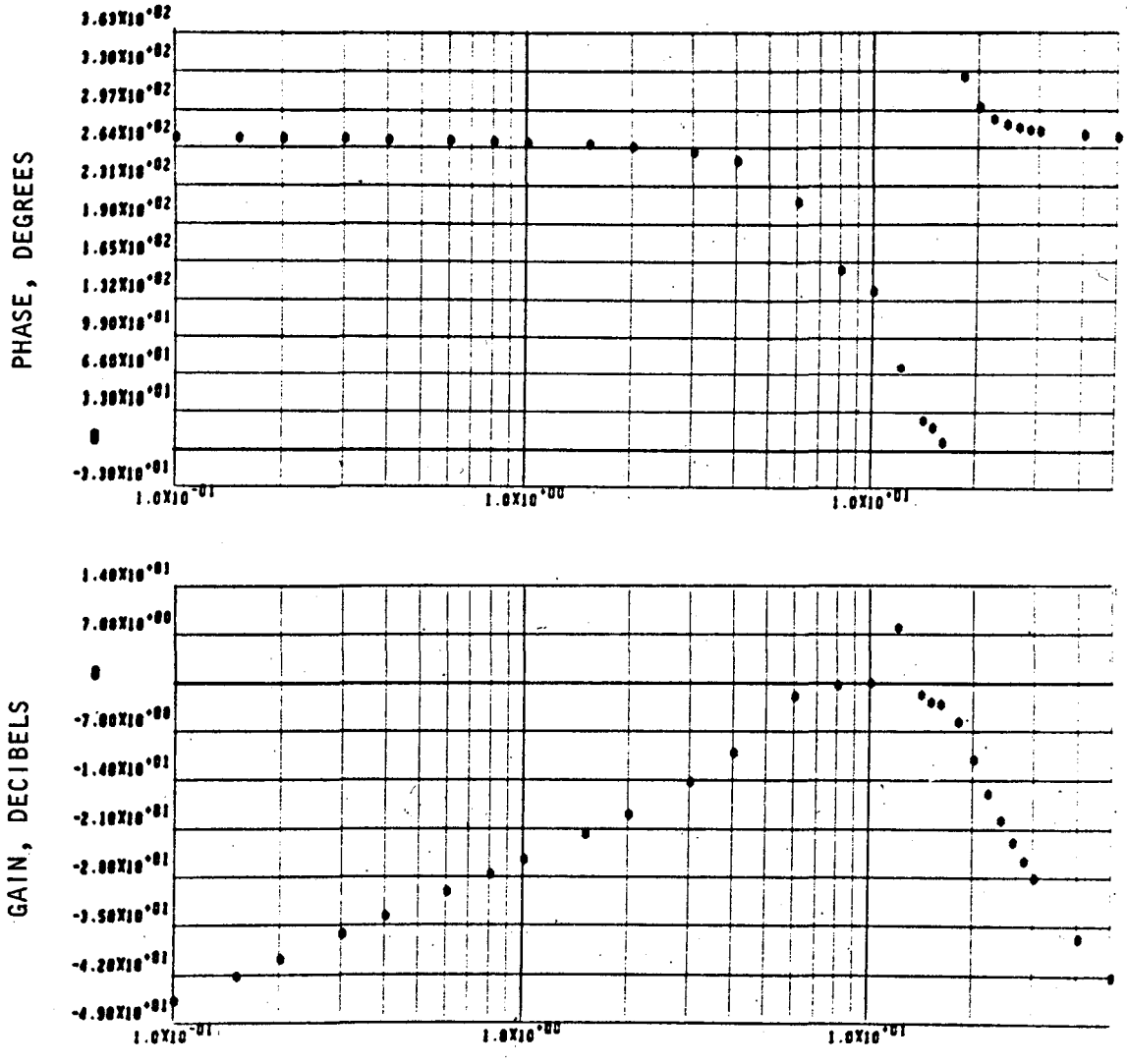

Figure 4. Response of Pump Inlet Pressure (P_s) to Disturbance Pulser Flowrate (W_{P1}) With Inducer Remote Coupled to the Pump Inlet and NPSH = 6.1 Meters (20 ft)

Page intentionally left blank

CONTROL SYSTEM ANALYSIS AND DESIGN

With the dynamic characteristics of the fluid system defined, an analysis to establish the suppressor control requirements was made. Design of the control systems requires that the servo-actuated piston maintain its null point regardless of either the steady load produced by pressure on the face of the piston or the steady value of an input signal. In addition, the most desirable characteristic for the piston is that its velocity be proportional to the input signal over a wide frequency range (2 to 50 Hz). The design transfer function was therefore chosen as:

$$\frac{X}{V} = \frac{KS}{1 + S/\omega_o + S^2/\omega_o^2}, \text{ where } \omega_o \approx 4\ \pi \text{ rad/sec} \qquad (1)$$

X is control piston position, inches
V is controller input signal, volts

Figure 5 is a schematic of the controller piston and servovalve second stage spool. An existing 0.756 liters/sec servovalve was used for which the following transfer function was determined from a Bode plot curve fit of no load frequency response test data:

$$\frac{Z \text{ (percent spool position)}}{i \text{ (ma of current)}} = \frac{25}{(1 + S/125)(1 + S/1000} \qquad (2)$$

The response of the piston position to spool position and piston face pressure was found to be:

$$X = \left[0.148(1 + S/667)\ P_s + 1.02\ Z\right] / S\left[1 + 0.16S/3100 + S^2/3100^2\right] \qquad (3)$$

In order to obtain approximately 50-Hz response for the piston positioning loop, the following circuit was used for the inner loop:

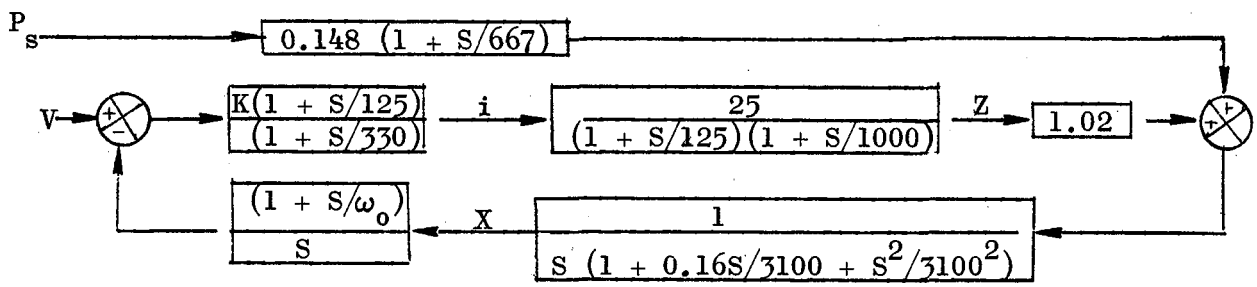

where ω_o = 12 rad/sec. The term K(1 + S/125)/(1 + S/330) represents the inner loop electronic compensation.

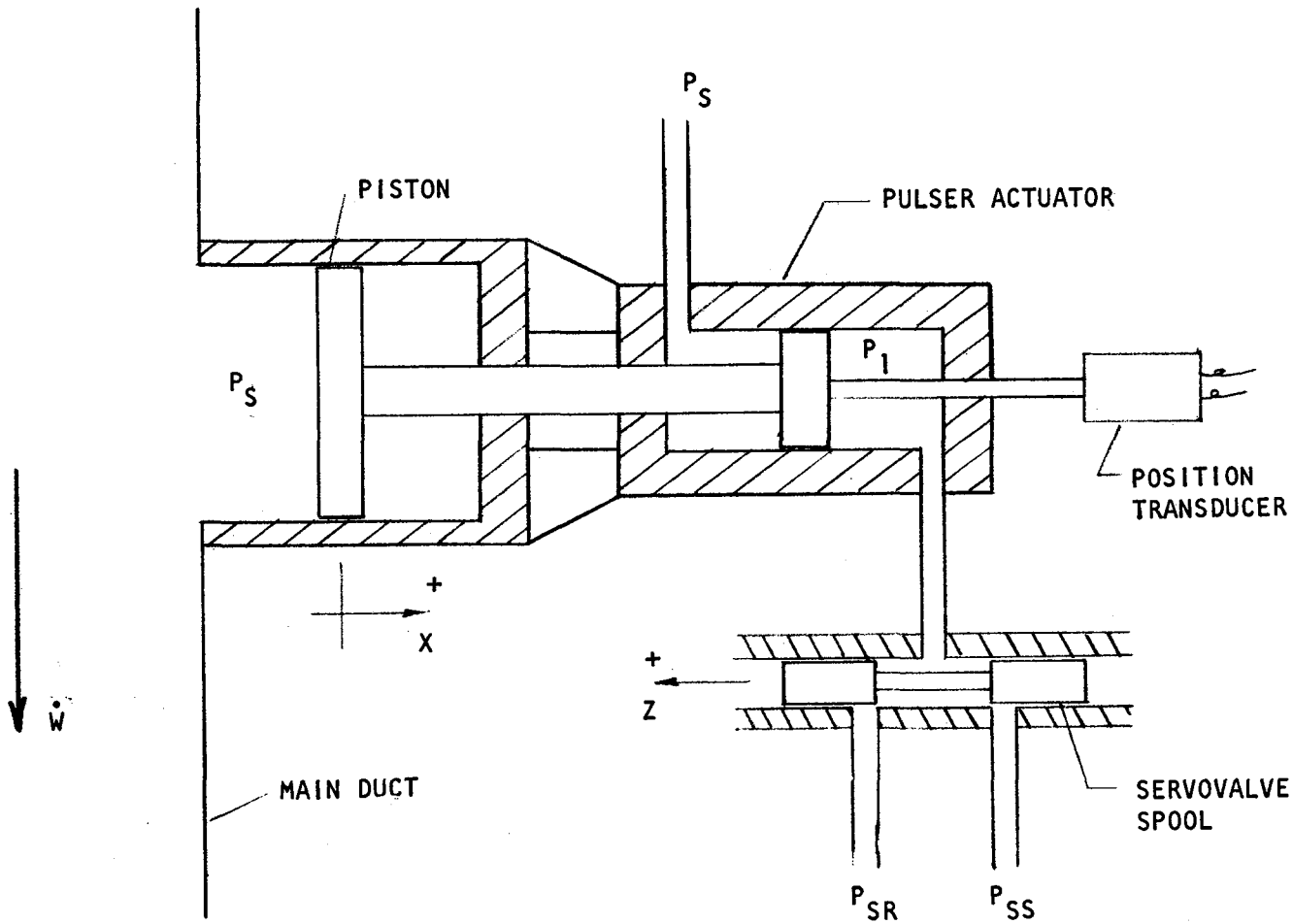

Figure 5. Pulser Piston, Actuator and 3-Way Servovalve Schematic

Ignoring frequencies higher than 330 rps (50 Hz) and the P_s input, results in:

$$\frac{X}{V}(S) = \frac{K\ (25)\ (1.02)}{S(1 + S/330) + (1 + S/\omega_o)\ (K)\ (25)\ (1.02/S)}$$

$$= \frac{S}{\frac{S^2}{25\ (1.02K)}\ (1 + S/330) + (1 + S/\omega_o)} \qquad (4)$$

Choosing $(25)\ (1.02)K \doteq \omega_o^2$ a root locus analysis for 50-percent damping gave the approximate equivalent closed loop transfer function of:

$$\frac{X}{V}(S) = \frac{S}{(1 + S/\omega_o + S^2/\omega_o^2)\ (1 + S/300)} \qquad (5)$$

Ignoring system dynamics above 330 rads/sec, the block diagram becomes:

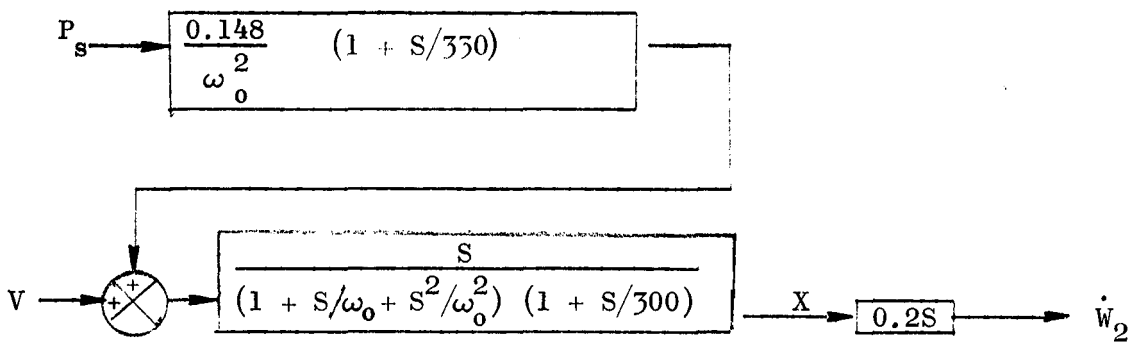

With the exception of the pole at 300 rps (≈48 Hz), the desired inner loop transfer function, as given in Eq. 1, is obtained. This transfer function allows the pulser piston to respond to commands at frequencies above 2 Hz.

To complete the design of the controller, the desired form of the input had to be determined. For the close coupled inducer configuration, an estimate of the feed system dynamics was obtained from Fig. 6 . Ignoring the minor effects of the second order dipole in the 10-Hz range, a reasonable estimate of the transfer function of inducer inlet pressure (P_{II}) to pulser disturbance flowrate (W_{PI}) is:

$$\frac{P_{II}}{W_{PI}} = \frac{1.605S}{1 + 0.086\ (S/111) + (S/111)^2} \quad \text{sec/cm}^2$$

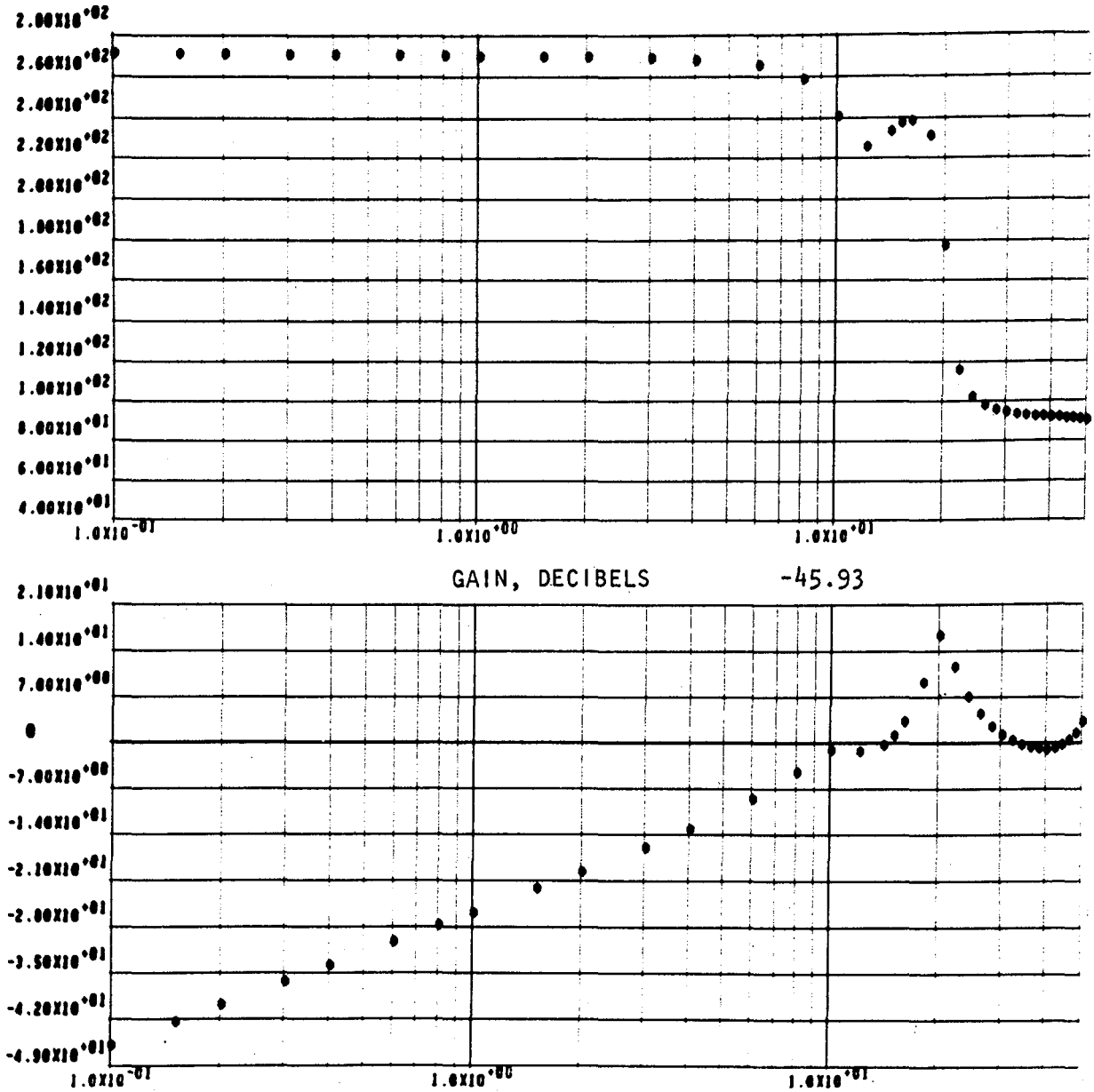

Figure 6. Response of Pump Inlet Pressure (P_s) to Disturbance Pulser Flowrate ($\hat{W}_{P1}$) Without Inducer in Feed System

Knowing that only one significant resonance exists in the 0- to 50-Hz range, and referring to Fig. 38 for subscript locations, the following equations can be written for the feed system:

$$P_T - P_2 = L_1 S \dot{W}_{T2} \tag{6}$$

$$P_2 - P_{II} = L_2 S \dot{W}_{2s} \tag{7}$$

$$(CS + 1/R)P_{II} = \dot{W}_{2s} - \dot{W}_{P2} \tag{8}$$

$$\dot{W}_{2s} = \dot{W}_{T2} - \dot{W}_{P1} \tag{9}$$

where

C = terminating capacitance, $in.^{-2}$

$L1$ and $L2$ = fluid inertia in duct, $sec^2/in.^2$

P_T = tank outlet pressure, psia

P_{II} = inducer inlet pressure, psia

P_2 = pressure at disturbance pulser, psia

$\dot{W}_{T2}$ = flowrate in duct between tank outlet and point 2, lb/sec

$\dot{W}_{2s}$ = flowrate in duct between point 2 and pump inlet, lb/sec

$\dot{W}_{P2}$ = controller, flowrate, lb/sec

$\dot{W}_{P1}$ = disturbance flowrate at point 1, lb/sec

Combining these equations and defining $\Delta P_T = P_T - L_1 S W_{P1}$ and $L1 + L2 = L$, the following equation results:

$$P_{II} = \left[\Delta P_T - LS \dot{W}_{P2}\right] / \left[1 + LS/R + LCS^2\right] \tag{10}$$

One method of achieving POGO control is to reduce the first mode resonant frequency of the feedline below that of a critical mode. This can be accomplished by increasing the terminating compliance.

A resistance-compliance effect can be achieved if a control is built represented by the form:

$$\dot{W}_{P2} = \left[C' S + D\right] P_{II} \tag{11}$$

Substituting this into Eq. 10, the feed line equation becomes:

$$P_{II}/\Delta P_T = 1/\left[1 + \left(\frac{L}{R} + DL\right) S + L\,(C + C')\,S^2\right] \qquad (12)$$

From Eq. 12 the new system natural frequency is $\omega = 1.0/\sqrt{(C + C')L}$ and the damping factor is given by $\zeta = \frac{1}{2}\left(\frac{L}{R} + LD\right)/\sqrt{L\ (C + C')}$, Thus, by choosing the value of C' we can control the system frequency while the value of D sets the system damping.

Defining $V = H \times P_s$

where

H = Input Compensation

Combining with the controller equation and solving for H, an input compensation of the form of (C'S + D) is obtained.

Desirable design values for 50-percent damping are:

Required frequency (Hertz)	C'	D	Break frequency of lead compensation (rad/sec)
17-1/2	0	0	-
10	$4.8\ (10^{-4})$	$5.2\ (10^{-2})$	108
6	$1.7\ (10^{-3})$	$8.2\ (10^{-2})$	48

This results in a controller input of the form $P_s\ (C'S + D)/(1 + S/314)$. The lag at 50 Hz (314 rps) is added to eliminate problems with high frequency noise due to the lead compensation. Additional details and alternate approaches are presented in Appendix B.

A second controller input, other than the pressure measurement at the controller, was analyzed and designed into the controller. This input was an upstream pressure, the input compensation being designed to cancel the effect of upstream inputs on pump inlet pressure. This results in a compensation of $V = 68P_1/(1 + S/12)$. The final control system is shown in block diagram form in Fig. 7.

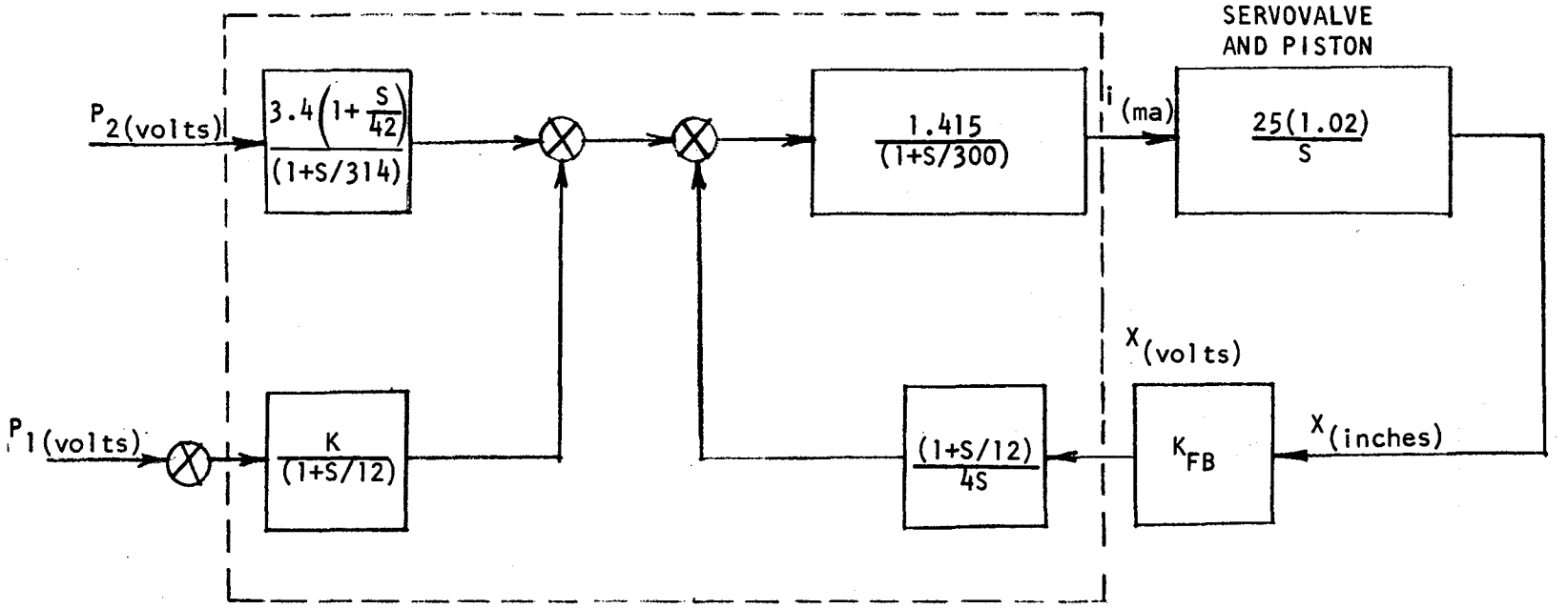

Figure 7. Block Diagram of Pressure Oscillation Suppression Control System

In addition to the digital frequency response model, a nonlinear analog computer model of the test stand and controller was developed. Fig. 8 shows predicted results, from the model, of the inducer and main pump inlet pressures for no control and with control. As can be seen, it was estimated that almost total suppression was achieved below about 40 Hz.

The close-coupled inducer configuration was also analyzed with the digital model, first with no control, then with the active control and finally, with the active control plus upstream pressure lead. The lead pressure (P_l) was sensed at the discharge of the disturbance pulser; the active control feedback pressure (P_S) was measured at the control piston station. Without control (Fig. 9), the feed system contains a resonant mode at 16 Hz that is less than the 18 Hz resonance of Fig. 1 due to a slightly different value of pump compliance. Use of the active control, with 2-Hz high pass control, effectively reduces the gain of the system by more than 25 db at the resonant frequency, 16 Hz. The addition of the lead pressure compensation serves to further reduce the gain over a broader frequency range.

The control system was then examined with the remote inducer installation wherein the control device was mounted between the main pump and the inducer. In this case, the lead pressure was measured at the outlet of the inducer. Again, three cases were run with this installation: (1) no control, (2) with the active control, and (3) with the active control plus pressure lead. The results are in Fig. 10. Since initial analysis indicated that radical phase changes result in unstable loops in the control, the lead pressure measurement was mounted relatively close to the inducer in a section of line that responds as though it were primarily inertive throughout the frequency range of interest. Locating the control between the main pump and inducer and measuring the lead pressure upstream of the inducer would produce instabilities in the 30-Hz frequency range. It was acceptable, however, to mount both the control and the lead pressure measurement downstream of the inducer.

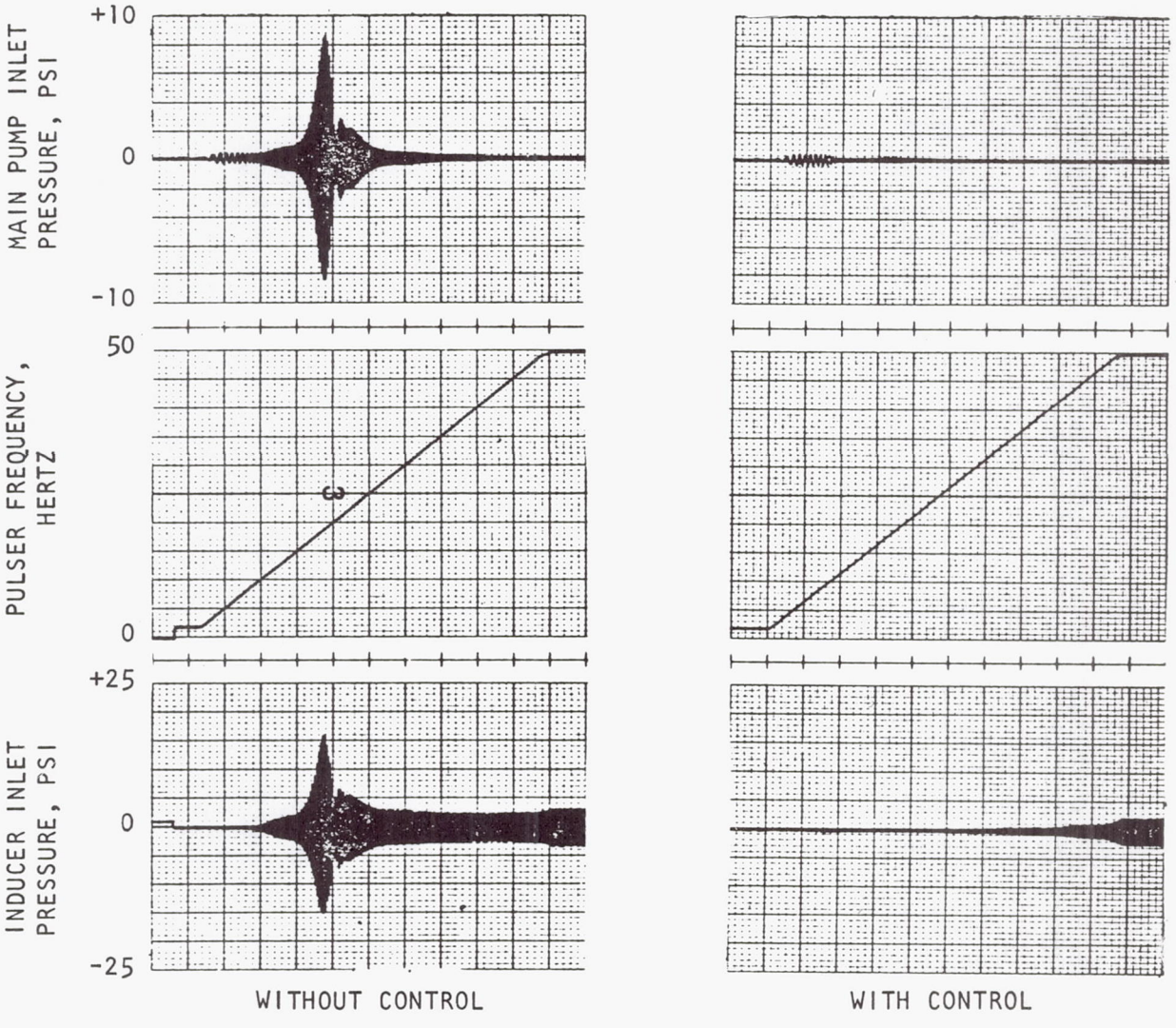

Figure 8. Performance of Close-Coupled Inducer With and Without Active Control

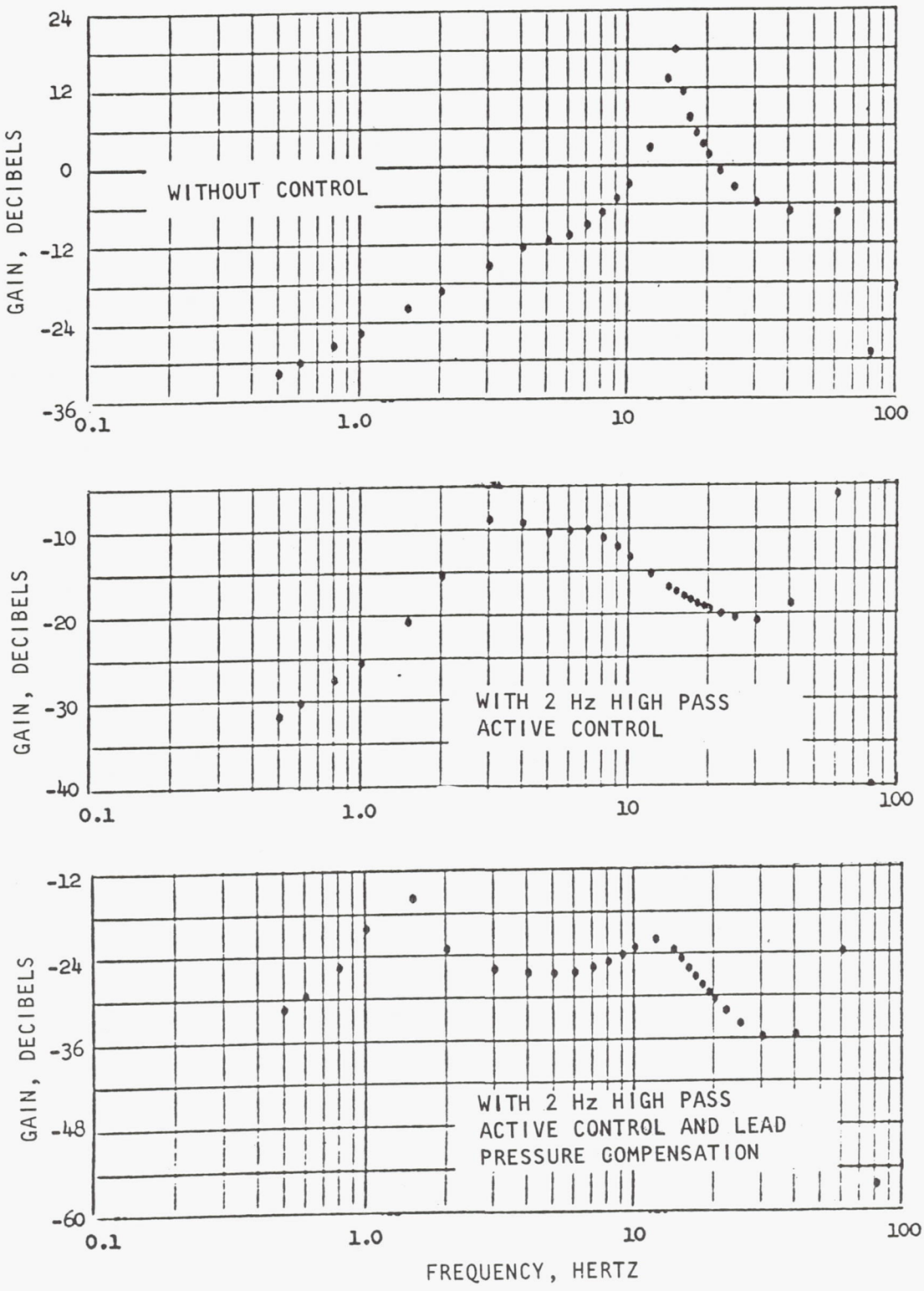

Figure 9. Gain Between Main Pump Inlet Pressure and Disturbance Pulser Flowrate Showing Attenuation Caused by the Control Configurations for the Close-Coupled Inducer Installation

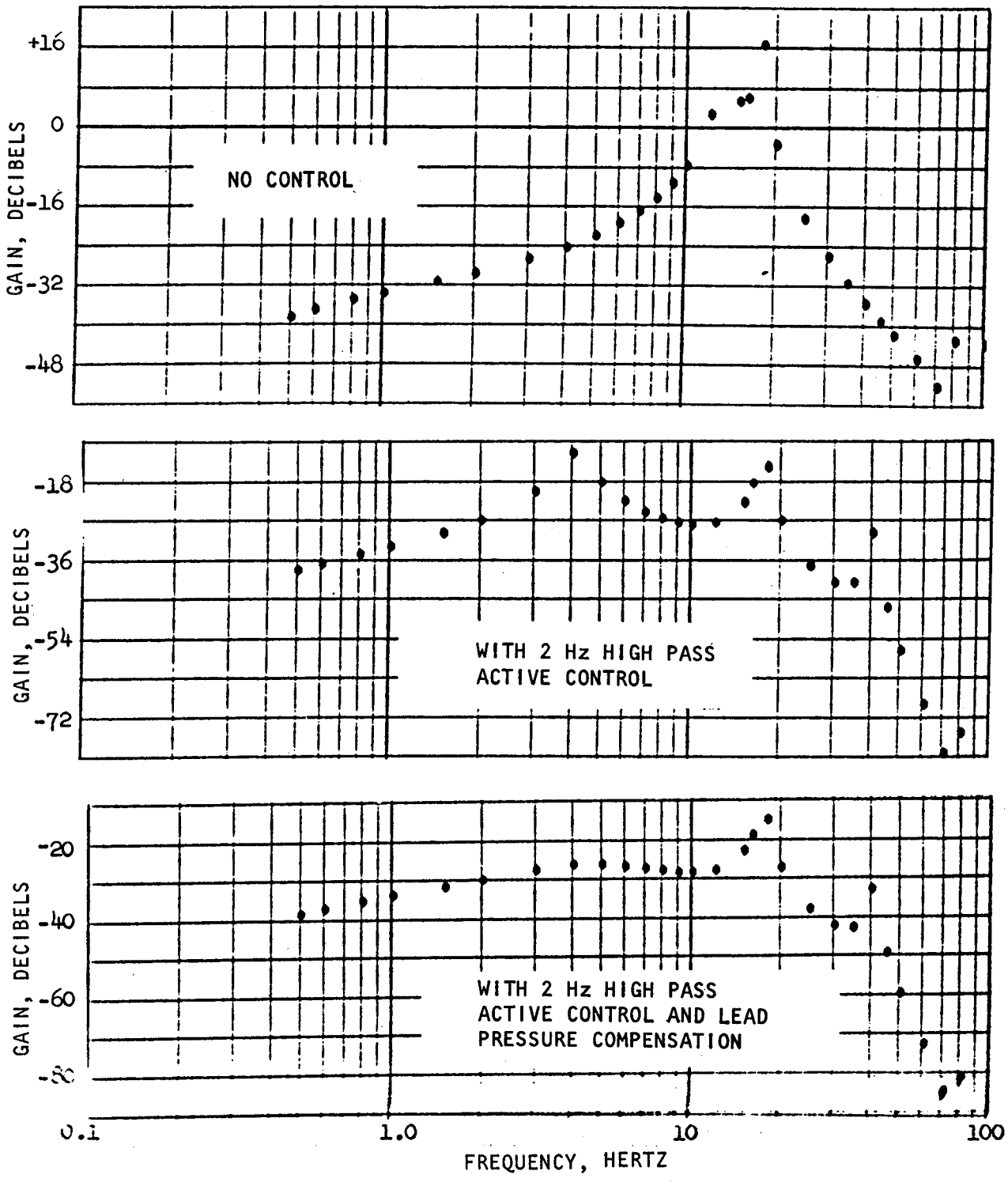

Figure 10. Gain Between Main Pump Inlet Pressure and Disturbance Pulser Flowrate Showing Attenuation Caused by the Control Configuration for the Remote-Coupled Inducer Installation

Page intentionally left blank

TEST PROGRAM

A test program was conducted in Cell 2A of Rocketdyne test facility CTL-I to experimentally determine the frequency response characteristics of a low-speed inducer high-speed pump system in liquid oxygen, and the effectiveness of the analyzed and designed POGO instability suppression system. The test hardware consisted of a J-2S liquid oxygen pump modified with a J-2 pump inducer, a low-speed hydraulic-turbine driven inducer, a hydraulic driven flow pulser, and a hydraulic driven anti-POGO controller with associated electronics.

Tests listed in Table VI of Appendix C were run for two different configurations. These configurations had the low-speed inducer close-coupled to the main pump and remote-coupled to the main pump. In the close-coupled configuration, the flow pulser was the first component in the test section followed by a reducer section, an expander section, the anti-POGO manifold and piston, a bellows for absorbing thermal displacements, the low-speed inducer, and the main pump. The remote-coupled configuration interchanged the low-speed inducer and the reducer section. The turbine drive for the low-speed inducer was liquid oxygen tapped from the main pump discharge.

A total of 41 tests were run, 20 tests with the inducer remote-coupled and 21 tests with the inducer close-coupled. The remote-coupled tests consisted of calibration runs, pulsing runs at two inducer Q/N values, and two inlet pressures and controller runs at two inducer Q/N values and two inlet pressures. The calibration runs were made to check out the system and to determine the regions of self-driven oscillations. To determine the region, the tank pressure was set for 27.6×10^4 newtons/m^2 gage. The tank pressure was then vented off until pump cavitation occurred. A review of the pressure data showed self-driven oscillation between 6.2×10^4 and 7.6×10^4 newtons/m^2 gage. The high NPSP tests were run with the low-speed inducer inlet pressure at about 31×10^4 newtons/m^2 gage, while the low NPSP tests were made with the pressure at about 8.3×10^4 newtons/m^2 gage.

The close-coupled configuration tests consisted of pulsing tests at two inducer Q/N values and two inlet pressure levels, controller runs at two inducer Q/N values and two inlet pressures, and a set of tests without the inducer or main pump operating. The high NPSP tests were run with a low-speed inducer inlet pressure of about 31×10^4 newtons/m^2 gage, while the low NPSP tests were run with the pressure at about 6.9×10^4 newtons/m^2 gage. The tests run without the inducer or main pump operating were to evaluate various controller gains and lead pressure inputs. Reduction of the data indicated results for the test section were comparable to those obtained when the inducer and pump were operating. For details of the test program, see Appendix C.

There were no major problems encountered in running the test series, no hardware damage, and all test objectives were met.

SYSTEM TEST RESULTS

CLOSE-COUPLED CONFIGURATION

In this configuration, Fig. 37 , the low-speed inducer was mounted immediately upstream of the main pump. The controller was located several pipe diameters upstream of the low-speed inducer to ensure that it would not be adversely affected by back flow along the duct wall. Data were monitored at a number of points in the system and typical data for a pulsing sequence are shown in Fig. 11 and 12. The parameter chosen for controller evaluation was the response of the ratio of pressure, measured in the duct at the control, to the stroke of the input pulser.

Phase and gain data are shown in Fig. 13 and 14 for high NPSP tests with and without the controller operating. The gain plot shows that at 20 Hz, an attenuation of approximately 12 db at high Q/N and 8 db at low Q/N is obtained with the controller. In some areas the statistical coherence of the data was low due to either the low amplitude of the input pulser stroke or low system response. These areas have been smoothed to present the best estimate of the actual system response. The actual phase-gain-coherence plots of Test 069 are shown in Fig. 15 , 16, and 17 to indicate the extent to which smoothing was used to obtain the results of Fig. 13 and 14. For correlation purposes, an average of the two uncontrolled responses of Fig. 13 and 14 is compared with Fig. 6 and shown as Fig. 18. The simulation was for a case with no inducer and no control. It can be seen by comparing the two responses that the effect of including the low-speed inducer close to the main pump is primarily to add system damping to the 20-Hz resonance. For comparison purposes, the pulser motion was converted to an input disturbance flowrate by knowing that 1-cm motion displaces 37.0 gms of liquid oxygen.

The resonant peak from data with no control indicates 30 percent of critical damping. Since the most significant dynamics are the second order resonance, the controller was evaluated as to its effect on those dynamics. The response of the system without the control is approximately:

$$P_s/X_p = K\,S^2/\left[1 + LS/R + LCS^2\right] \triangleq F(S)$$

where $K = -\rho A_p\, L_1$

Consider next a control that obeys the equation:

$$\dot{W}_c/P_s = G(S)$$

The equation for the system with this control, Eq. 10, then becomes:

$$P_s/X_p = KS^2/\left[1 + LS/R + LSG(S) + LCS^2\right] \triangleq H(S)$$

LERC ACTIVE POGO SUPPRESOR TEST DATA, CLOSE-COUPLED INDUCER
(ALL DATA FILTERED 1 TO 50 Hz, NOMINAL PUMP SPEED)

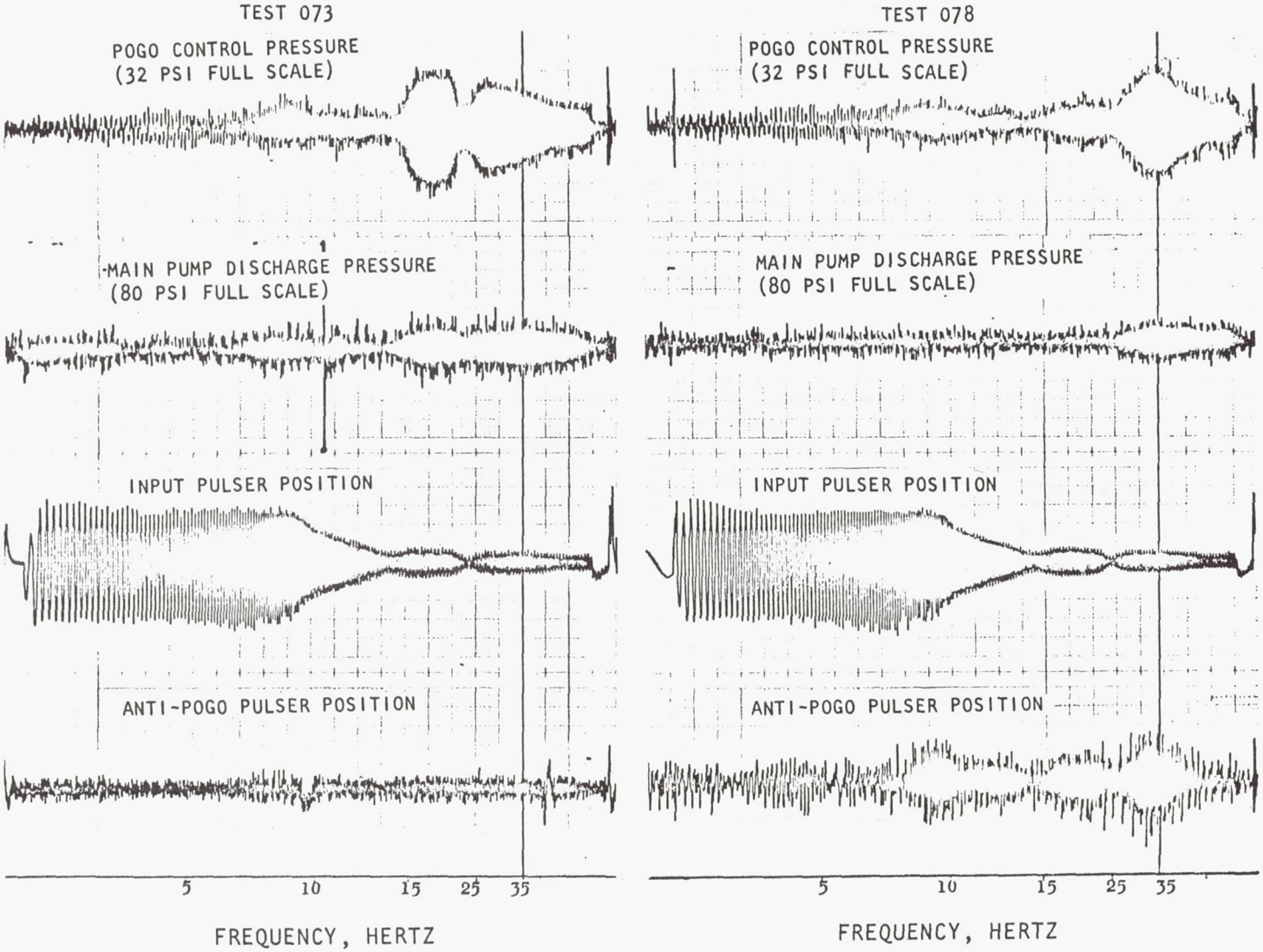

Figure 11. Active POGO Suppressor Test Data, Close-Coupled Inducer

LERC ACTIVE POGO SUPPRESSOR TEST DATA, CLOSE-COUPLED INDUCER
(ALL DATA FILTERED 1 TO 50 Hz, NOMINAL PUMP SPEED)

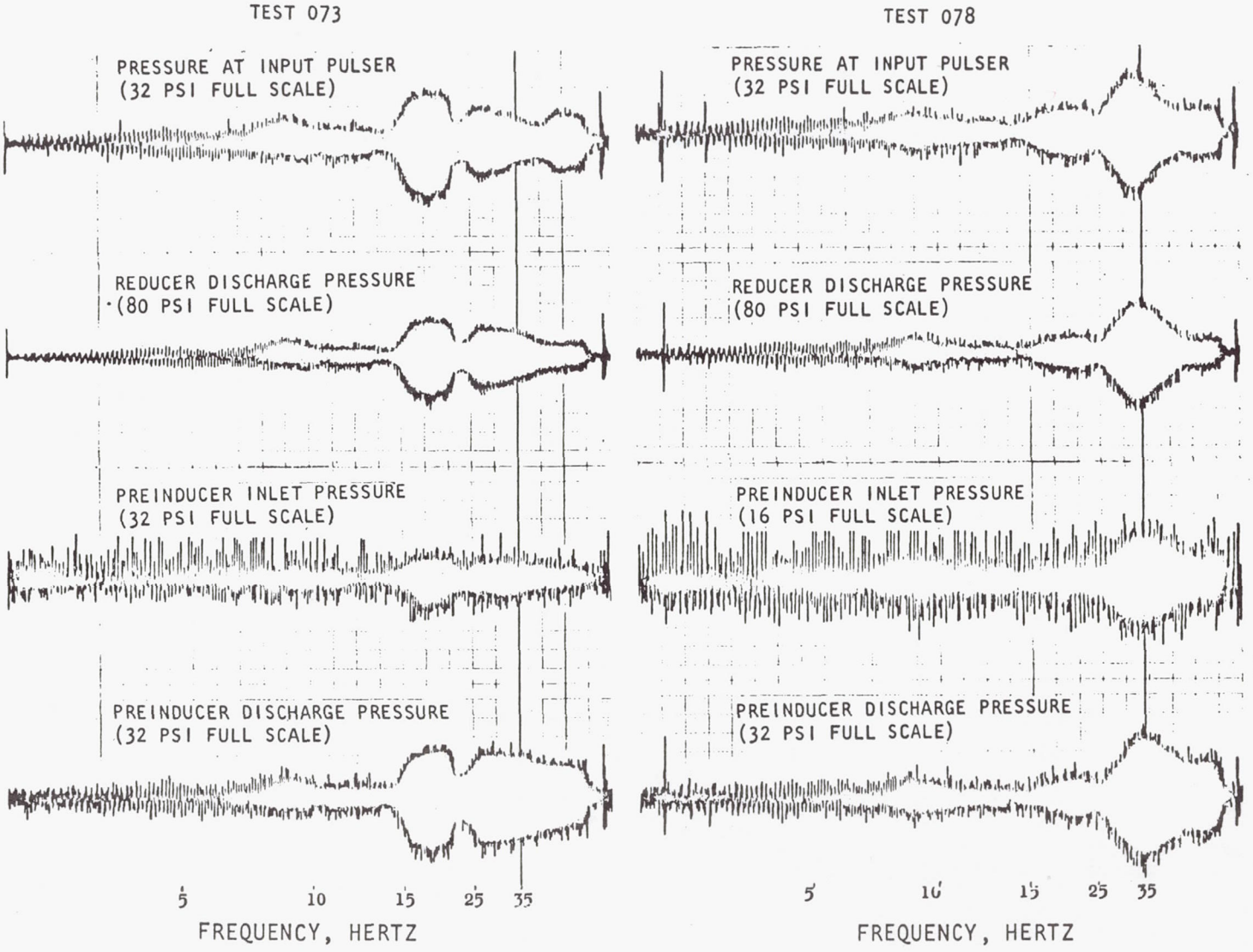

Figure 12. Active POGO Suppressor Test Data, Close-Coupled Inducer

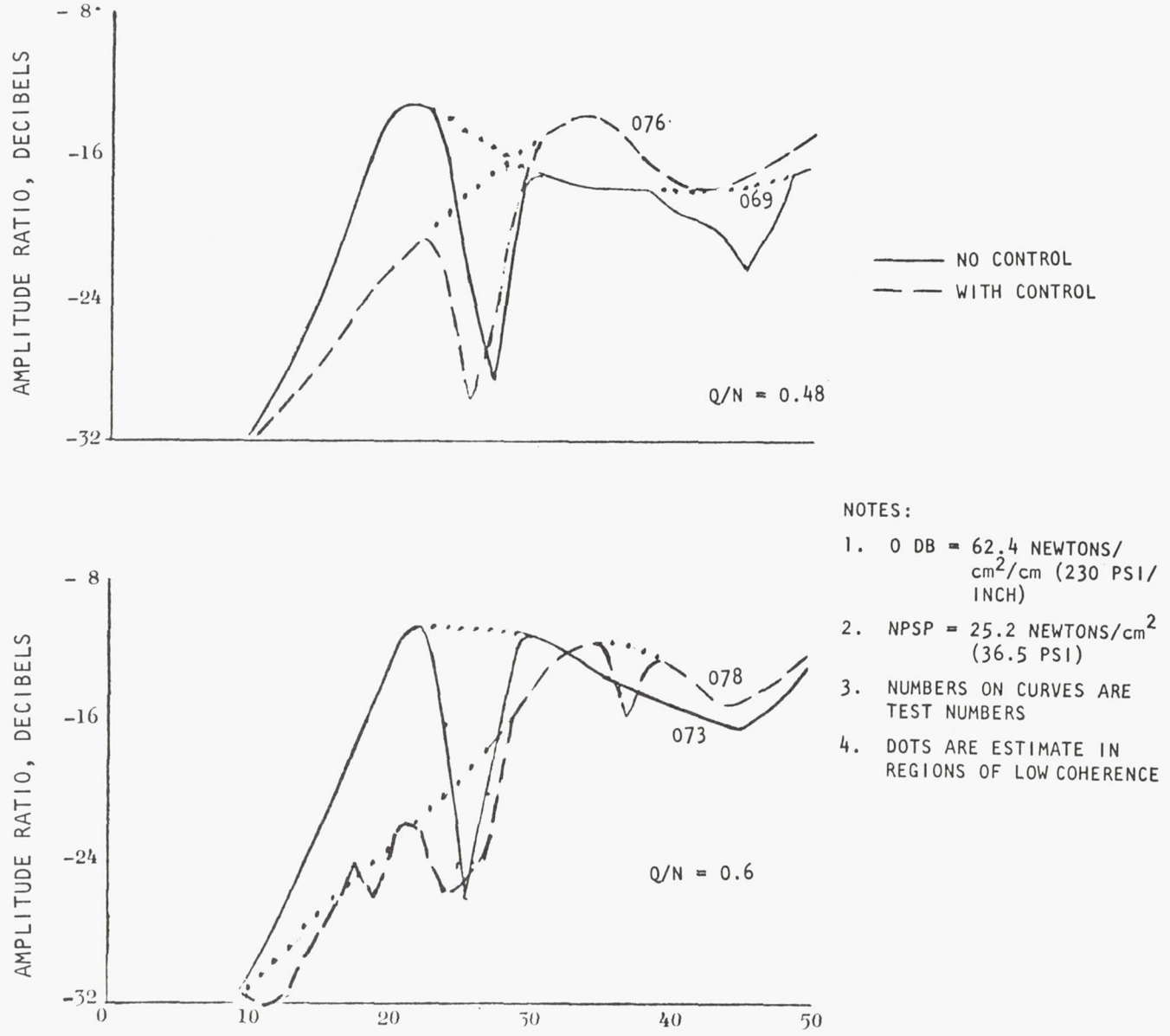

Figure 13. Gain of Controller Duct Pressure/Disturbance Pulser Stroke Close-Coupled High NPSP Tests

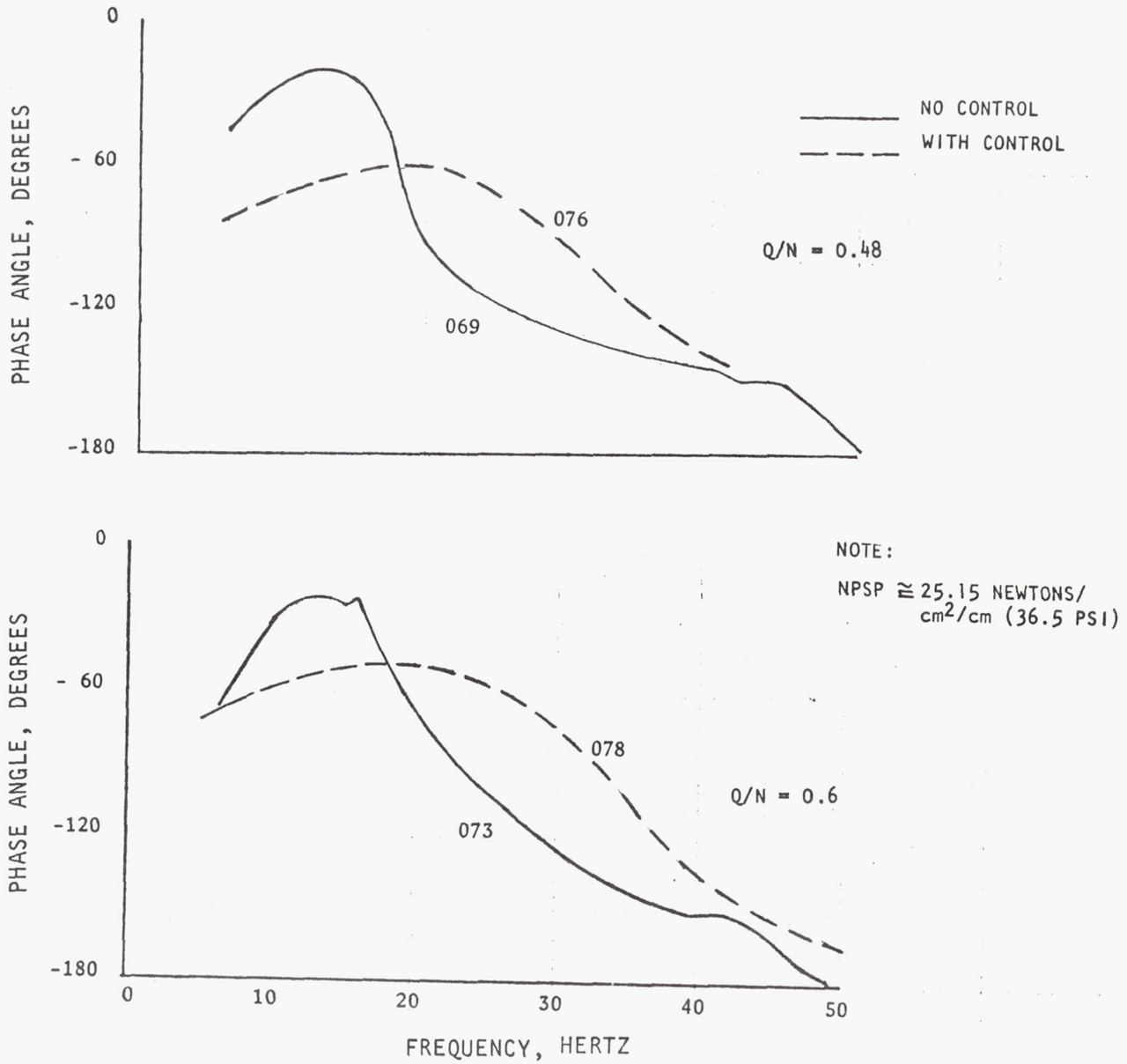

Figure 14. Phase of Controller Duct Pressure/Disturbance Pulser Stroke Close-Coupled Tests

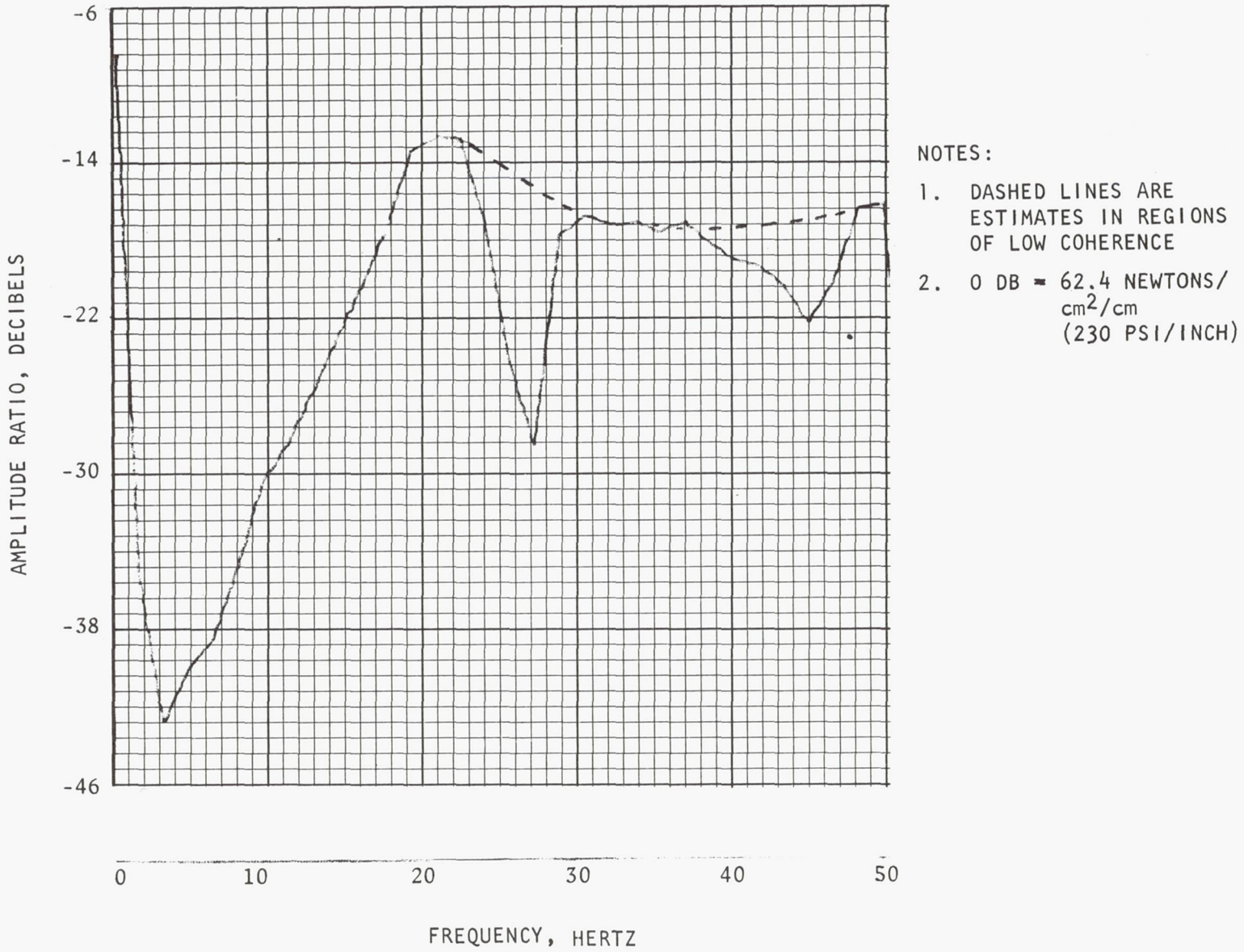

Figure 15. Gain of Controller Duct Pressure/Disturbance Pulser Position Test-069

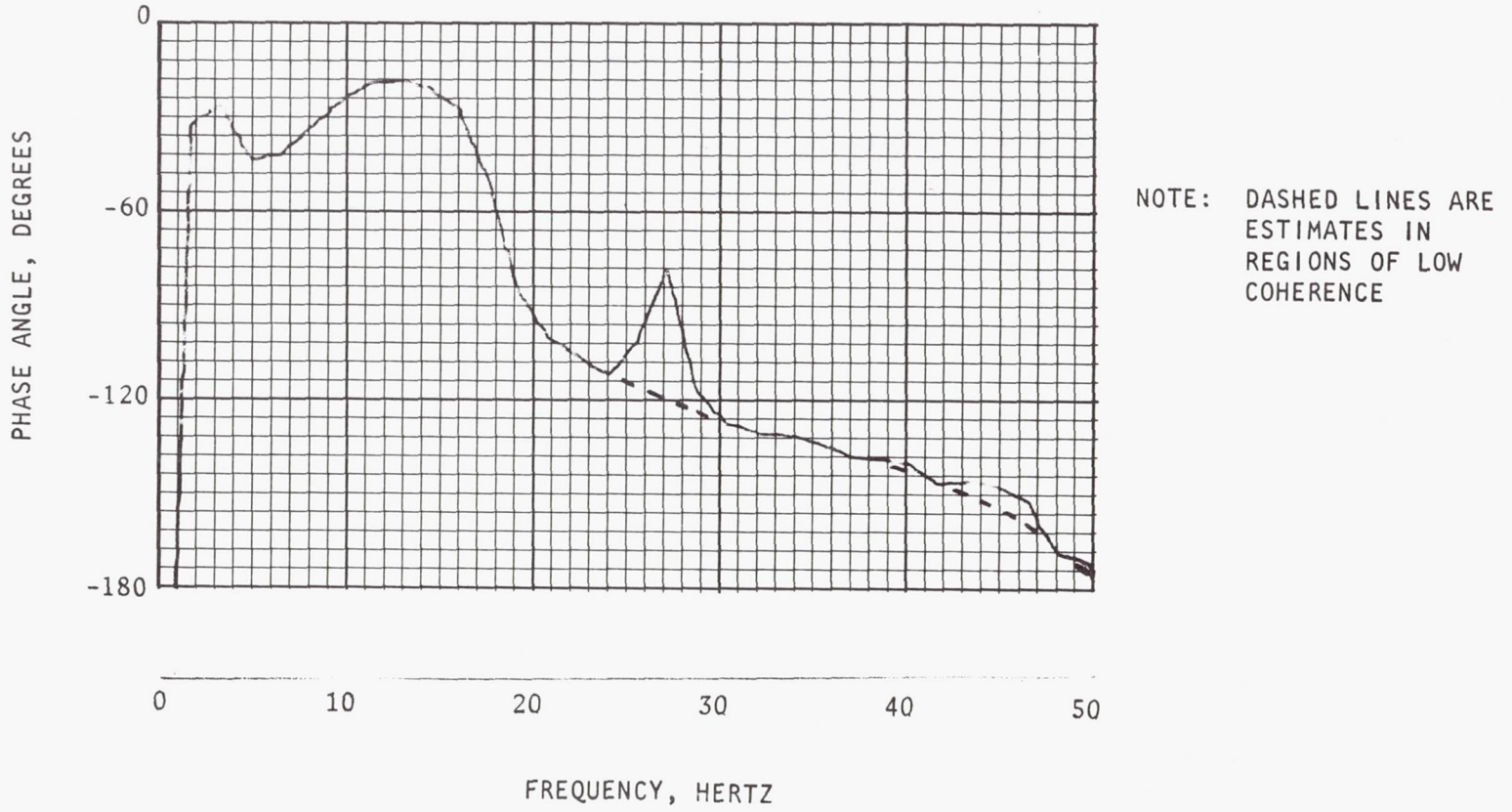

Figure 16. Phase of Controller Duct Pressure/Disturbance Pulser Position Test-069

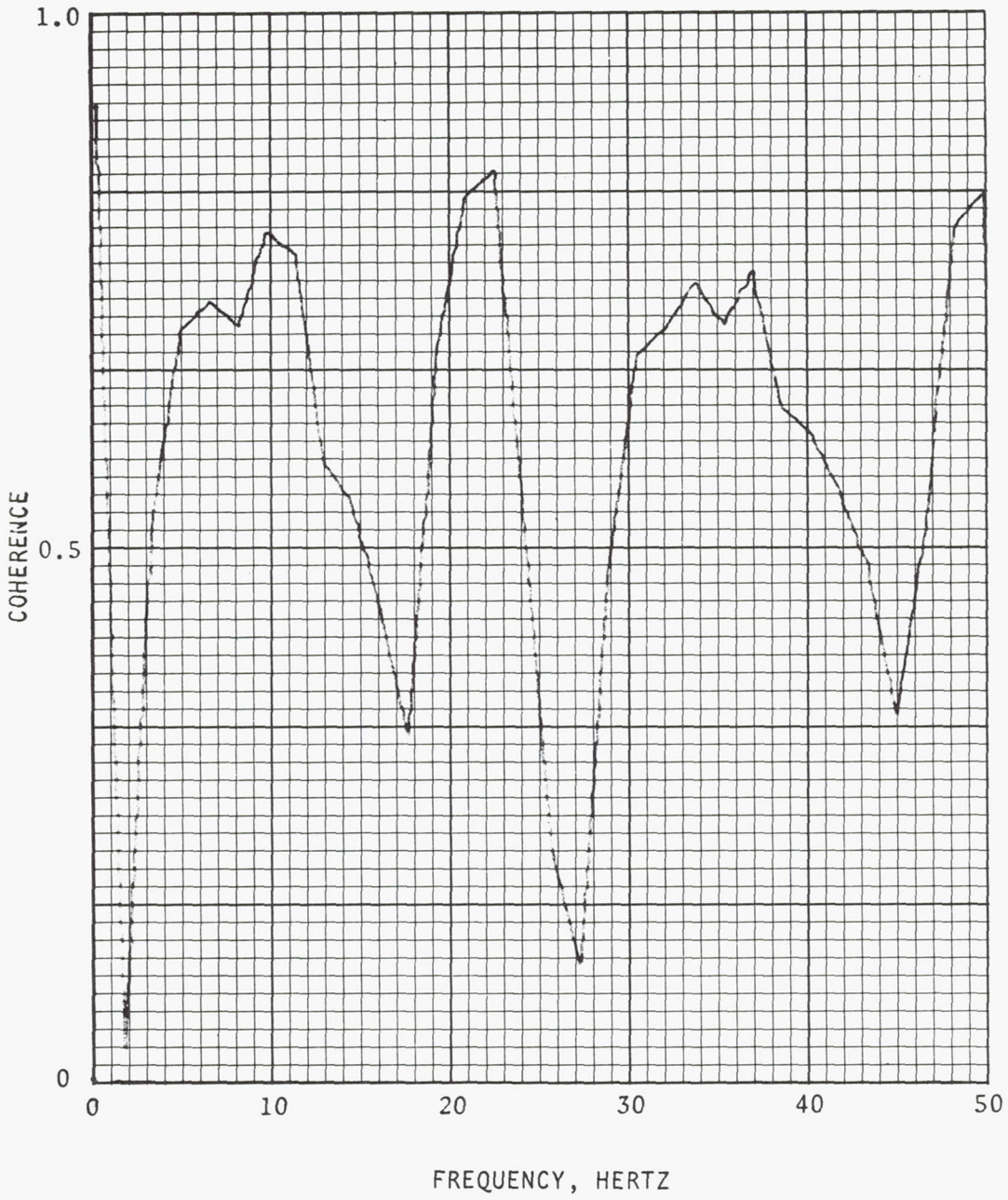

Figure 17. Coherence of Controller Duct Pressure/Disturbance Pulser Position Test-069

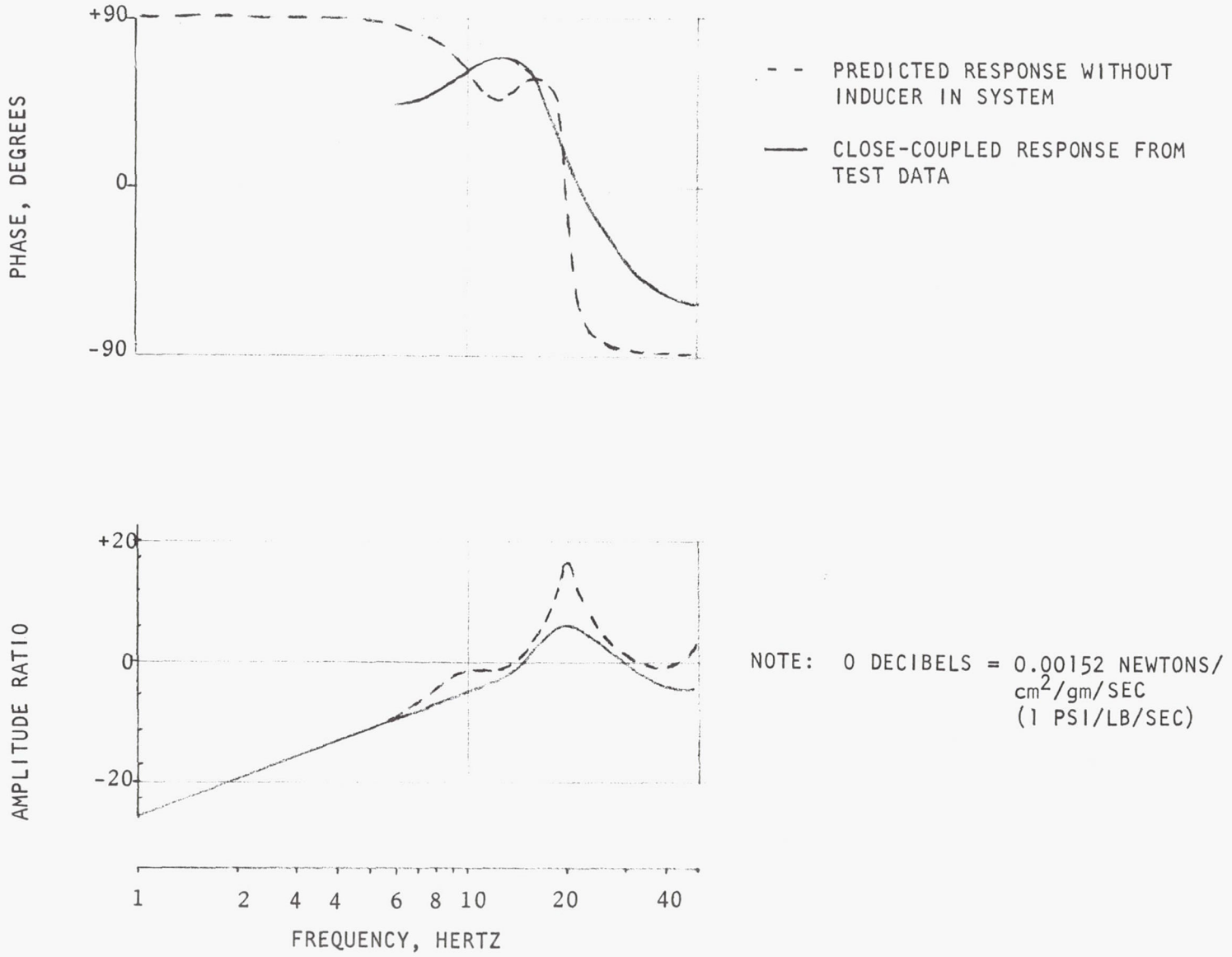

Figure 18. Comparison of Test and Predicted Controller Duct Pressure/Disturbance Pulser Flowrate

Solving for G(S):

$$G(S) = \frac{SK}{LF(S)} \left[\frac{F(S)}{H(S)} - 1\right]$$

$$G(S) = -\frac{L_1 \rho A_p S}{L\ F(S)} \left[\frac{F(S)}{H(S)} - 1\right]$$

This equation allows us to use the controlled H(S) and uncontrolled F(S) gain and phase data from Fig. 13 and 14 to solve for the response of the control. The resultant polar plot is shown in Fig. 19 . Also shown on the figure for reference is the system admittance $\left(\frac{1}{R} = \frac{2300\ \text{Kg/sec}}{\text{newtons/m}^2}\ (0.35\ \frac{\text{lb/sec}}{\text{psi}})\right)$ determined from the response of the uncontrolled system. Since damping is dependent on the vector sum of $\frac{1}{R}$ and G(S), it is obvious that in the 10- to 25-Hz range the control adds appreciable system damping. At 31 Hz, the phase shift in the control adds no additional damping, and at frequencies between 31 and 38 Hz, the system damping is actually decreased due to the control.

Additional tests were run on the close-coupled configuration with low NPSP such that the system resonant frequency was lowered from 20 Hz to about 12 Hz. Figures 20 and 21 show the system performance with and without the control; only in the 20- to 30-Hz band could any improvement in performance be seen. The reason for this lies in the large inherent damping of the suction system when it is operated close to cavitation. The uncontrolled system shows damping in the order of 70 percent of critical for the 12-Hz resonance. This high damping implies a pump admittance of approximately $\frac{9880\ \text{Kg/sec}}{\text{newton/m}^2}\left(1.5\ \frac{\text{lbs/sec}}{\text{psi}}\right)$. At 12 Hz, the controller effective admittance is only about half of the pump admittance, and this vector sum represents a minor change in total system damping.

Although the signal to noise was generally poor in the pump discharge pressure data, the transfer function amplitude ratio was computed for three high NPSP tests. These transfer functions are shown on Fig. 22 . One test was with no control and the data showed good coherence throughout most of the frequency band. Two tests were included using the control. Both of these tests show reduced response in the 13- to 50-Hz frequency range. With the reduced pressure oscillation amplitude there was also a decrease in signal/noise ratio and in coherence. Comparison of the tests do, however, indicate a reduction in transmission to the discharge system of 8 to 12 db at frequencies above 15 Hz.

REMOTE-COUPLED CONFIGURATION

In this configuration, Fig. 37 , the low speed inducer was located about six feet upstream of the main pump. The disturbance pulser was upstream of the inducer while the controller was located between the inducer discharge and main pump inlet.

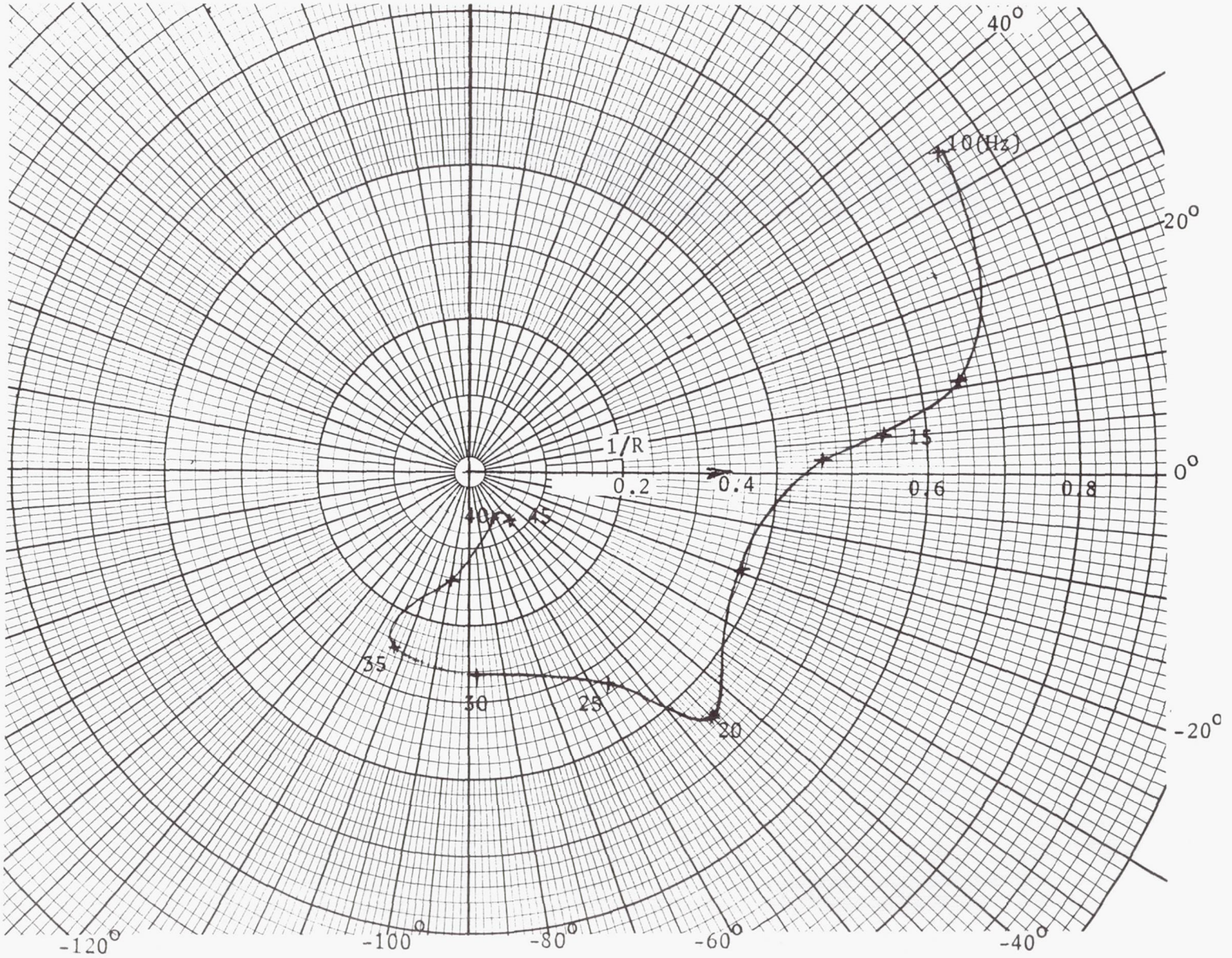

Figure 19. Control Response (Controller Flowrate/Controller Duct Pressure) From Test Data System Frequency Response lbs/sec/psi

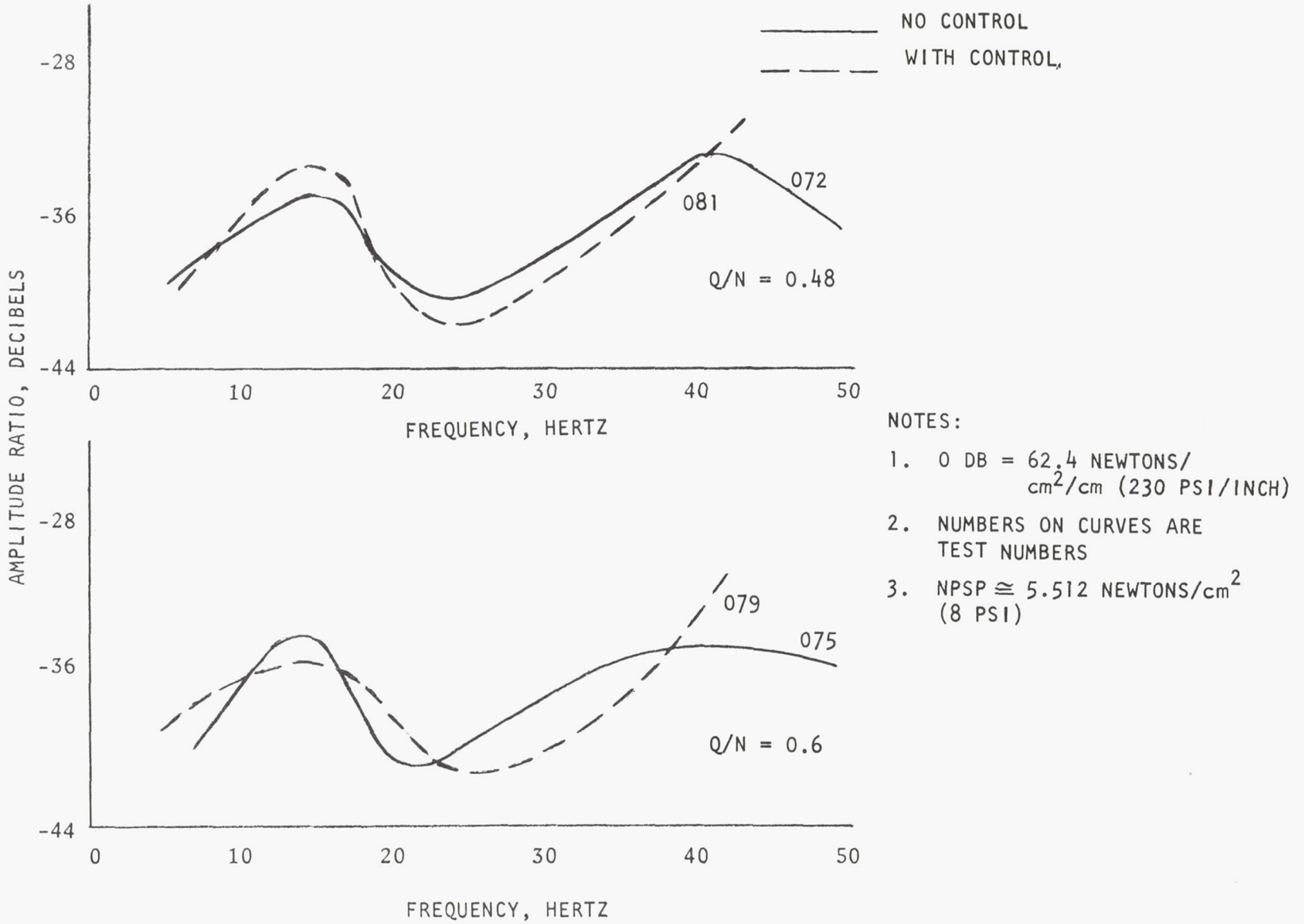

Figure 20. Gain of Controller Duct Pressure/Disturbance Pulser Position Close-Coupled Tests Low Inducer NPSP

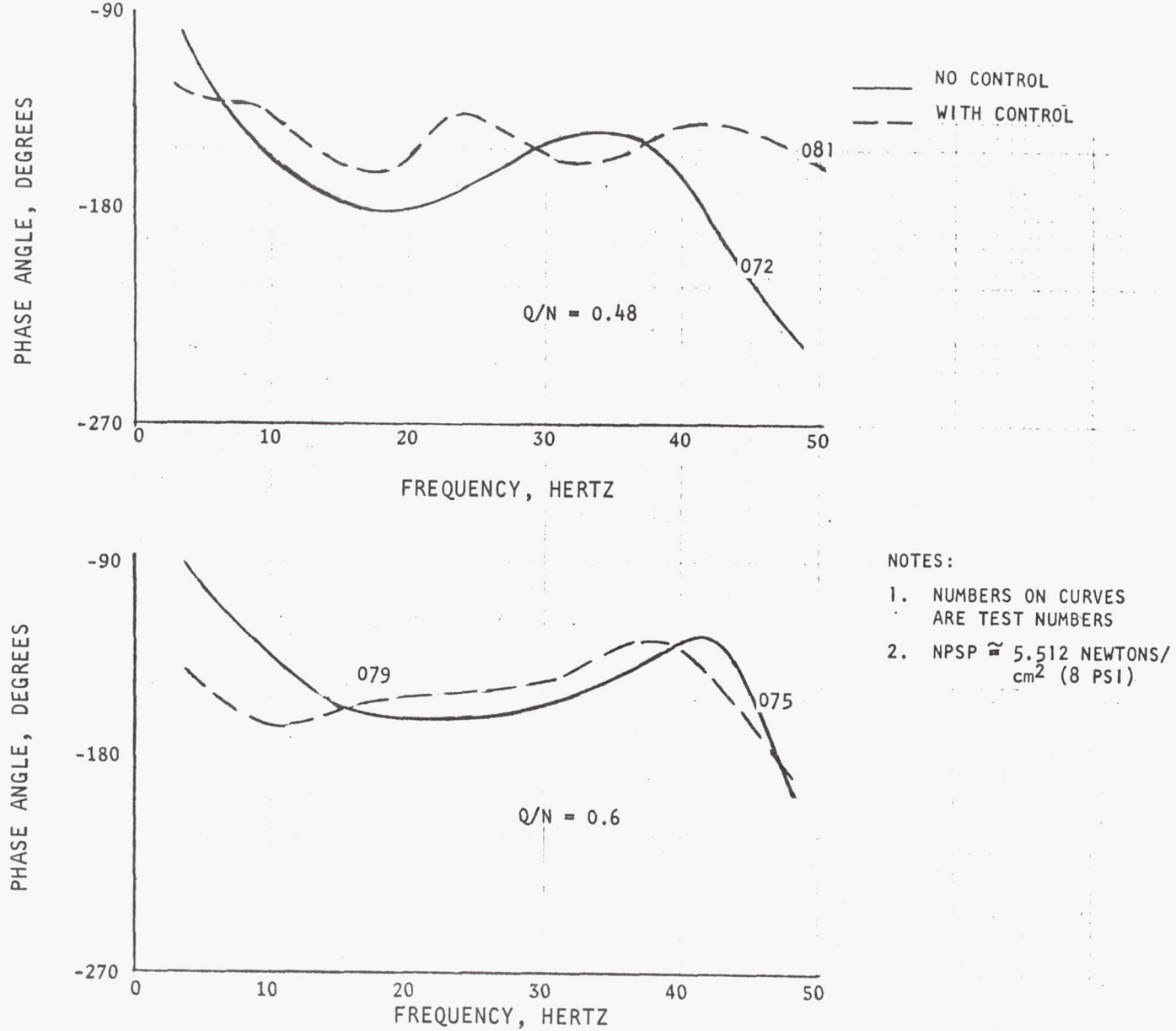

Figure 21. Phase of Controller Duct Pressure/Disturbance Pulser Position, Close-Coupled Tests, Low Inducer NPSP

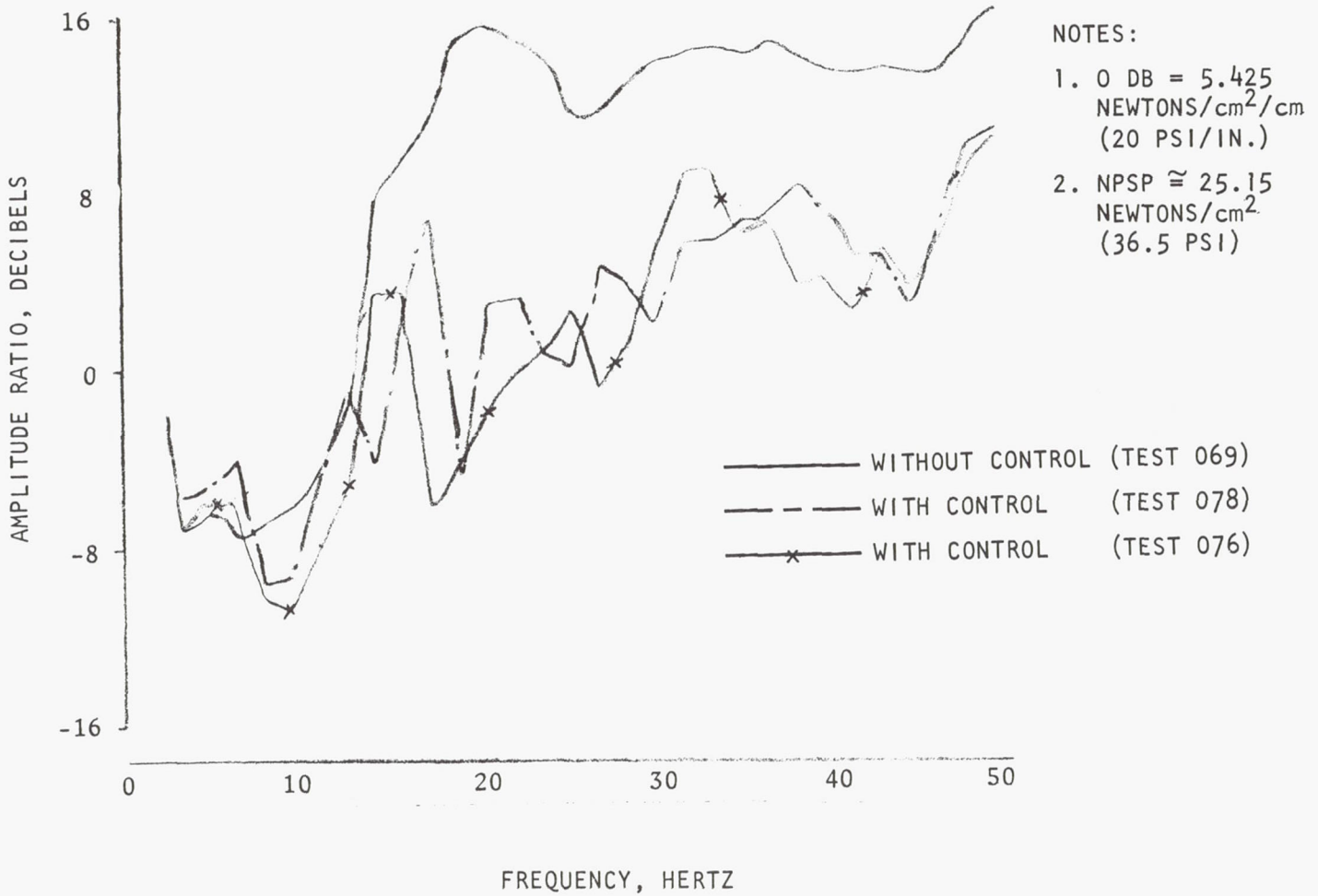

Figure 22. Gain of Pump Discharge Pressure/Disturbance Pulser Position Close-Coupled High NPSP Tests

Phase and gain data are shown in Fig. 23 and 24 for high NPSP tests with and without the controller operational. The gain plots show that, as for the close-coupled configuration, approximately 8-db control attenuation is obtained in the 18- to 25-Hz range. The dip obtained in the data at 25 Hz is in a region of low coherence and was also observed on close-coupled data. This does correspond to the region where an anti-resonance is predicted when a structural vibration mode is included (see Appendix D).

Figure 25 shows the gain data for the low NPSP remote-coupled configuration. These results shown an approximate 8-db controller attenuation from 10 to 25 Hz. This is because the pressure level at the inducer discharge is high enough to prevent fluid cavitation. As a result, the damping looks the same over a range of inducer inlet pressures from at least 12 to 40 psig. Based on these results, it is concluded that effective control is available over a wider range of inducer inlet pressure when the controller can be located in a section between an inducer and a high head pump.

CONTROLLER PERFORMANCE

The theory of controller operation requires that over the effective bandwidth of operation, the control piston velocity must be proportional to a command voltage. Position and rate signals are integrated and used in a feedback loop to provide for low frequency nulling below 2 Hz. Since the operating band for the control was set at 50 Hz, first order roll-off was provided in the control to limit its bandwidth.

Block diagrams of the intended system and the actual performance are shown in Fig. 26. Parameters were measured in the control during pump tests to obtain transfer function data. Data from several tests were reduced and are presented in Fig. 27, 28, and 29 and are the source of the actual performance in Fig 26.

Figure 27 represents the compensation used on the pressure signal to provide command voltage. The in-phase component (0 degrees) produces effective compliance in the system. It can be seen that the lead compensation performed as designed.

The indicated position response to the servo coil current is shown in Fig. 28. It can be seen that while the amplitude ratio follows the theoretical quite well, considerable phase shift is apparent, indicative of either a lag or a time delay. The additional phase lag is associated with either the forward loop in the servo valve drive system, or in the variable reluctance position sensing system. A phase shift in the sensing system is of little consequence since the feedback signal is very weak above 2 Hz. Phase shift in the servo drive system is in the forward loop and can adversely affect system performance. The solution would be to use a higher response servovalve and/or two in series to prohibit early phase roll-off.

The current/command voltage response is shown in Fig. 29. The amplitude should be essentially flat with nearly 0 percent phase across the bandwidth of the control. From 20 Hz to 50 Hz about 12-db attenuation takes place with

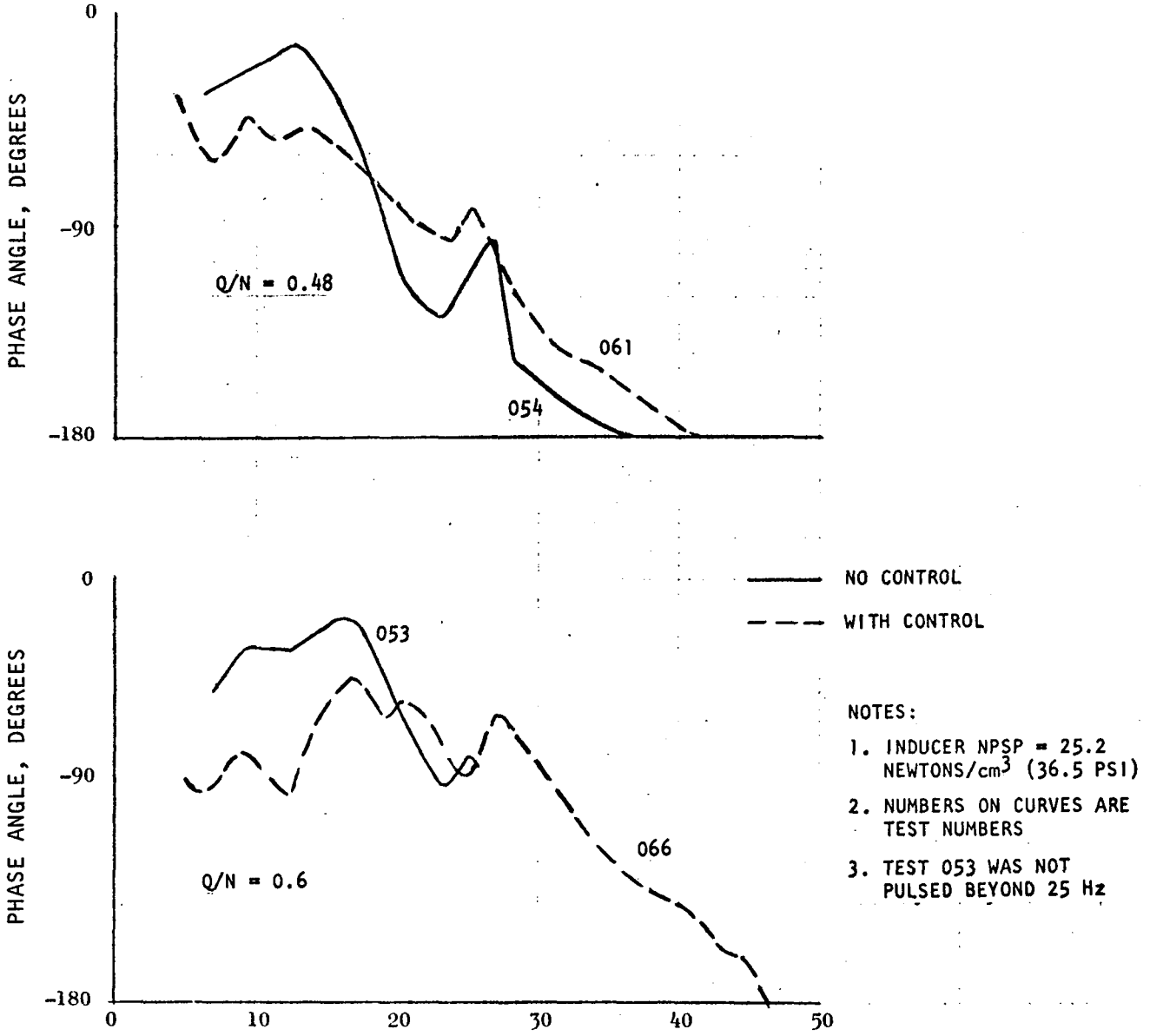

Figure 23. Phase of Control Inlet Pressure/Disturbance Pulser Position, Remote-Coupled High NPSP

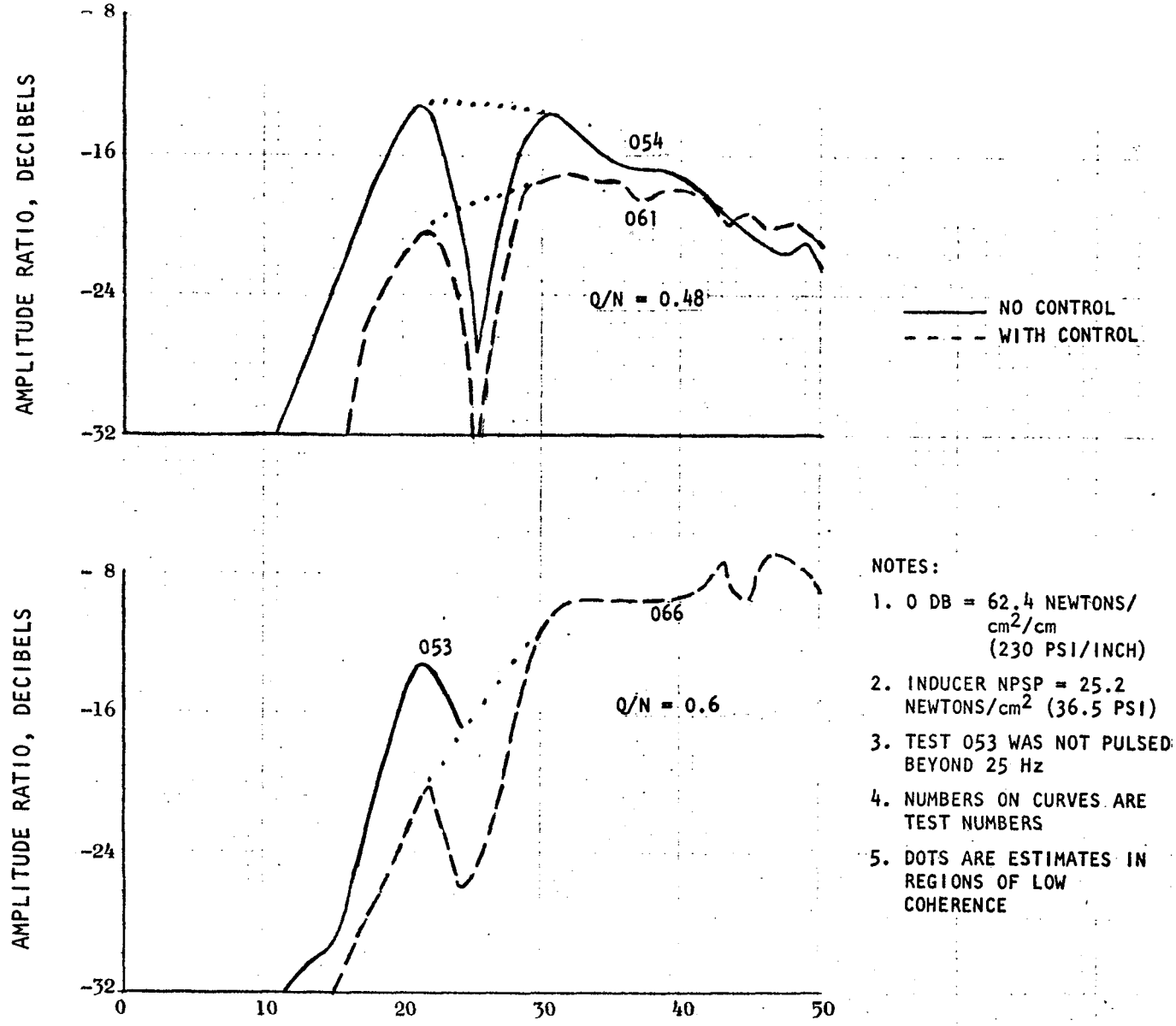

Figure 24. Gain of Control Inlet Pressure/Disturbance Pulser Position, Remote-Coupled High NPSP Tests

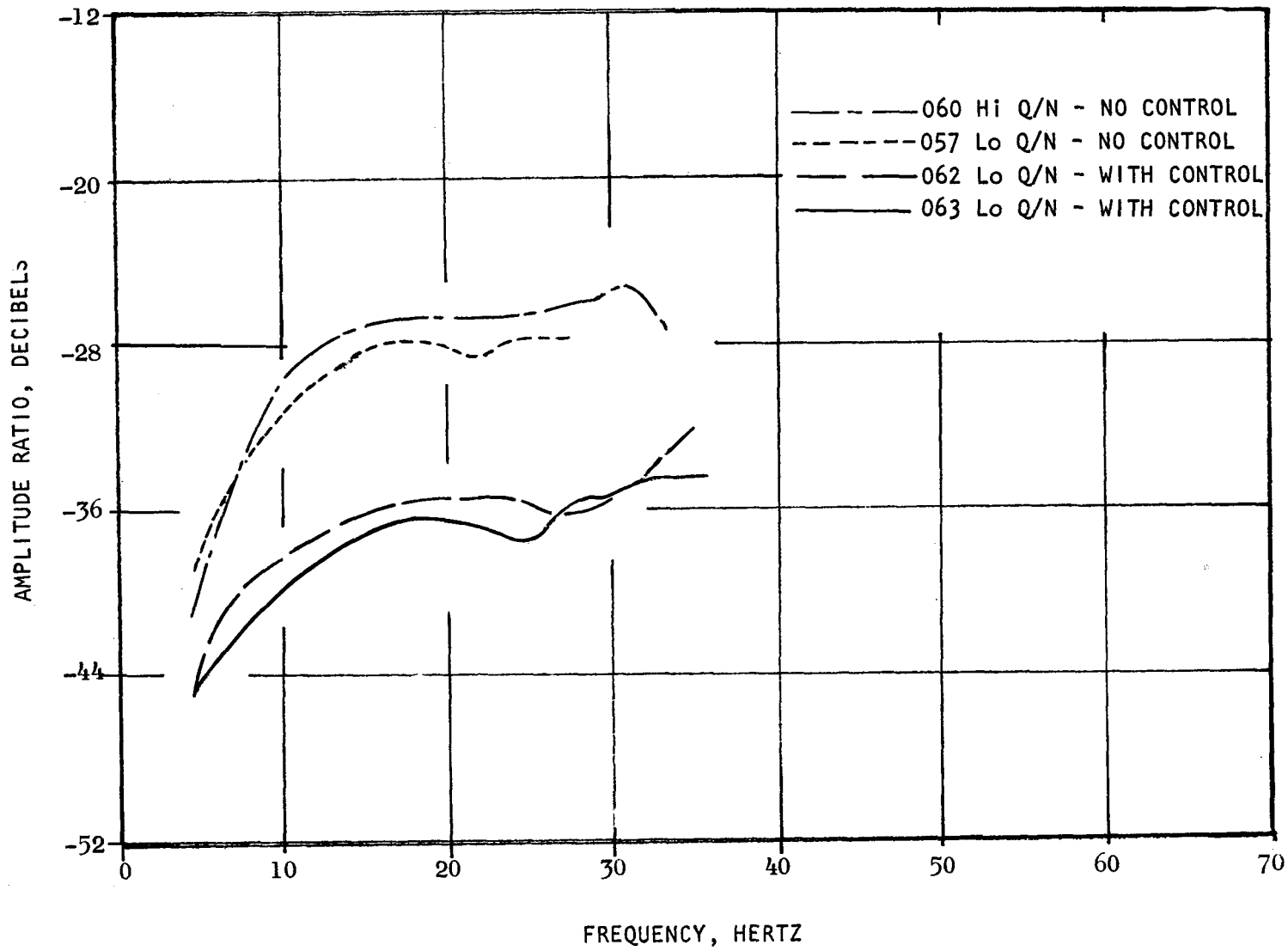

Figure 25. Gain of Control Inlet Pressure/Disturbance Pulser Position, Low NPSP, Remote-Coupled

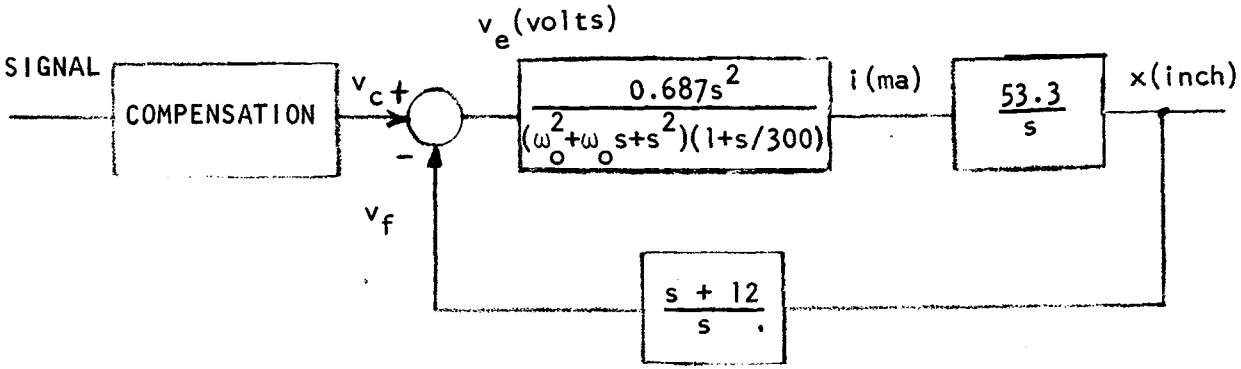

ANALYZED

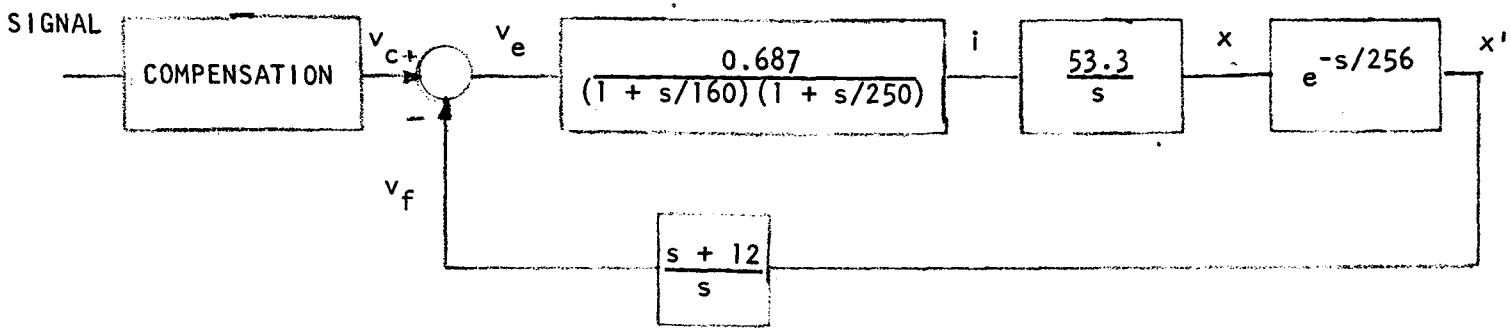

TEST DATA

Figure 26. Block Diagrams of Control System As Analyzed and Performance Derived From Test Data

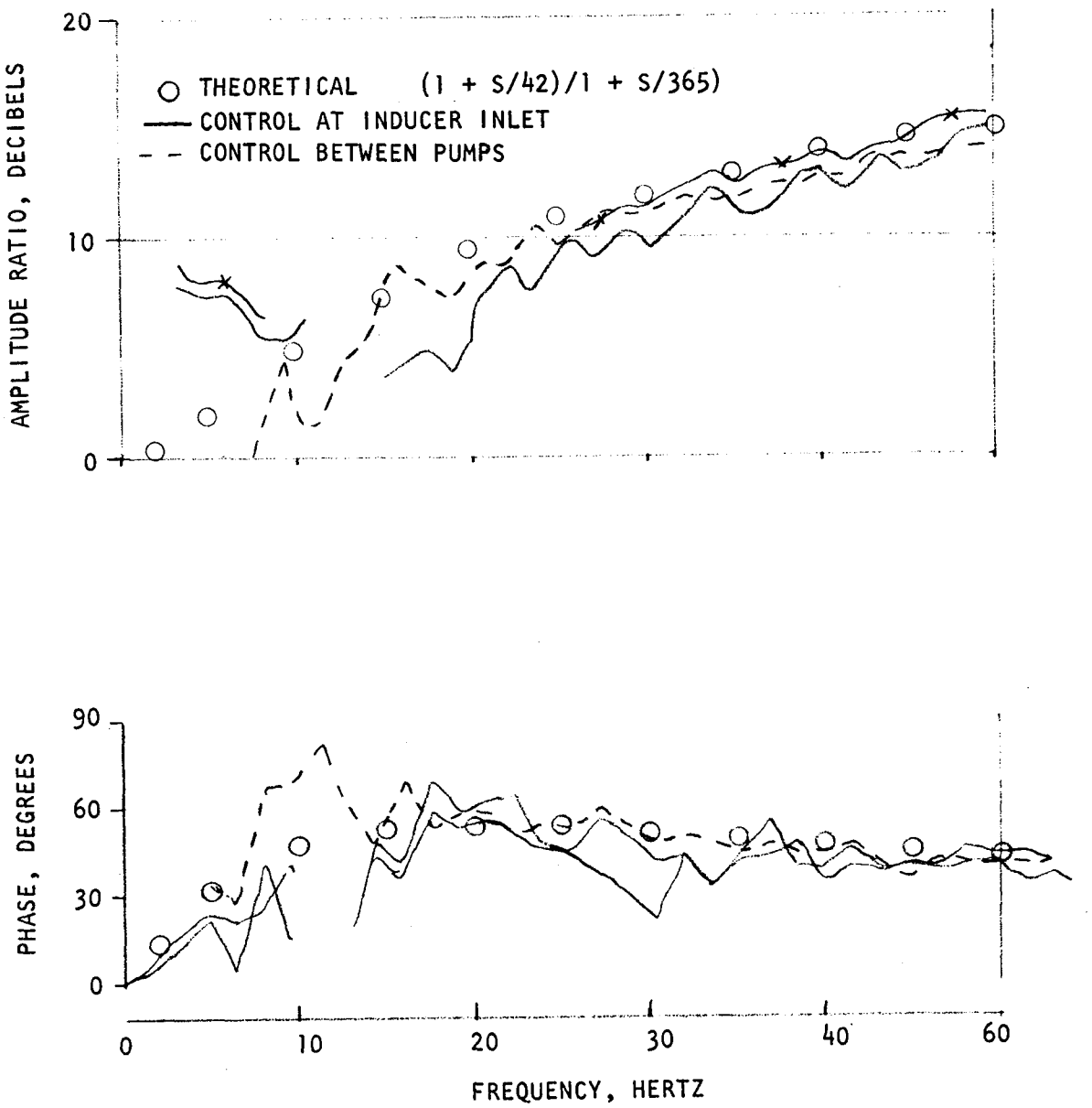

Figure 27. Gain and Phase of Controller Command Voltage/Sensed Pressure (Compensation Network)

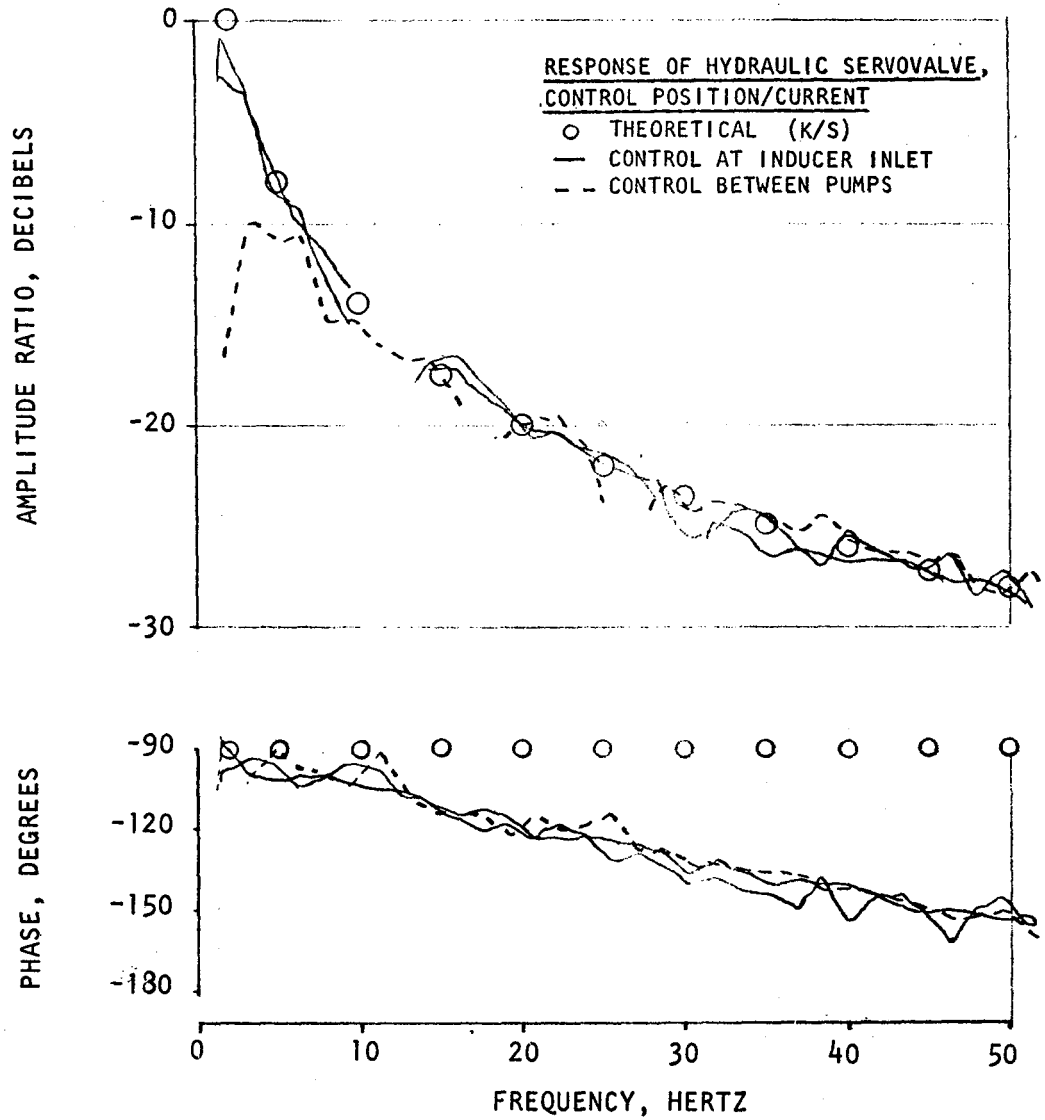

Figure 28. Gain and Phase of Control Piston Position/ Servovalve Current

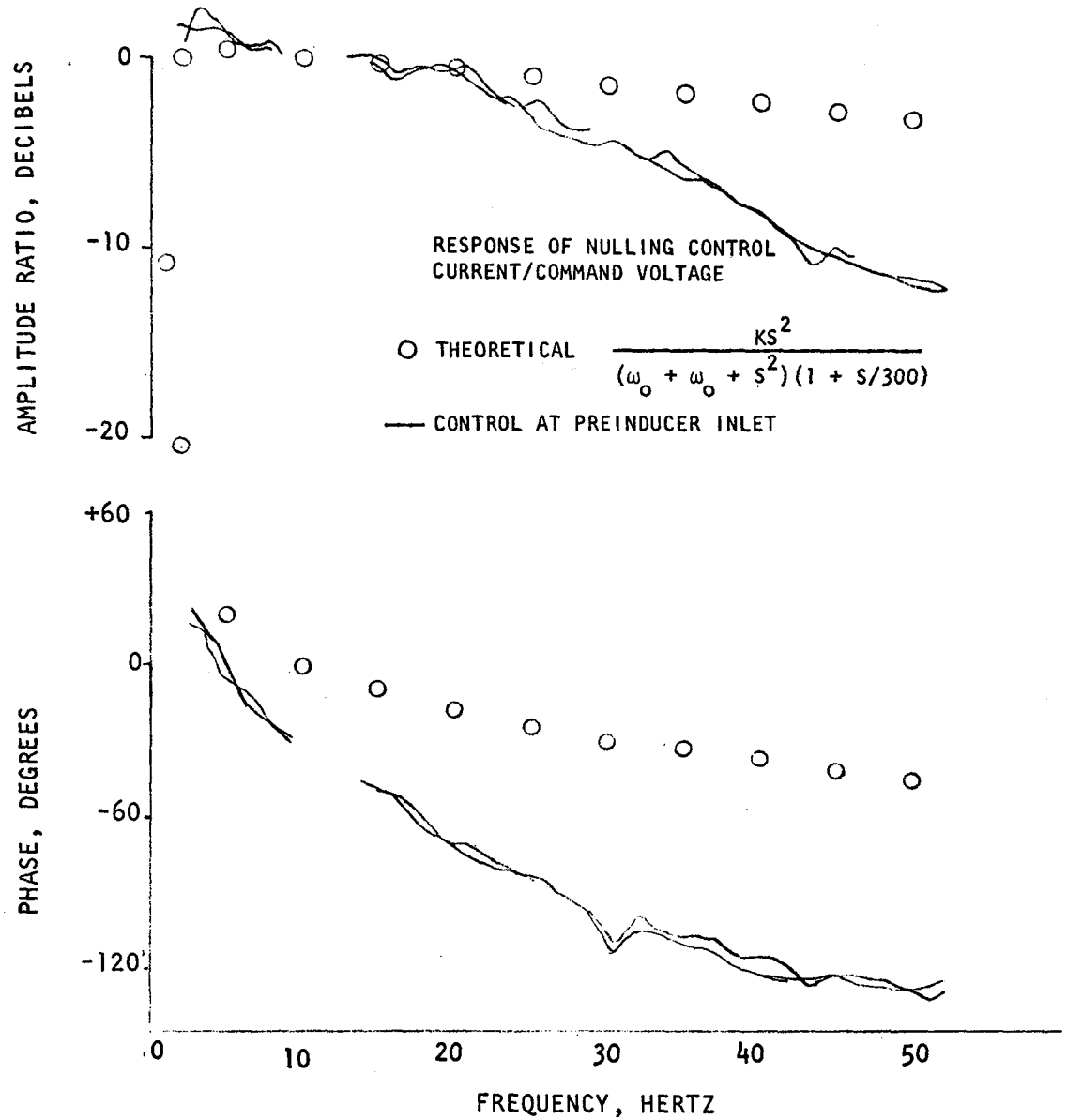

Figure 29. Gain and Phase of Servovalve Current/Controller Command Voltage

phase lag of about -130 degrees at 50 Hz. This is indicative of second order dynamics in this portion of the system.

Detailed investigation indicated that one first order lag at 40 Hz was due to an R-C network that had been included in the controller electronics as shown in Fig. 30. The capacitor should have been removed before testing.

The second dynamic term was the result of the wiring of the current drive system for the servovalve. Figure 31 shows the circuit actually used where the amplifier feedback voltage for the servo current drive was taken upstream of the servovalve coil. At frequencies in excess of 160 rad/sec, the coil inductance causes a reduction in current. The voltage monitored during testing (v_{ref}) Fig. 31, indicated a reduction in current through the 10Ω resistor at high frequencies. To avoid this problem the amplifier feedback voltage should be taken at v_{ref}, as shown in Fig. 32. This circuit change was made after the completion of pump testing, and at frequencies as high as 50 Hz, the system did produce flat phase response. Analytical transfer functions of the system tested and the revised circuit are shown in Fig. 33 and 34. Figure 34 also shows the control phase shift (piston velocity/command voltage) under the assumptions that the phase error indicated in Fig. 28 occurs in the servovalve and second that it occurs in the position transducer.

One item that was not pursued, but may be useful in application, is the saturation effects of the transistor drive amplifier. The transistor drive amplifier peak-to-peak output becomes proportional to frequency above 160 rad/sec in order to overcome the coil inductance. At high frequencies, if the command voltage is significant, the saturation characteristics of the amplifier (about ± 12 volts) will limit controller velocity. This saturation would itself limit the amplitude of the system oscillations augmented by adverse phase shift.

In order to reduce the amplitude response of the system at frequencies that result in 90-degrees phase lag, some type of filter is required. Unfortunately, attenuation is associated with severe phase errors in most filters. Figure 33 presents one type of allowable filter that has less than 45-degrees phase lag while producing 10 db/decade of attenuation. It is essentially a number of lag networks in series that could be readily included as the feedback network of an amplifier. By using this type of filter the critical phase point (-90 degrees) could be shifted to a frequency range high enough so that any oscillations which might be augmented by the presence of the control, would have negligible transmission through the engine.

INDUCER PERFORMANCE

During the analytical phase of the program, the dynamic performance of the inducer was represented by a compliance at the inducer inlet and a fluid inertance representing the inducer fluid passages. With this representation and a fluid inertia value, determined by assuming a centrifugal flow path pump, of 0.04 psi/lb/sec^2 the results for pressures downstream of the inducer

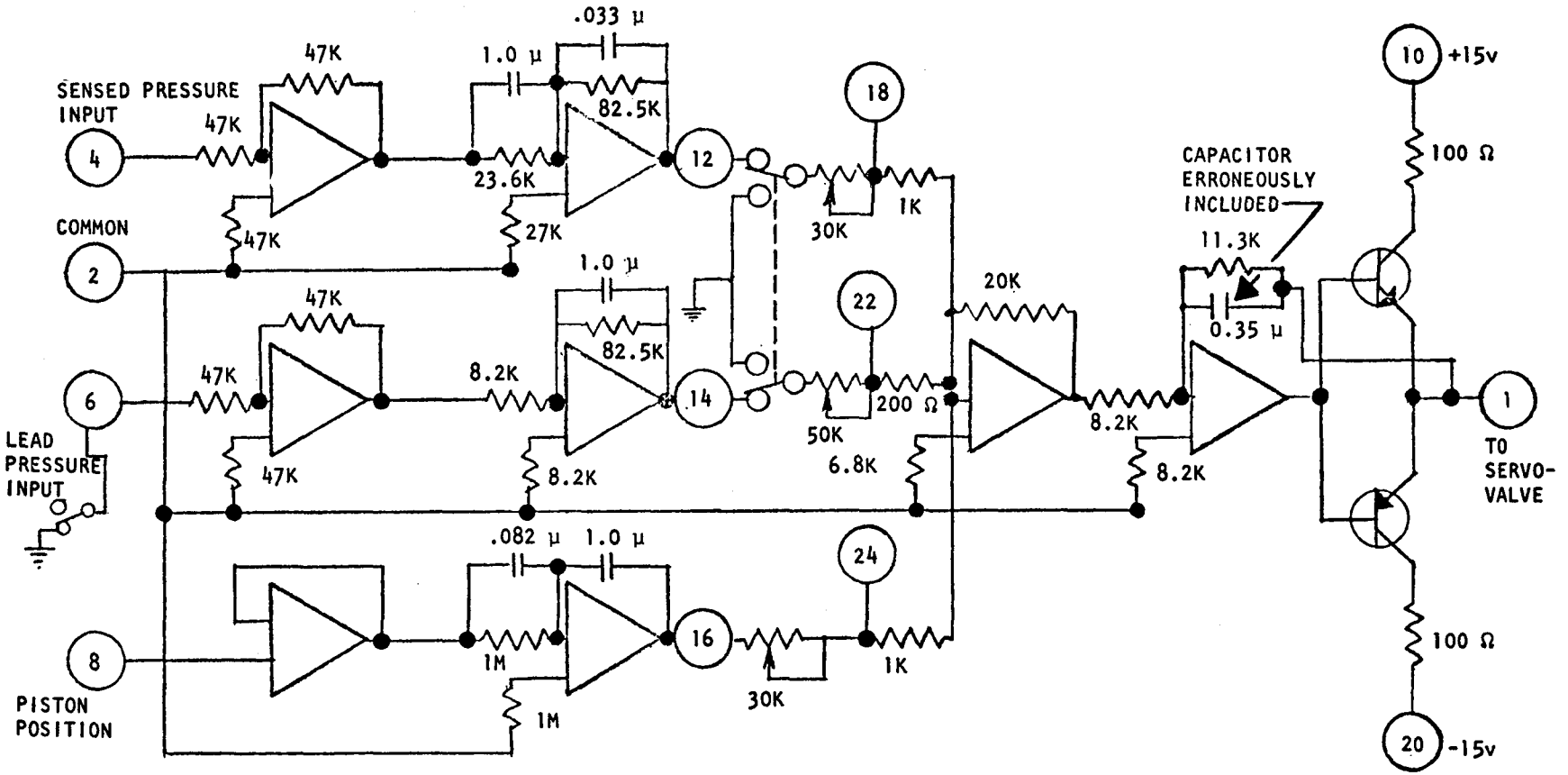

Figure 30. Schematic of Controller Electronics

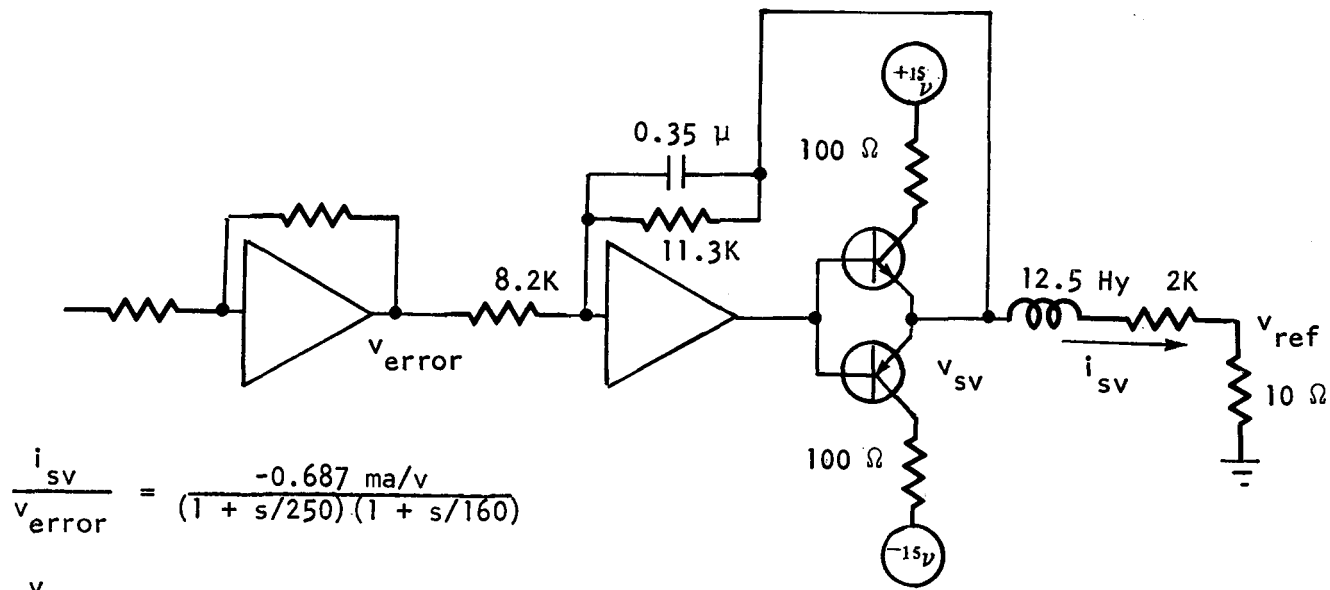

$$\frac{i_{sv}}{v_{error}} = \frac{-0.687 \text{ ma/v}}{(1 + s/250)(1 + s/160)}$$

$$\frac{v_{sv}}{v_{error}} = \frac{-1.38}{(1 + s/250)}$$

Figure 31. Current Drive Used in Tests

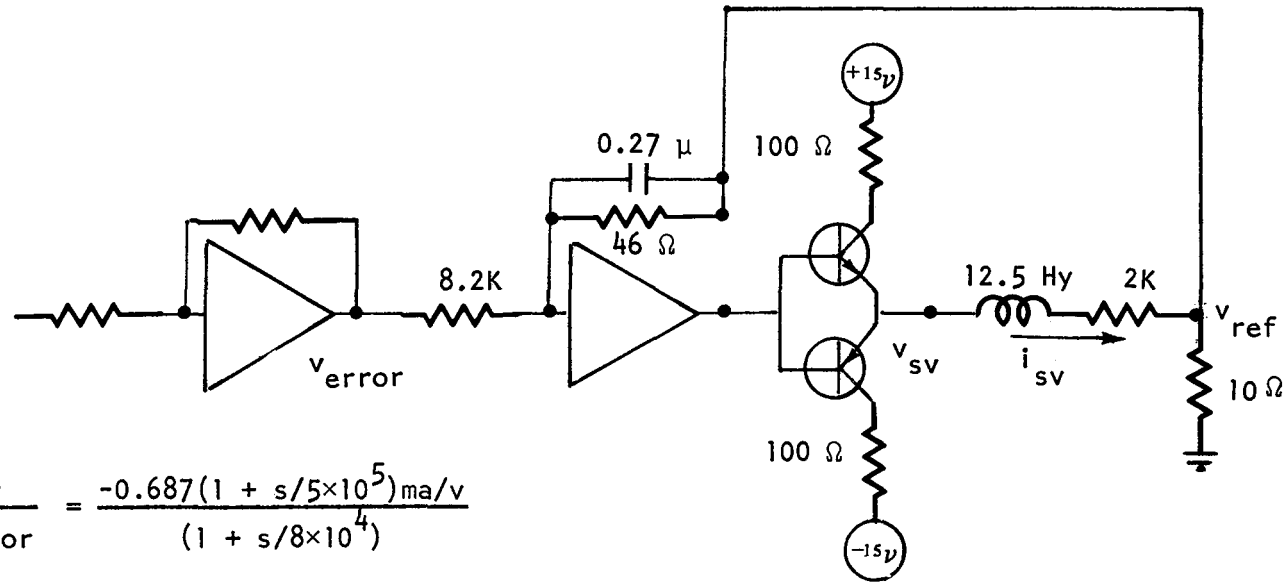

$$\frac{i_{sv}}{v_{error}} = \frac{-0.687(1 + s/5\times10^{5})\,ma/v}{(1 + s/8\times10^{4})}$$

$$\frac{v_{sv}}{v_{error}} = \frac{-1.38(1 + s/250)(1 + s/5\times10^{5})}{1 + s/8\times10^{4})}$$

Figure 32. Improved Electrical Drive System

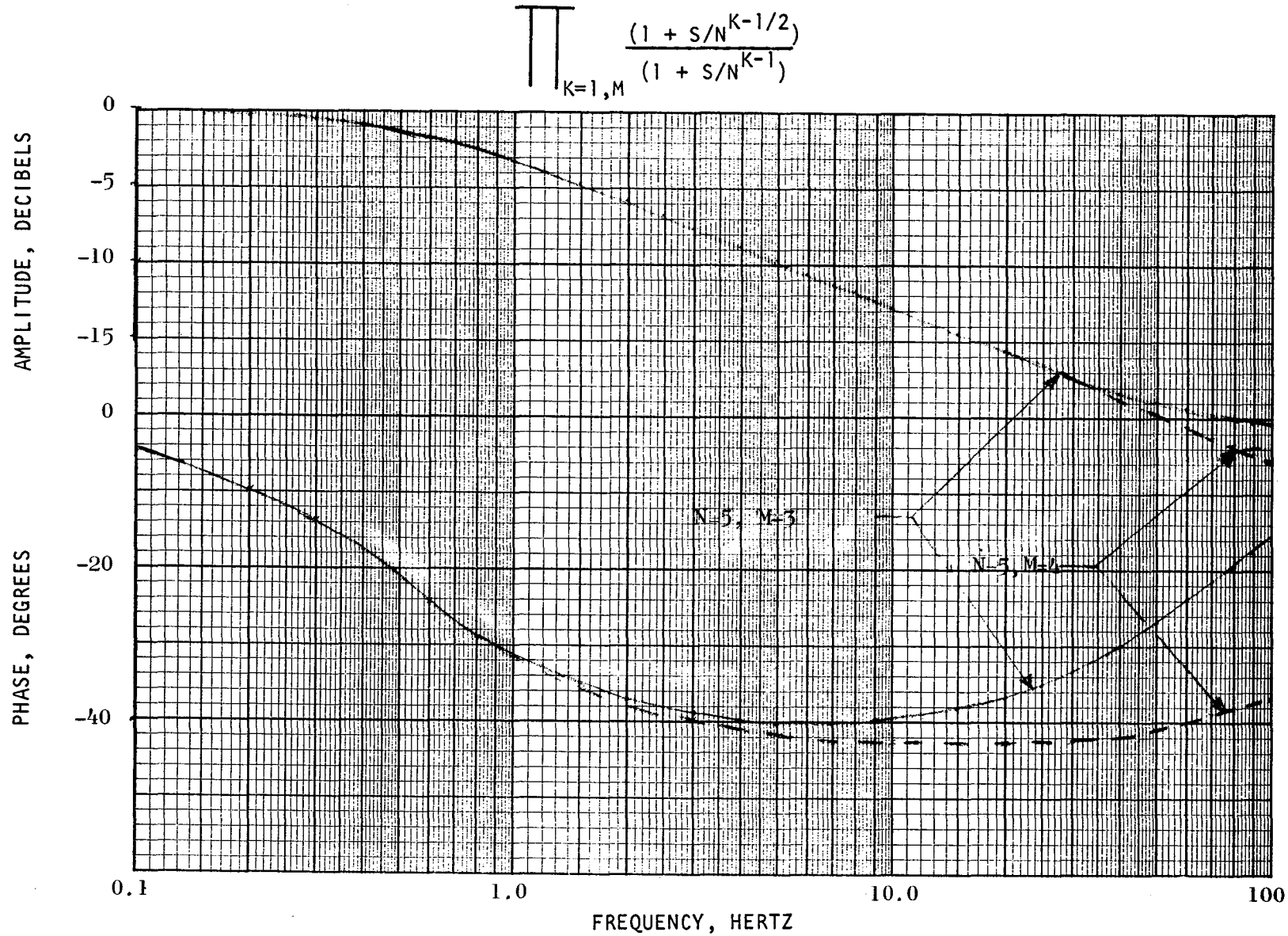

Figure 33. Improved System Dipole Filter

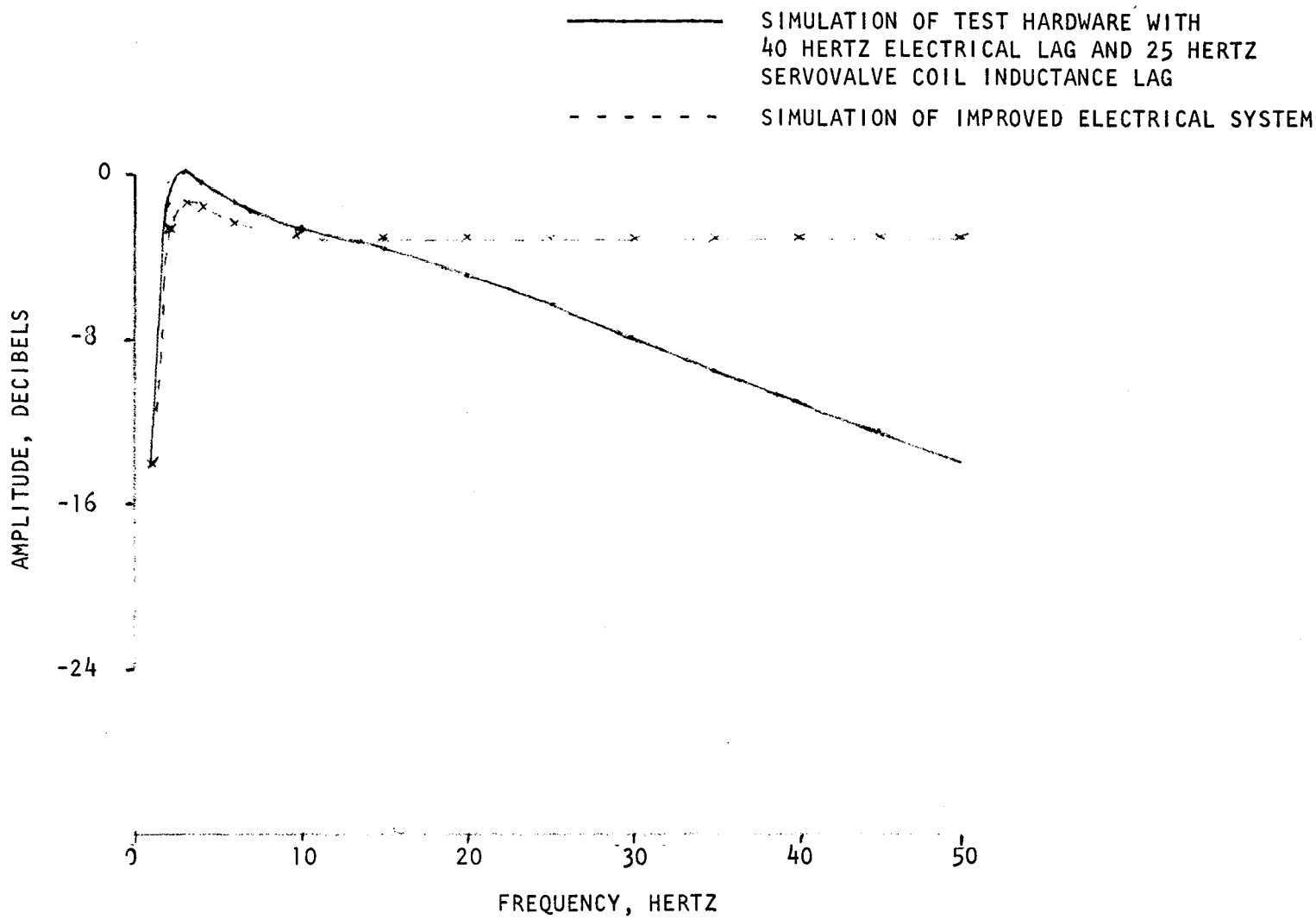

Figure 34. Analytical Amplitude Response of Control Piston Velocity/Controller Command Voltage

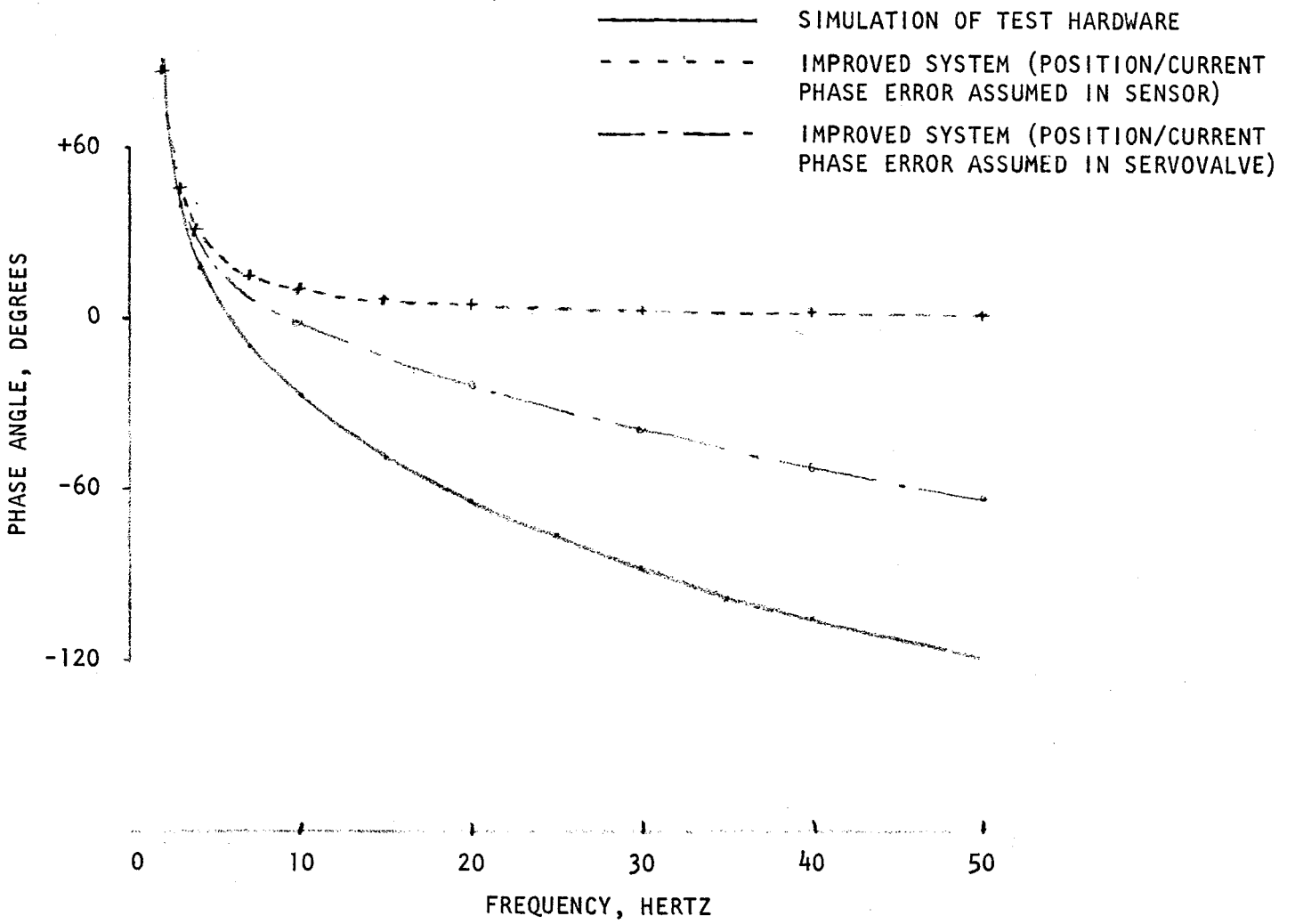

Figure 35. Analytical Phase Response of Control Piston Velocity/Controller Command Voltage

are shown by Fig. 3. The response of pressures upstream of the inducer looked like the close-coupled configuration of Fig. 1. The significant predicted affect of the inducer was, within the 50-Hz range, a 360-degree phase shift in pressures downstream of the inducer; the inducer itself contributing 180 degrees. When the test data was reduced, the major difference between the analytical and test data was that the data did not show a 180-degree phase shift across the inducer. Within the 50-Hz frequency range, only a total of 180 degrees was seen. In efforts to correlate the model and test data phase shift, various compliances and inertances in the system were varied. The predominant variables that produced the desired results were the inducer fluid inertia and main pump inlet capacitance. The inertia value of 0.04 was reduced to 0.001 and the MP inlet capacitance was reduced from 0.0124 to 0.0006 to give the results shown in Fig. 36. To refine the values more would require data beyond 50 Hz. It is concluded that the inertia value based on a centrifugal pump flow path does not hold for an axial pump flow path. The axial pump is best represented by a very small or zero value of fluid inertia. For additional test results see Appendix D.

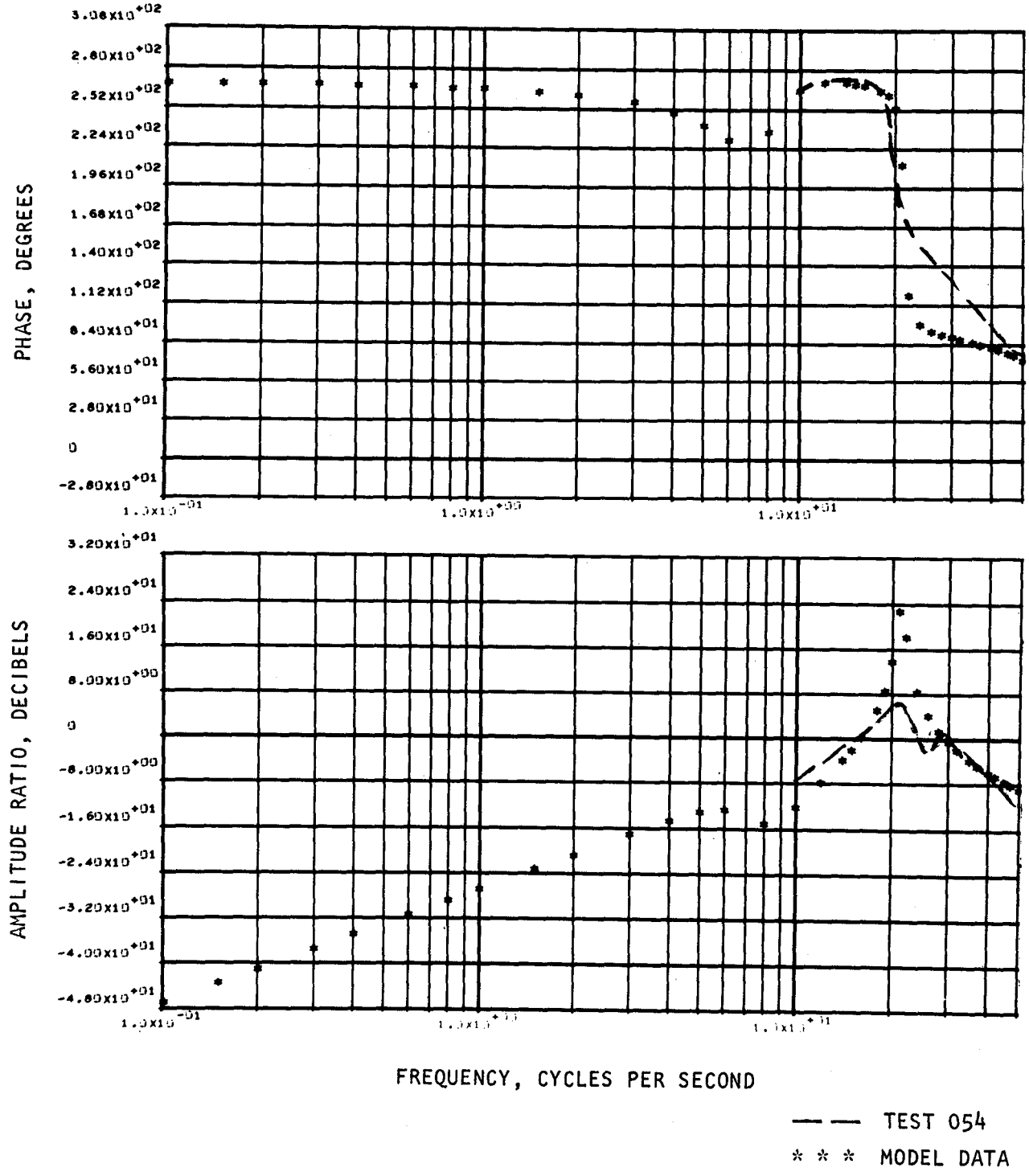

Figure 36. Gain and Phase Comparison of Controller Duct Pressure/ Disturbance Piston Flowrate for Analytical Model and Test Data

Page intentionally left blank

CONCLUSIONS

From the results of the analysis of the experimental and analytical model data, the following conclusions are drawn:

1. Large values of fluid inertia, normally present in a centrifugal pump, were not found to be associated with the axial flow inducer.

2. Liquid oxygen used to power the hydraulic turbine did not produce noticeable fluid compliance when injected into the main flow stream.

3. The presence of the active controller resulted in no observable change in self-induced pump oscillation.

4. The control functioned, as designed, below 25 Hz. In the 35-Hz range, an accumulated phase error resulted in some loss of sytem damping. Circuit changes are recommended to reduce the phase error.

5. The upper bandwidth of the control should be limited by use of a filter causing less than 45-degree phase shift. A usable filter would consist of a series of lag networks spaced at frequencies of 5 Hz apart so that -45 degrees and -3 db/octave will result.

6. At high NPSP values, similar attenuation was obtained when the control was placed upstream or downstream of the inducer. At low NPSP values the pressure sensing control was much more effective when placed downstream of the inducer.

7. The operating Q/N, from nominal to 0.8 nominal, has a minor, if any, affect. The resonant frequencies, for runs without control, do not appear to shift and the remote-coupled control effectiveness appears to increase by about 3 db at the nominal Q/N.

8. The control admittance operates in parallel with the pump admittance. Under cavitating conditions, small inlet pressure variations cause large pump flow variations compared to those caused by the control. The control thus becomes ineffective when the pump is near cavitation.

9. The system analysis resulted in a control that, desirably, adds damping and compliance to the system. The data showed that the damping effect was as expected, while the compliance effect was not significant. The damping effect was shown in the data by the reduced resonant frequency amplitude, while the approximately constant resonant frequency indicated an insignificant change in compliance.

10. Data did not indicate that cavitation occurred in the control manifold or piston. To avoid any possibility of a closed loop instability from such an occurrence, the reference pressure transducer should sense the pressure in the manifold itself.

11. Upstream local vibration associated with the ducting and its support structure was interpreted by the control as additional resonances and anti-resonances of the feed system itself and resulted in no unexpected change in performance.

12. The 4-in. turbine flowmeter used in the discharge system was observed to follow the input pulsing in a manner similar to the pump discharge pressure. The limit to the turbine flowmeter response appears to be associated with resolution of the digital (pulse rate) output rather than the response of the rotor itself.

13. The control appeared to have an admittance of about 1.6 lb/sec per psi over its effective frequency range. This is compared with the pump admittance of approximately 0.6 in non-cavitating conditions.

REMARKS

The feasibility of an active device to suppress oscillations produced by forced inputs to the inlet system was shown in this study. Sensing pressure variations in order to control oscillations were shown to produce 8 db of quieting at the pump inlet. Various studies of the POGO problems encountered during the Saturn V launches indicate that this degree of quieting would have been sufficient to eliminate the buildup of oscillations seen during flight.

In addition to the quieting produced by sensing pressure, it is expected that additional reduction in pressure amplitude can be obtained by using pump face acceleration as an additional input. Test data was not obtained for this type of input due to the high costs required for facility modifications.

With either type of input the important requirement of the control is that it have no more than 45-degrees phase lag for good control and that at frequencies where the phase lag is in excess of 90 degrees, reduced damping can result due to the control.

Circuit modifications to achieve a flat phase response in the electronic sections were discussed in the body of the report. It was, however, impractical to reconnect the hydraulic system and install an improved position sensor and servovalve in order to ensure that a flat phase response is indeed produced with the complete system. In any additional study this should be the first item of interest.

The upper bandwidth limit for the system should be such that the amplitude is reduced with no appreciable phase error. A dipole filter giving 10 db per decade and -45-degrees phase error should be sufficient to reduce the amplitude to a negligible value at frequencies where the remainders of the forward control loop dynamics furnish -45-degrees phase lag. The design of the filter is dependent on the response of the forward loop and specific values should be determined when the actual electronics servovalve response is known.

Bench testing with the improved circuits should provide assurance that the control will work as expected, but a final verification could be made in a facility. Since the response of the feed system in the high frequency range (~35 Hz) was similar when the pump was powered and when it was stationary, it would not be necessary to power the pump to verify the control response.

It is recommended that effort be continued on an active suppressor primarily in the analytical and specific design areas. Good models of vehicles that have experienced POGO are available. Use of the enclosed control description in such models would provide as much experience as is possible to achieve without an actual flight. The relative merit of pressure and/or acceleration sensing can also be determined for these specific cases. In cases where one propellant system is driving while the other is actually

stabilizing a vehicle POGO loop, it is likely that acceleration sensing might provide better control than pressure sensing. Only model studies can provide the answers to such questions.

Although it appears that a broad band control of the type developed during this study has a great amount of flexibility and should have general application, there are limitations. For example, when a propellant line has negligible fluid inertia so that the pump inlet pressure and tank bottom pressure are essentially equal, neither a passive or active device may cure the problem since flow cavitations into or out of the duct will not affect suction pressure. Again, vehicle studies are required to determine the limitations quantitatively.

APPENDIX A

ANALYTICAL MODELS

To conduct the system analysis, mathematical models of the CTL I Cell 2A test system, shown schematically in Fig. 37, were constructed. The test system consists of a 3000-gallon liquid oxygen run tank, facility ducting from the tank to the test section inlet, test section, main pump, and facility discharge ducting terminating in a 5000-gallon catch tank. The test section, a block diagram of which is shown in Fig. 38, consists of the flow distrubance pulser, a reducer-expander section, a second pulser used for pressure oscillation suppression, a bellows, and the low-speed inducer for the condition where the inducer is close-coupled to the main pump. For the condition where the inducer is remote-coupled, the reducer-expander sections and low-speed inducer positions are interchanged.

To determine the frequency response characteristics of this system, a set of linerarized equations describing the dynamic performance of the system were written. These equations, presented in Table I (nomenclature given in Table II) and corresponding to the block diagram of Fig. 39, were solved using a digital computer frequency response program. The supply and catch tanks are each at constant pressure. The facility lines are represented by delay equations between the run tank and the test section, and between the main pump discharge and the catch tank. The test section and main pump are represented by lumped parameter segments. The equations given in Table I are in the form used by the frequency response program where the flowrates are eliminated by substituting the appropriate equation in terms of ΔP and the system constants (line inertance, compliance, and resistance). Table III gives the nominal values of these constants.

Output from the program consists of plots of phase angle (in degrees) and amplitude (in decibels) as a function of frequency for various system pressures with respect to pulser flowrate. Figures 1 and 2 show the predicted response of main pump inlet pressure to pulser flowrate for a close-coupled inducer at high and low inducer inlet NPSH. For the inducer operating at high inlet NPSH, the model predicts a fluid resonance at about 8 Hz, followed by an anti-resonance at about 11 Hz, and a double resonance in the range of 18 to 20 Hz as shown in Fig. 1 . The main pump inlet pressure response for a close-coupled inducer operation at low inducer NPSH, was obtained by increasing the inducer inlet compliance (C11), thereby softening the feed system and reducing the fluid resonant frequencies. These results are presented in Fig. 2, where the 8-Hz resonance is reduced to about 3.5 Hz, both of the higher resonances appear to move down (one of them canceling the 11-Hz antiresonance), leaving a single significant resonance at about 12 Hz. The inducer compliance versus NPSP was determined during a study reported in Ref 2. The curve is reproduced here for reference, Fig. 40.

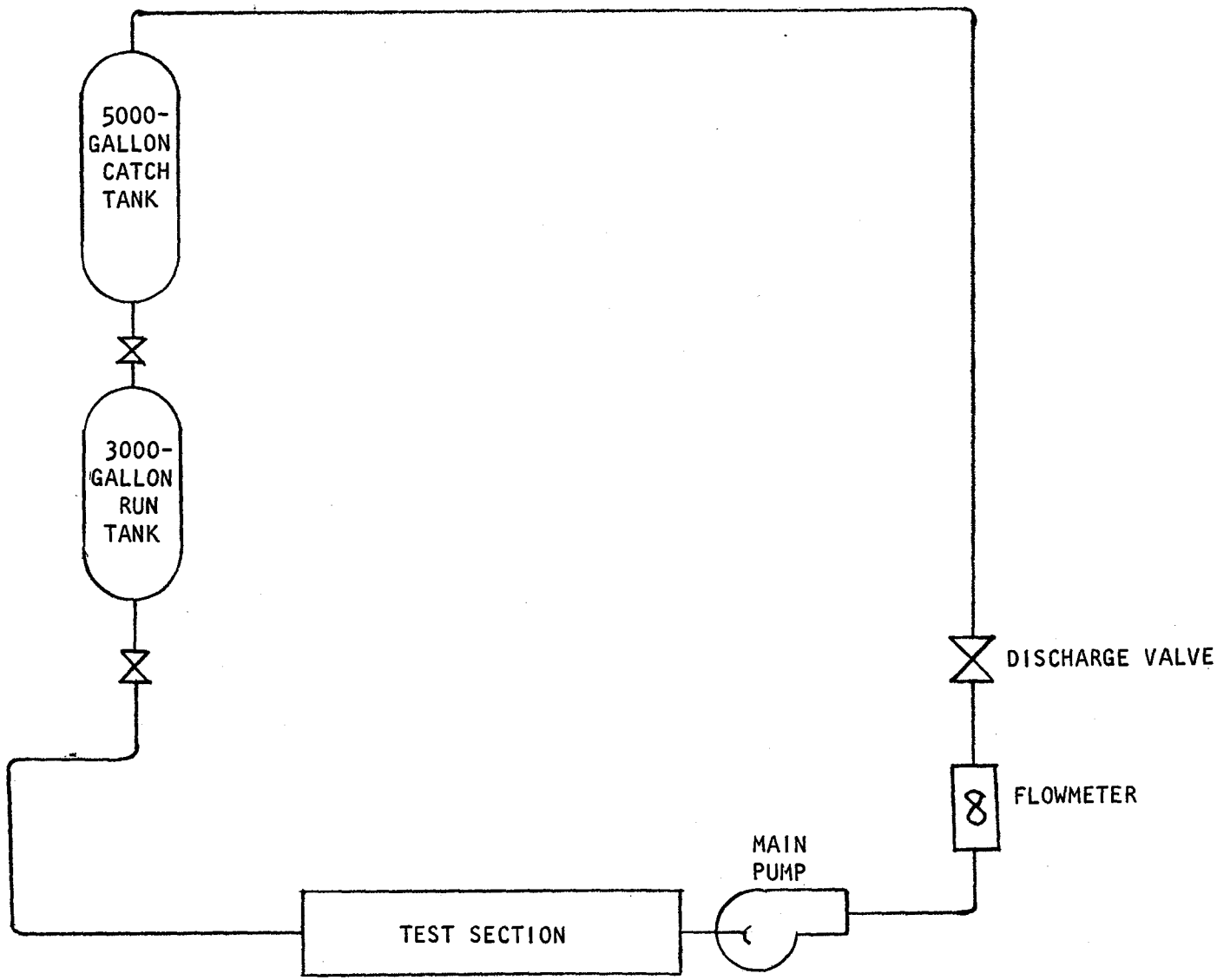

Figure 37. CTL I Cell 2A Schematic

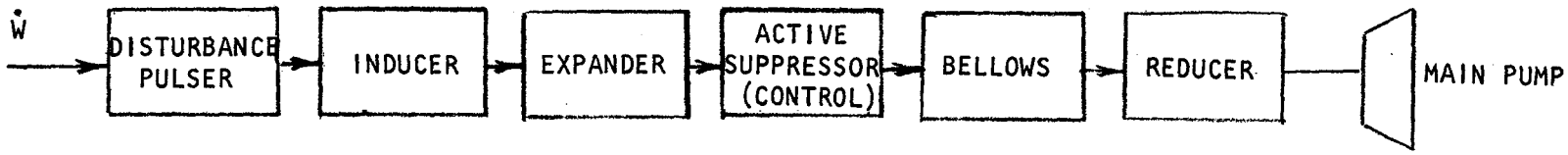

INDUCER REMOTE-COUPLED TO MAIN PUMP

INDUCER CLOSE-COUPLED TO MAIN PUMP

Figure 38. Test Section Block Diagram

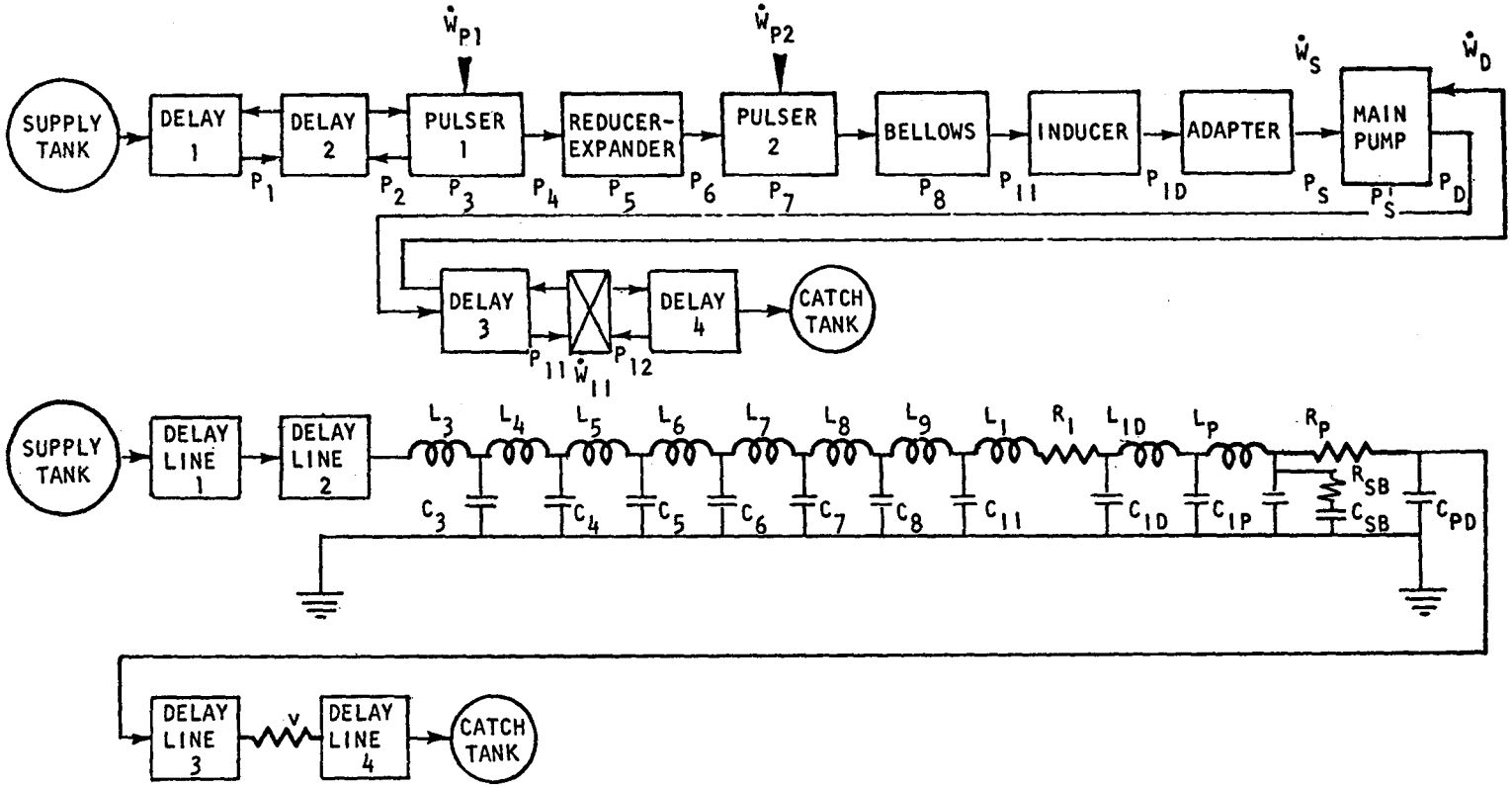

Figure 39. Block Diagram and Electrical Analogy of CTL-1 Facility Dynamic Model

TABLE I. FREQUENCY RESPONSE MODEL EQUATIONS

1. $$P_1\left(1 + e^{-2\tau_1 S}\right) + \frac{a}{A_1 g}\left(1 - e^{-2\tau_1 S}\right)\dot{W}_1 = 0.0$$

2. $$P_1 - \frac{a}{A_1 g}\dot{W}_1 - \left[P_2 - \frac{a}{A_2 g}\dot{W}_2\right] e^{-\tau_2 S} = 0.0$$

3. $$P_2 + \frac{a}{A_2 g}\dot{W}_2 - \left[P_1 + \frac{a}{A_2 g}\dot{W}_1\right] e^{-\tau_2 S} = 0.0$$

4. $$P_2 - P_3 - L_3 S \dot{W}_2 = 0.0$$

5. $$L_4 P_2 + L_3 P_4 + L_3 L_4 S \dot{W}_{P1} - \left[L_3 + L_4 + L_3 L_4 C_3 S^2\right] P_3 = 0.0$$

6. $$L_5 P_3 + L_4 P_5 - \left[L_4 + L_5 + L_4 L_5 C_4 S^2\right] P_4 = 0.0$$

7. $$L_6 P_4 + L_5 P_6 - \left[L_5 + L_6 + L_5 L_6 C_5 S^2\right] P_5 = 0.0$$

8. $$L_7 P_5 + L_6 P_7 - \left[L_6 + L_7 + L_6 L_7 C_6 S^2\right] P_6 = 0.0$$

9. $$L_8 P_6 + L_7 P_8 + L_7 L_8 S \dot{W}_{P2} - \left[L_7 + L_8 + L_7 L_8 C_7 S^2\right] P_7 = 0.0$$

10. $$L_9 P_7 + L_8 P_{11} - \left[L_8 + L_9 + L_8 L_9 C_8 S^2\right] P_8 = 0.0$$

11. $$\left(R_I + L_I S\right) P_8 - \left[R_I + \left(L_9 + L_I\right) S + L_9 R_I C_{11} S^2 + L_9 L_I C_{11} S^3\right] P_{11} + L_9 S P_{ID} = 0.0$$

TABLE I. (Concluded)

12. $$L_{12}P_{11} - \left[R_I + L_I + L_{ID}\ S + L_{12}\,R_I\,C_{ID}\,S^2 + L_I L_{12} C_{ID}\,S^3\right]\ P_{ID} + \left(R_I + L_I\,S\right)\,P_S = 0.0$$

13. $$L_P P_{ID} - \left[\left(L_{ID} - L_P\right) + L_{ID} L_P C_{PS}\,S^2\right]\ P_S + L_{ID} P'_S = 0.0$$

14. $$\left(R_P + R_P R_{SB}\,C_{SB}\,S\right)\,P_S - \left[R_P + \left(L_P + R_P\,R_{SB}\,C_{SB}\right)\,S + \left(L_P\,C_{SB}\,R_P + L_P\,R_{SB}\,C_{SB} + C_{PD}\,R_P\,L_P\right)\,S^2 + C_{PD}\,R_P\,L_P\,R_{SB}\,C_{SB}\,S^3\right]\ P'_S + \left(L_P\,S + L_P\,R_{SB}\,C_{SB}\,S^2\right)\ P_D = 0.0$$

15. $$P'_S - P_D - R_P\,\dot{W}_D = 0.0$$

16. $$P_D - \frac{a}{A_3 g}\,\dot{W}_D - \left[P_{11} - \frac{a}{A_3 g}\,\dot{W}_{11}\right]\ e^{-\tau_3 S} = 0.0$$

17. $$P_{11} + \frac{a}{A_3 g}\,\dot{W}_{11} - \left[P_D + \frac{a}{A_3 g}\,\dot{W}_D\right]\ e^{-\tau_3 S} = 0.0$$

18. $$P_{11} - P_{12} - R_V\,\dot{W}_{11} = 0.0$$

19. $$P_{12} - \frac{a}{A_4 g}\,\dot{W}_{11} + \left[P_{12} + \frac{a}{A_4 g}\,\dot{W}_{11}\right]\ e^{-\tau_4 S} = 0.0$$

TABLE II. NOMENCLATURE

Symbol	Description	Units
a	Fluid Acoustic Velocity	m/sec
A	Line Cross-Sectional Area	m^2
C	Compliance	sec^2 m
g	Gravitational Constant	m/sec^2
L	Fluid Inertia	1/m
P	Pressure	newtons/m^2
R	Resistance	1/m sec
S	Laplace Operator	1/sec
τ	Wave Travel Time	sec
$\dot{W}$	Flowrate	kg/sec

TABLE III. NOMINAL PARAMETER VALUES

Parameter	Value	Units
a	810	m/sec
A_1	3.23×10^{-2}	m^2
A_2	5.09×10^{-2}	m^2
A_3	7.5×10^{-3}	m^2
A_4	2.94×10^{-2}	m^2
C_3	1.176×10^{-8}	sec^2 m
C_4	1.45×10^{-8}	sec^2 m
C_5	2.89×10^{-8}	sec^2 m
C_6	1.45×10^{-8}	sec^2 m
C_7	1.176×10^{-8}	sec^2 m
C_8	5.48×10^{-8}	sec^2 m
C_{11}	3.87×10^{-7}	sec^2 m
C_{ID}	6.56×10^{-9}	sec^2 m
C_{PS}	5.24×10^{-7}	sec^2 m
C_{SB}	5.57×10^{-7}	sec^2 m
C_{PD}	6.56×10^{-9}	sec^2 m
g	9.8	m/sec^2
L_3	3.01	1/m
L_4	3.01	1/m

TABLE III. (Concluded)

Parameter	Value	Units
L_5	15.4	1/m
L_6	15.4	1/m
L_7	3.01	1/m
L_8	7.9	1/m
L_9	3.89	1/m
L_I	610.	1/m
L_{ID}	1.922	1/m
L_P	175.	1/m
R_I	6.73×10^3	1/m sec
R_{SB}	7.06×10^3	1/m sec
R_P	2.08×10^4	1/m sec
R_V	6.08×10^4	1/m sec
τ_1	2.3033×10^{-3}	sec
τ_2	3.9173×10^{-3}	sec
τ_3	4.459×10^{-3}	sec
τ_4	14.72×10^{-3}	sec

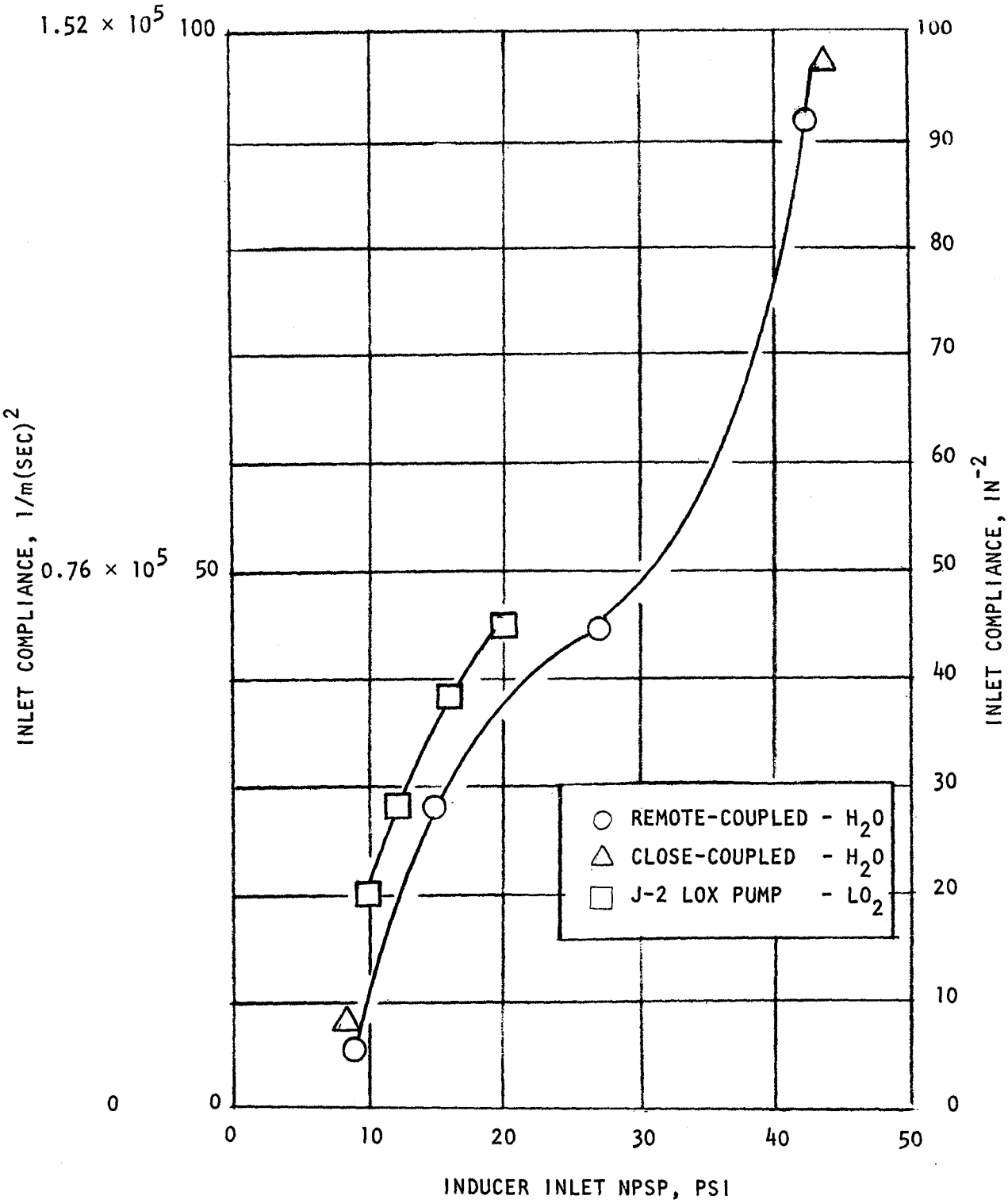

Figure 40. Inducer Inlet Compliance Versus Inducer Inlet NPSP

In addition to considering operation at low NPSH, the effects of varying the bellows compliance was investigated. The bellows compliance was varied over a range of 1/5 to 5 times the calculated nominal value; the results indicated no affect.

Frequency response characteristics were also determined for the configuration where the reducer was remote-coupled to the main pump. The high NPSH condition produces a 6- to 7-Hz resonance, an antiresonance about 12 Hz and a double resonance in the range of 17 to 22 Hz. The low NPSH condition showed a lowering of the 17- to 22-Hz resonances into the 12-Hz range.

To assist in evaluating the control system and to establish the disturbance pulser command requirements, an analog computer model of the test system was mechanized. The analog model is a nonlinear mathematical representation of the system compared to the linearized representation used for the digital model; the system block diagrams presented in Fig. 37 and 38 are applicable to this model. To ensure that the analog computer was programmed properly, the model was compared to the digital program results on a frequency response basis. This comparison is shown in Fig. 41 .

The results from these models established the controller design requirements, test disturbance pulser requirements and estimated performance data for use in correlation to test data.

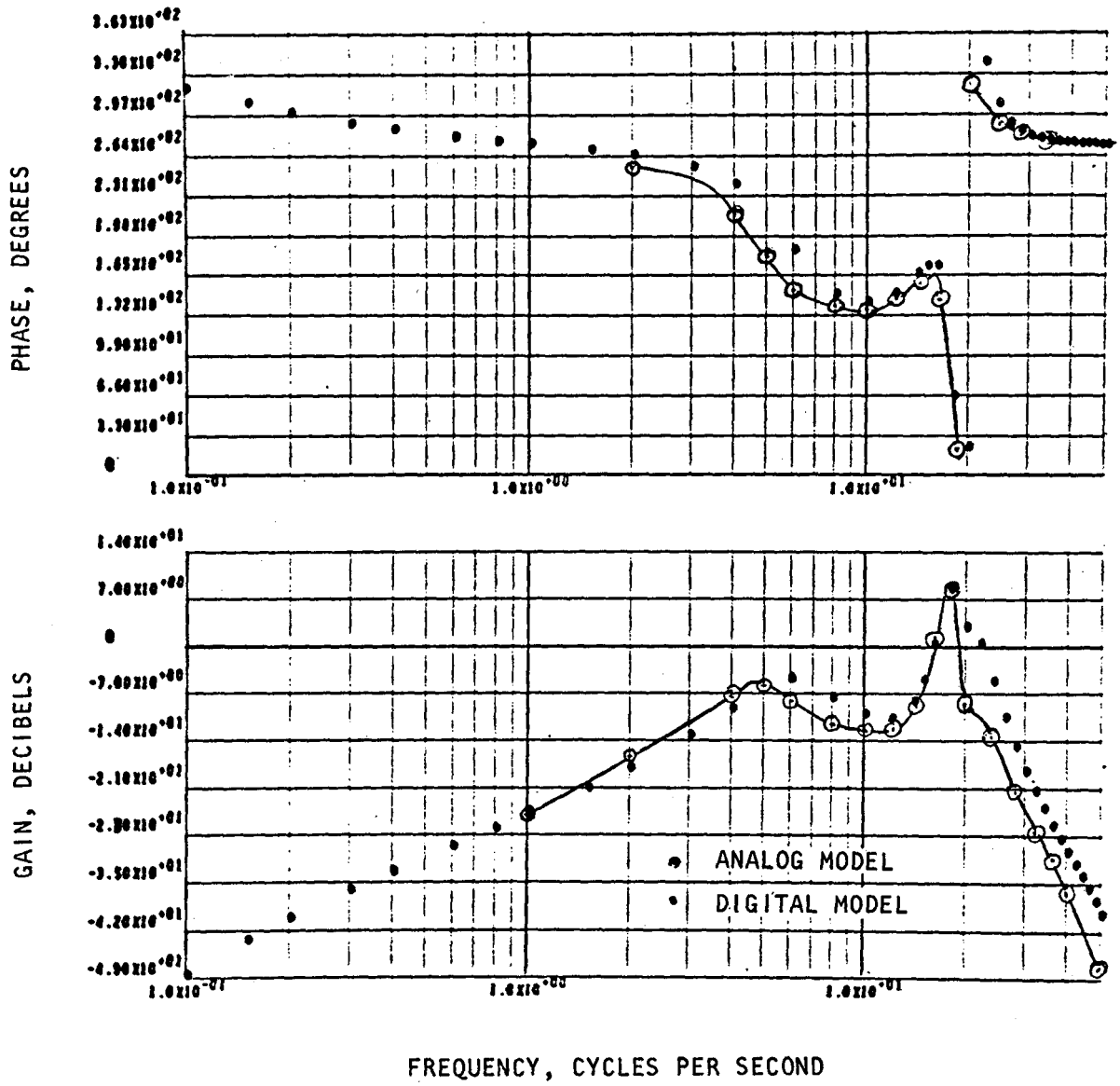

Figure 41. Comparison of Frequency Response Results From the Digital and Analog Models, Close-Coupled Inducer

APPENDIX B

CONTROLLER DESIGN

As presented in the body of the report, the controller design was based on electrical R-C compensation of the controller manifold inlet pressure. Provision was also made to provide some sensing lead with a second pressure input sensed upstream of the controller manifold. The system is shown schematically in Fig. 42 , while the details of the design equation derivation are given below.

The results of the feed system frequency response analyses showed that the feed system, at least up to 50 Hz, could be represented by the fluid inertia and resistance in the inlet line terminated by a capacitance at the inducer inlet. This resulted in the feedline equation of:

$$P_s = \left[P_T - LS\,\dot{\omega}_2\right] / \left[1 + L/RS + LCS^2\right] \qquad \text{(B-1)}$$

where

C = inducer inlet capacitance, m sec^2

L = inlet line fluid inertia, 1/m

P_s = inducer inlet pressure oscillation, newtons/m^2

P_T = effective upstream pressure oscillation, newtons/m^2

R = inlet line resistance, 1/m sec

S = Laplace operator, rads/sec

$\dot{\omega}_2$ = controller flowrate, kg/sec

The transfer function for the servo valve and piston combination with inner loop compensation was derived to be:

$$X = \left[\frac{0.546\times10^{-6}}{\omega_o^2}(1+S/667)(1+S/330)\,P_s + V\right] S/\left[1+S/\omega_o+S^2/\omega_o^2\right]\left[1+S/300\right] \qquad \text{(B-2)}$$

where

X = suppressor piston position, m

V = summation of input and feedback voltages

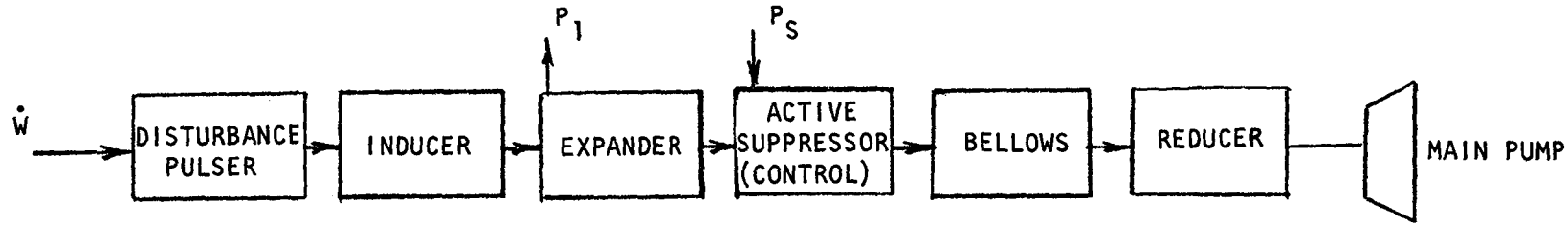

INDUCER REMOTE-COUPLED TO MAIN PUMP

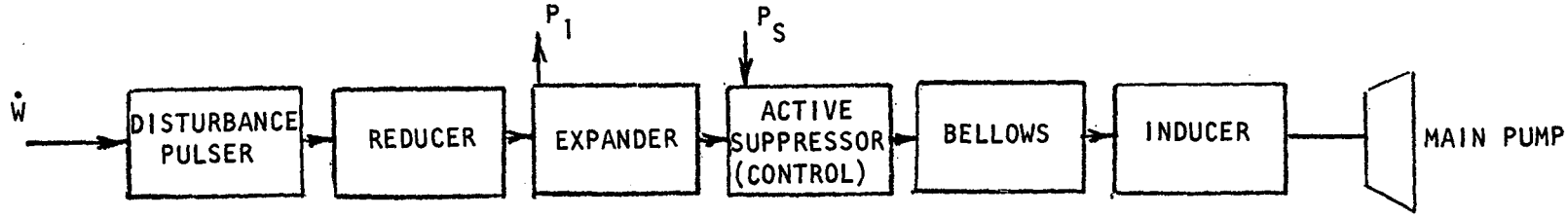

INDUCER CLOSE-COUPLED TO MAIN PUMP

NOTE:

1. P_S IS PRIMARY CONTROLLER INPUT PRESSURE
2. P_1 IS CONTROLLER LEAD PRESSURE INPUT

Figure 42. Test Section Block Diagram

Now, if a control is built representing an active R-C component, the desired controller action is represented by an equation of the form:

$$\dot{w}_2 = [C' S + D] P_s \tag{B-3}$$

where

C' = effective capacitance added by the controller, sec^2 m

D = effective 1/R added by the controller, m sec

substituting in the feedline Eq. B-1:

$$P_s/P_T = 1/[1 + (L/R + DL) S + L (C + C') S^2] \tag{B-4}$$

From Eq. B-4, the new system natural frequency is $\omega = 1.0\sqrt{L (C + C')}$ and the damping factor is given by $\zeta = 1/2 (L/R + LD)/\sqrt{L (C + C')}$. Thus, by choosing the value of C' we can control the system frequency while the value of D sets the system damping.

Using the nulling-integrating piston equation (B-2), the following set of equations apply to the control system:

$$V = H \times P_S \tag{B-5}$$

$$\dot{W}_2 = \rho A_p S X \tag{B-6}$$

where H = input precompensation required

ρ = fluid density, (Kg/m^3)

A_p = controller piston area, (m^2)

for frequencies where $300 > \omega > \omega_o$ the transfer function is approximately:

$$\frac{\dot{W}_2}{P_S} = \rho A_p \left[0.546 \times 10^{-6} + \omega_o^2 H\right] \tag{B-7}$$

therefore,

$$\rho A_p (0.546 \times 10^{-6}) + \rho A_p \omega_o^2 H = C'S + D \tag{B-8}$$

or

$$H = \frac{1}{\rho A_p \omega_o^2} \left[C'S - \rho A_p 0.546 \times 10^{-6} + D\right] \tag{B-9}$$

Considering Eq. B-1 and B-4 and values for the close-coupled inducer configuration on CTL-1, $\omega = 2\ \pi 17\ 1/2$ rps, $\zeta = 5$ percent and $L \approx 150$, values of $C \approx 6.6 \times 10^{-7}$ and $R \approx 1.5 \times 10^{5}$ are obtained. In order to reduce the frequency from 17-1/2 to 5 Hz, the effective compliance (C + C') needs to be changed by a factor of 12; in order to achieve 20-percent damping at 5 Hz a value of LD of about 0.013 is required (compared to L/R = 0.001). These values (a frequency reduction of 3 1/2 and minimum damping of 20 percent) are typical of the type of requirement which might be necessary to stabilize POGO in a particular vehicle.

For the tested system:

$$\rho = 1133.\ \text{Kg/m}^3 \quad (0.041\ \text{lb/in.}^3)$$

$$A_p = 0.00322\ \text{m}^2 \quad (5\ \text{in.}^2)$$

$$\omega_o = 12\ \text{rad/sec}$$

Substituting these values into Eq. B-9 gives:

$$\frac{V}{P_S} = H = 0.002\left[C'S + D - 2 \times 10^{-6}\right] \tag{B-10}$$

The item that results in the number 2×10^{-6} is damping resulting from the feedline pressure force on the piston, forcing hydraulic fluid through the lands of the servovalve. In this application, the effect is about 1/3 times the natural damping of the system.

Substituting Eq. B-9 and B-2 into Eq. B-6 for $\omega < (330)$ yields:

$$\frac{\dot{W}}{P_S} = \frac{\frac{\rho A_p S^2}{2}\left(\frac{1}{\omega_o}\right) 0.546 \times 10^{-6} + \frac{S^2}{2}\left(\frac{1}{\omega_o}\right)\left[C'S + D - 0.03\right]}{\left(1 + S/\omega_o + S^2/\omega_o^2\right)\left(1 + S/300\right)} \tag{B-11}$$

$$\cong \frac{\frac{S^2}{2}\left(\frac{1}{\omega_o}\right)\left(C'S + D\right)}{\left(1 + S/\omega_o + S^2/\omega_o^2\right)\left(1 + S/300\right)} \tag{B-12}$$

MATERIAL INSPECTION AND RECEIVING REPORT

1. PROC. INSTRUMENT IDEN (CONTRACT) NAS3-14382 (ORDER) NO. | 6. INVOICE NO. DATE | 7. PAGE 1 OF 1 | 8. ACCEPTANCE POINT D

2. SHIPMENT NO. ERC0019Z | 3. DATE SHIPPED 73N0V20 | 4. B/L TCN Not assigned Z | 5. DISCOUNT TERMS

9. PRIME CONTRACTOR CODE
Rocketdyne Div./RIC
6633 Canoga Ave.
Canoga Park, Calif. 91304

10. ADMINISTERED BY CODE
NASA/LeRC, Cleveland, Ohio

11. SHIPPED FROM(IF OTHER THAN 9) CODE FOB:
See block 9

12. PAYMENT WILL BE MADE BY CODE
Finance Div./Audit Branch
NASA/LeRC, Ohio

13. SHIPPED TO CODE
NASA/LeRC,
21000 Brookpark Rd.
Cleveland, Ohio 44135

14. MARKED FOR CODE
NASA/LeRC, Cleveland, Ohio
Attn: Contracting Officer

15. ITEM NO.	16. STOCK/PART NO. DESCRIPTION (INDICATE NUMBER OF SHIPPING CONTAINERS-TYPE OF CONTAINER-CONTAINER NO.)	17. QUANTITY SHIP'D/REC'D.	18. UNIT	19. UNIT PRICE	20. AMOUNT
Exh. A	Task IV.C FINAL REPORT NASA CR-134500 R-9125 - Pogo Instabilities Suppression Evaluation Additional dist. made per contract	132 (1)			

21. PROCUREMENT QUALITY ASSURANCE

A. ORIGIN
☐ PQA ☐ ACCEPTANCE OF LISTED ITEMS HAS BEEN MADE BY ME OR UNDER MY SUPERVISION AND THEY CONFORM TO CONTRACT, EXCEPT AS NOTED HEREIN OR ON SUPPORTING DOCUMENTS.
DATE | SIGNATURE OF AUTH GOVT REP
TYPED NAME AND OFFICE

B. DESTINATION
☐ PQA ☐ ACCEPTANCE OF LISTED ITEMS HAS BEEN MADE BY ME OR UNDER MY SUPERVISION AND THEY CONFORM TO CONTRACT, EXCEPT AS NOTED HEREIN OR ON SUPPORTING DOCUMENTS.
DATE | SIGNATURE OF AUTH GOVT REP
TYPED NAME AND TITLE

22. RECEIVER'S USE
QUANTITIES SHOWN IN COLUMN 17 WERE RECEIVED IN APPARENT GOOD CONDITION EXCEPT AS NOTED.
DATE RECEIVED | SIGNATURE OF AUTH GOVT REP
TYPED NAME AND OFFICE
* IF QUANTITY RECEIVED ON THIS CONSIGNMENT IS THE SAME AS QUANTITY SHIPPED, INDICATE BY (✓) MARK, IF DIFFERENT, ENTER ACTUAL QUANTITY RECEIVED BELOW QUANTITY SHIPPED AND ENCIRCLE.

23. CONTRACTOR USE ONLY
A. G.O. 9364 | B. SUB-ACCT | C. | D.
E. CONTROL NUMBERS
F. | G. GROSS WT. | H. CUBE
I. LENGTH | J. WIDTH | K. HEIGHT

OTHER CONTRACTOR INFORMATION:
P. UNCLASSIFIED

L. CERTIFICATION - INSPECTION & CONTRACT PERFORMANCE
E. L. Caudill

M. PACKAGING INFORMATION
GOLDENROD

R. PREP DATE 73N0V20 | O. PACKING LIST NO. Z-73-8557 PD

DD FORM 1 AUG 67 250 REPLACES EDITION OF 1 OCT. 1966 WHICH MAY BE USED

The system response from 0 to 330 rps is then given by Eq. B-12 and B-1. Combining these two equations results in:

$$P_S \left[1 + \frac{LS}{R} + LCS^2 + \left(\frac{L\,S^3}{\omega_o^2}\right) \frac{(C'S + D)}{(1 + S/\omega_o + S^2/\omega_o^2)\ (1 + S/300)} \right] = P_T \qquad \text{(B-13)}$$

Letting $\omega_n = \frac{1}{\sqrt{LC}}$ and rearranging gives:

$$\frac{P_S}{P_T} = \frac{\omega_o^2\ (300/LC)(1+S/\omega_o+S^2/\omega_o^2)(1+S/300)}{(S^2+2\xi_n\omega_n S+\omega_n^2)(\omega_o^2+S\omega_o+S^2)(300+S) + \left(\frac{300\ C'}{C}\right)\ S^3\cdot\ (S+D/C')} \qquad \text{(B-14)}$$

The denominator of Eq. B-14 contains the pertinent stability information. Root loci plots for variation in C' are required to determine the control characteristics.

Several root loci were plotted to determine the effect of D/C' and C'/C values. The closed loop roots close to the origin ($\bar{\omega}_o$) remain close to the open loop roots (ω_o). This infers that over a wide variation of D/C' and C'/C, the transfer function is essentially:

$$\frac{P_S}{P_T} = \frac{(1 + S/\omega_o + S^2/\omega_o^2)\ (1 + S/300)}{(1 + S/\bar{\omega}_o + S^2/\bar{\omega}_o^2)\ (1 + S/330)\ (1 + 2\bar{\xi}_n S/\bar{\omega}_n + S^2/\bar{\omega}_n^2)} \qquad \text{(B-15)}$$

where

$\bar{\xi}_n$ = damping ratio for controlled system

$\bar{\omega}_n$ = natural frequency of controlled system

where

$$\omega_o = \bar{\omega}_o$$

and in the low frequency range, this becomes:

$$\frac{P_S}{P_T} = \frac{1}{1 + 2\bar{\xi}_n S/\bar{\omega}_n + S/\bar{\omega}_n^2} \qquad \text{(B-16)}$$

From the root locus analysis, a summary plot was obtained (Fig. 43) that indicates the effect of C' on the system resonant frequency and the effect of D on system damping factor.

Using Fig. 43 and the criteria of 50-percent damping, the following values of C' and D for various desired natural frequencies are obtained.

Required frequency (Hertz)	C'	D	Break frequency of lead compensation = D/C' (rad/sec)
17-1/2	0	0	-
10	3.2×10^{-8}	3.4×10^{-6}	108
6	1.1×10^{-7}	5.4×10^{-6}	48

This results in one controller input of the form P_S (C' S + D)/(1 + S/314). The lag at 50 Hz (314 rps) is added to eliminate problems with high frequency noise due to the (C' S + D) lead compensation.

In an attempt to improve the controller performance, the concept of sensing a second upstream pressure and using this pressure as a lead input was analyzed. Two sensing schemes were considered.

1. A pressure upstream of the control was sensed and used, with appropriate compensation, as an additional input.

2. A pressure difference, across a line section upstream of the control, is sensed and used, with appropriate compensation, as an additional input.

The first lead compensated control used an additional input signal from a pressure measurement upstream of the control in the feed line. The compensating network for the upstream pressure measured was chosen to cancel the effects of tank pressure inputs on pump suction pressure. This system appears to have good dynamic characteristics for pressure oscillation control.

Expanding Eq. B-5 to include the additional input gives:

$$V = \frac{(C' S + D)}{(1 + S/314)} P_S + GP_1 \qquad \text{(B-17)}$$

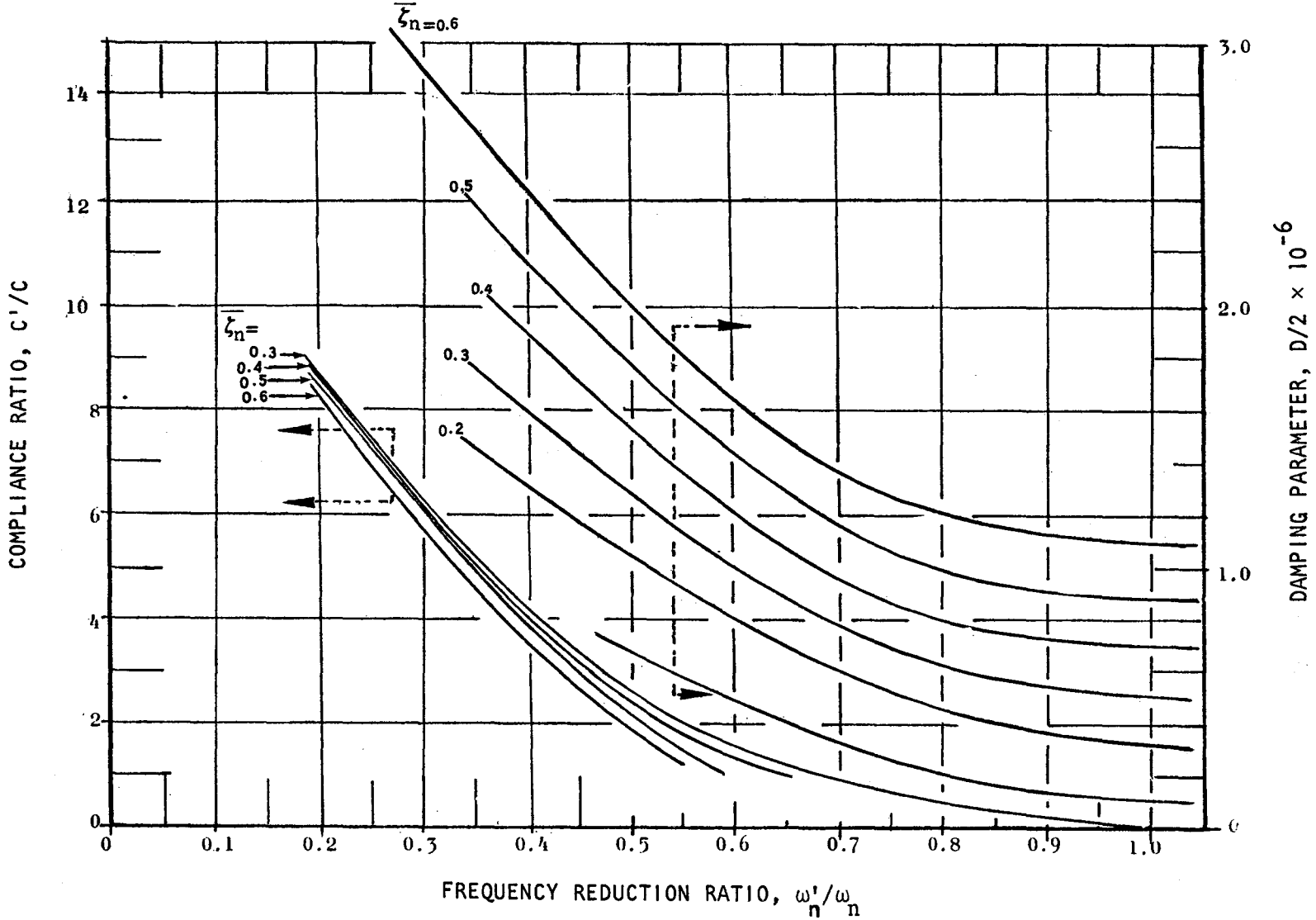

Figure 43. Summary Plot From Root Locus Analysis Showing Effect of the Damping Parameter (D) and Compliance Ratio (C'/C) on the Closed Loop System Damping Ratio (ζ) and System Frequency Reduction Ratio (ω_n'/ω_n)

where

G = lead pressure precompensation

P_1 = lead pressure

This modifies Eq. B-13 to:

$$P_S\left[1 + L/R\ S + LCS^2 + \frac{(L\ S^3)\ (3.6)}{(1+S/\omega_o+S^2/\omega_o^2)}\ \frac{(C'S+D)}{(1+S/314)}\right] = P_T - \frac{3.6\ (L\ S^3)\ GP_1}{(1+S/\omega_o+S^2/\omega_o^2)} \quad \text{(B-18)}$$

Substituting for P_1 in terms of P_T and P_S gives:

$$P_S\left[1 + L/R\ S + LCS^2 + \frac{3.6\ LS^3\ (C'S + D)}{(1+S/\omega_o+S^2/\omega_o^2)\ (1+S/314)}\right] = \quad \text{(B-19)}$$

$$P_T - \left[\frac{3.6\ L\ S^3}{1+S/\omega_o+S^2/\omega_o^2}\ G\ (L_2/L\ P_T + L_1/L\ P_S)\right]$$

This can be factored to give:

$$P_S\left\{1 + L/R\ S + (L)\ CS^2 + \frac{3.6\ (L)\ S^3}{1+S/\omega_o+S^2/\omega_o^2}\left[\frac{C'S+D}{1+S/314} + G\ L_1/L\right]\right\}$$

$$= P_T\left[1 - \frac{3.6\ S^3}{1+S/\omega_o+S^2/\omega_o^2}\ (L_2)\ G\right] \quad \text{(B-20)}$$

In this case, if the coefficient of $P_T = 0$ then $G = \left[\frac{1+S/\omega_o+S^2/\omega_o^2}{3.6\ S^3\ L_2}\right]$

or for $S > \omega_o$, $G \longrightarrow \left[\frac{1}{3.6\ \omega_o^2\ S\ L_2}\right]$.

To eliminate the integral effect at very low frequencies ($\omega_o < 4\pi$) we can let

$$G = \frac{0.28}{\omega_o^2 L_2 (\omega_o + S)} = \frac{0.28}{\omega_o^3 L_2 (1+S/\omega_o)} \qquad \text{(B-21)}$$

To evaluate the stability of the system the left side of Eq. B-20:

$$1+L/R\ S + (L)\ CS^2 + \left[\frac{3.6\ (L)\ S^3}{(1+S/\omega_o+S^2/\omega_o^2)(1+S/\omega_o)}\right]\left[(CS+D)(1+S/\omega_o) + L_1/L\ \frac{0.28}{\omega_o^3 L_2}\right]$$

is considered.

The most significant point is how the term $0.28\ L_1/\omega_o^3\ L\ L_2$ affects the roots of the equation since it adds damping to the system similar to the term D, as was discussed in the formulation of the R-C component.

The coefficient of P_T in Eq. B-20 becomes:

$$1-\left[\frac{3.6\ S^3\ L_2}{1+S/\omega_o + S^2/\omega_o^2}\right]\left[\frac{0.28}{\omega_o^3 L_2(1+S/\omega_o)}\right] = \frac{1+2\ S/\omega_o+2\ S^2/\omega_o^2}{(1+S/\omega_o+S^2/\omega_o^2)(1+S/\omega_o)} \qquad \text{(B-22)}$$

The transfer function for the system with lead compensation, determined from a root-locus plot, becomes:

$$P_S\left[\frac{(1+2\zeta S/\omega_o+S^2/\omega_o^2)(1+S/\omega_o'+S^2/\omega_o'^2)(1+S/\omega_o'')}{(1+S/\omega_o+S^2/\omega_o^2)(1+S/\omega_o)}\right]=$$

$$\left[\frac{(1+2\ S/\omega_o+2S^2/\omega_o^2)}{(1+S/\omega_o + S^2/\omega_o^2)(1+S/\omega_o)}\right]\ P_T \qquad \text{(B-23)}$$

since $\omega_o' \approx \omega_o'' \approx \omega_o$, the system very nearly becomes:

$$P_S = \frac{P_T}{(1+2\zeta_n S/\omega_n+S^2/\omega_n^2)(1+S/\omega_o)} \qquad \text{(B-24)}$$

In effect, then, the control results in:

1. Control of feed line frequency, ω_n

2. Control of feed line damping, ζ_n

3. Introduction of a 90-degree phase lag and direct attenuation with frequency for all frequencies above ω_o. At all suction system resonances, therefore, P_S will be nearly 180-degrees out of phase with the tank pressure disturbances.

The precompensation for this signal is defined using the control equation:

$$\dot{W} = \left[\frac{3.6\ S^2}{(1+S/\omega_o+S^2/\omega_o^2)(1+S/300)}\right]\cdot\left[\frac{C'S+D}{1+S/314}\ P_S + \frac{0.28}{\omega_o^3 L_2 (1+S/\omega_o)}\ P_1\right] \qquad \text{(B-25)}$$

ΔP LEAD

The second lead compensated control considered senses a ΔP across a section of the feed line from which the flow acceleration induced by tank pressure variations can be inferred. The control is then designed to provide a similar (out of phase) flow acceleration through motion of the compensating piston. By preventing fluid compression and therefore suction pressure variations, flow variations through the pump are theoretically eliminated. Stability calculations were required to indicate if such a system might enhance pump induced oscillations or if it might result in a closed-loop instability.

Once again the basic feedline equation is Eq. B-1. Defining the control requirement by:

$$W = G\ (P_1 - P_S) \qquad \text{(B-26)}$$

and substituting into the feed line gives:

$$\left[1 + (L_1 + L_2)\ (1/R + CS)\ S - L_2 S^2 G\right]\left[P_S\right] = P_T\left[1 - L_2 S^2 G\right] \qquad \text{(B-27)}$$

Ideally, the canceling control is chosen to eliminate the effect of the input, P_T. The effect of P_T on P_S can be eliminated by choosing G, so that the coefficient of P_T is zero $G = (1/L_2\ S^2)$. For this control, we obtain:

$$(L_1 + L_2)\ (1/R + CS)\ S\ P_S = 0 \qquad \text{(B-28)}$$

We must, however, use a less than perfect control based on the pulser nulling-integrating piston which has the approximate characteristics of:

$$W = \frac{3.6\ S}{(1+S/\omega_o+S^2/\omega_o^2)\ (1+S/300)} \left[V+0.546\text{x}10^{-6}\ (1+S/330)\ \ P_S\right] \qquad \text{(B-29)}$$

In the frequency range $\omega_o < S < 300$, the nulling piston equation is approximately:

$$W = \frac{3.6\omega_o^2}{S}\ \left[V + 0.546 \text{ x } 10^{-6}\ P_S\ \right] \qquad \text{(B-30)}$$

Ignoring the piston face force ($0.546 \text{ x } 10^{-6}\ P_S$):

$$W = 3.6\ \omega_o^2/S\ (H)\ (P_1 - P_S), \qquad \text{(B-31)}$$

where H is the electronic precompensation, $V/(P_1 - P_S)$. Then $3.6\ \omega_o^2/S$ x H $\doteq 1/L_2S^2$ or H $\doteq 1/3.6\ \omega_o^2 L_2\ S$ in the $\omega_o \leq 300$ rad/sec range. A suitable form for H is $1/3.6\ \omega_o^2\ L_2/(\omega_o + S)$ to prevent low frequency drift of the internal variables.

With this as the precompensation, we have from Eq. B-29:

$$W= \frac{3.6\ S}{(1+S/\omega_o+S^2/\omega_o^2)(1+S/300)} \left[\frac{1/(3.6\ \omega_o^2 L_2)}{(\omega_o+S)}\ (P_I-P_S)+\frac{0.546\text{x}10^{-6}}{\omega_o^2}(1+S/330)P_S\right] \qquad \text{(B-32)}$$

or

$$W = \frac{S/(\omega_o^3 L_2)}{(1\ +\ S/\omega_o\ +\ S^2/\omega_o^2)(1\ +\ S/300)(1\ +\ S/\omega_o)}\ P_1\ + \qquad \text{(B-33)}$$

$$\frac{S/(\omega_o^3 L_2)\{-1+(1.97\text{x}10^{-6}\ \omega_o L_2)[1+(1/\omega_o+1/300)S+S^2/\omega_o 330]\}}{(1+S/\omega_o+S^2/\omega_o^2)(1+S/300)(1+S/\omega_o)}\ P_S$$

Typically, $\omega_o = 12$, $L_2 = 30.4$ so that:

$$W = \frac{S/\ 52531\ \{P_1\ -(0.9993-6.1\text{x}10^{-5}\ S-1.8\text{x}10^{-7}S^2)P_S\}}{(1+S/12+S^2/12^2)(1+S/300)(1+S/12)} \qquad \text{(B-34)}$$

and for frequencies below about 100 Hz, we have approximately:

$$W/(P_1-P_S) = \frac{1.9\times10^{-5}}{(1+S/12+S^2/12^2)(1+S/12)(1+S/300)} = G \qquad \text{(B-35)}$$

From Eqs. B-27 and B-35, a descriptive equation for the system is found to be:

$$\left[1+\left[(L_1+L_2)/R\right]S+(L_1+L_2)CS^2 - \frac{S^3/\omega_o^3}{(1+S/\omega_o)(1+S/\omega_o+S^2/\omega_o^2)(1+S/300)}\right]P_S = \qquad \text{(B-36)}$$

$$\left[1 - \frac{S^3/\omega_o^3}{(1+S/\omega_o)(1+S/\omega_o+S^2/\omega_o^2)(1+S/300)}\right]P_T$$

Ignoring the pole at 300 radians and examining the low frequency stability by letting $(L_1 + L_2)/R = 2\zeta/\omega_n$ and $(L_1 + L_2)\ C = 1/\omega_n^2$, the characteristic equation for the system is:

$$\left[1+(2\zeta/\omega_n)S+S^2/\omega_n^2\right]\left[1+S/\omega_o\right]\left[1+S/\omega_o+S^2/\omega_o^2\right]-S^3/\omega_o^2 \qquad \text{(B-37)}$$

Figure 44 shows a root loci plot for the above polynominal normalized to the frequency, ω_o, as given in Eq. B-38:

$$\left[\left(\frac{\omega_n}{\omega_o}\right)^2 + 2\zeta_n\left(\frac{\omega_n}{\omega_o}\right)S' + S'^2\right]\left[1 + S'\right]\left[1 + S' + S'^2\right] - K\left(\frac{\omega_n}{\omega_o}\right)^3 S'^3 = 0 \qquad \text{(B-38)}$$

Since there is symmetry about the real axis, only the upper half plane is shown. The root locus plot was generated by selecting values of ω_n/ω_o and ζ_n that would satisfy the angle criterion for a positive feedback system and result in neutral stability at specific frequencies for some value of K. On these loci, locations were then established such that neutral stability would occur with K = 1.0. These points are shown with the symbol (□). The interpretation of the analysis is that the system would be stable only if the inherent feed system damping (with no control) is very high, greater than about 70 percent of critical damping. Since the feed line damping is generally in the 5- to 10-percent range, this type of control will not work because of loop instability, even though the effect of tank pressure variations would be significantly attenuated.

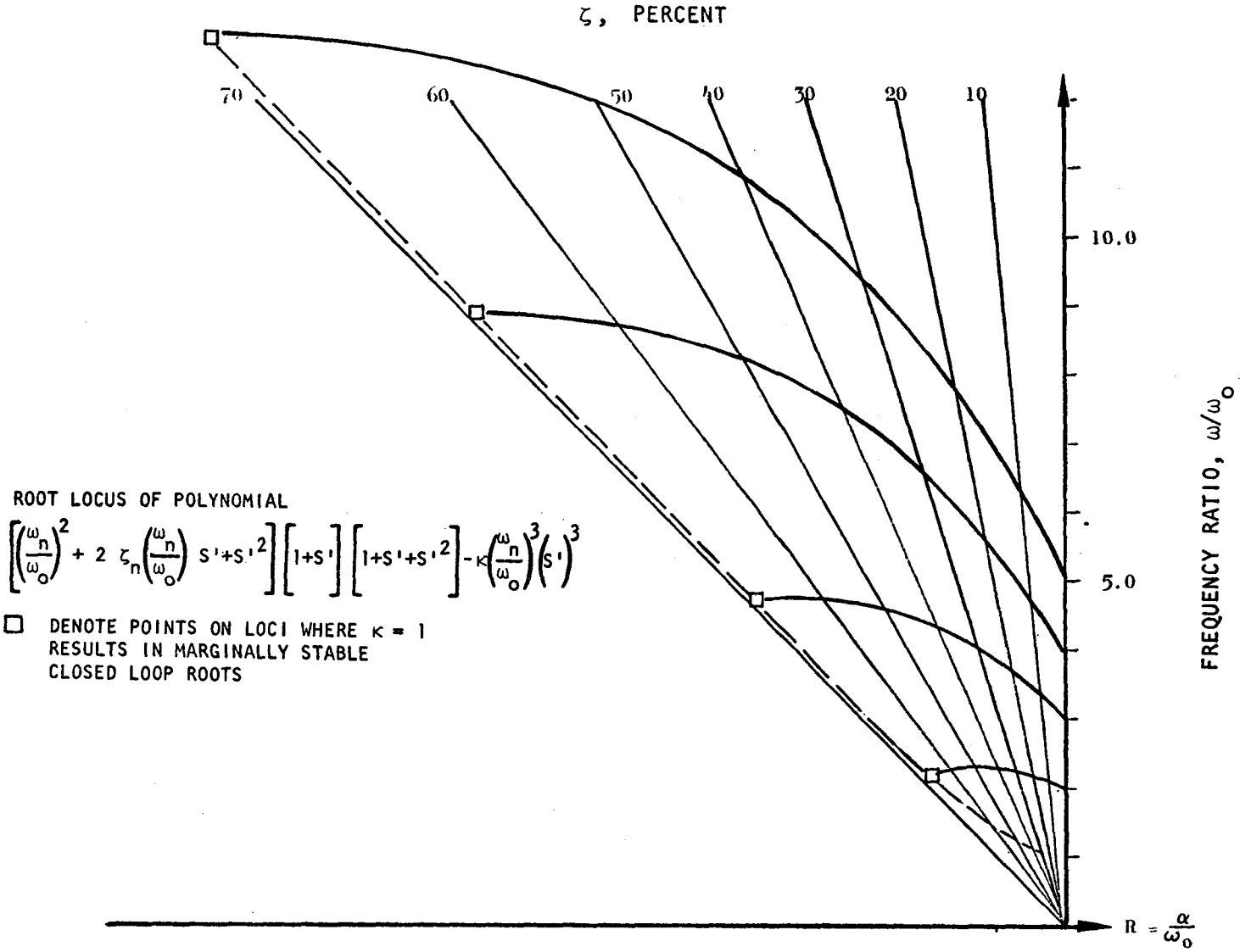

Figure 44. Root Locus Plot of Characteristic Equations Normalized to the Frequency (ω_o)

An additional control concept was considered but discounted early in the program. It consisted of using the active R-C component with an additional input from a pressure sensor downstream of the main pump to trim out any signal which might have passed through the pump. Initial frequency analysis of the system indicated that the pump dynamics can produce a significant (180 degrees) phase shift in pressures across the pump. The frequency at which the phase shift occurs is associated with a feed line-pump resonance which apparently is quite dependent on the cavitation characteristics and operating pressure level at the inlet to the pump. If a discharge pressure measurement were used for compensation at low frequencies, it could reverse sign and actually promote higher oscillations (positive feedback) at frequencies above the feedline frequency. Design of suitable electronic compensation would require that the compensation frequency response be a function of pressure level and that the frequency response of specific pumps be well known before the control is designed. The complexity and cost of such a system was not compatible with potential benefit and was therefore not pursued.

CONTROLLER ELECTRONICS

From the results of the system analysis, the electronic requirements for a control with a control pressure (P_S) input plus a lead pressure (P_1) input were found to be:

$$V_{out} = \left\{ P_S \left[\frac{3.4(1+S/42.4)}{(1+S/314)} \right] + P_1 \left[\frac{68}{(1+S/12)} \right] - X \left[\frac{(1+S/12)}{S} \right] \right\}$$

where

P_S = active R-C input (volts)
P_1 = lead input (volts)
S = Laplace operator d/dt
V_{out} = voltage to servovalve
X = position feed back (volts)

These requirements were built into a unit shown in Fig. 45 ; V_{out} being the voltage at the output of amplifier A7.

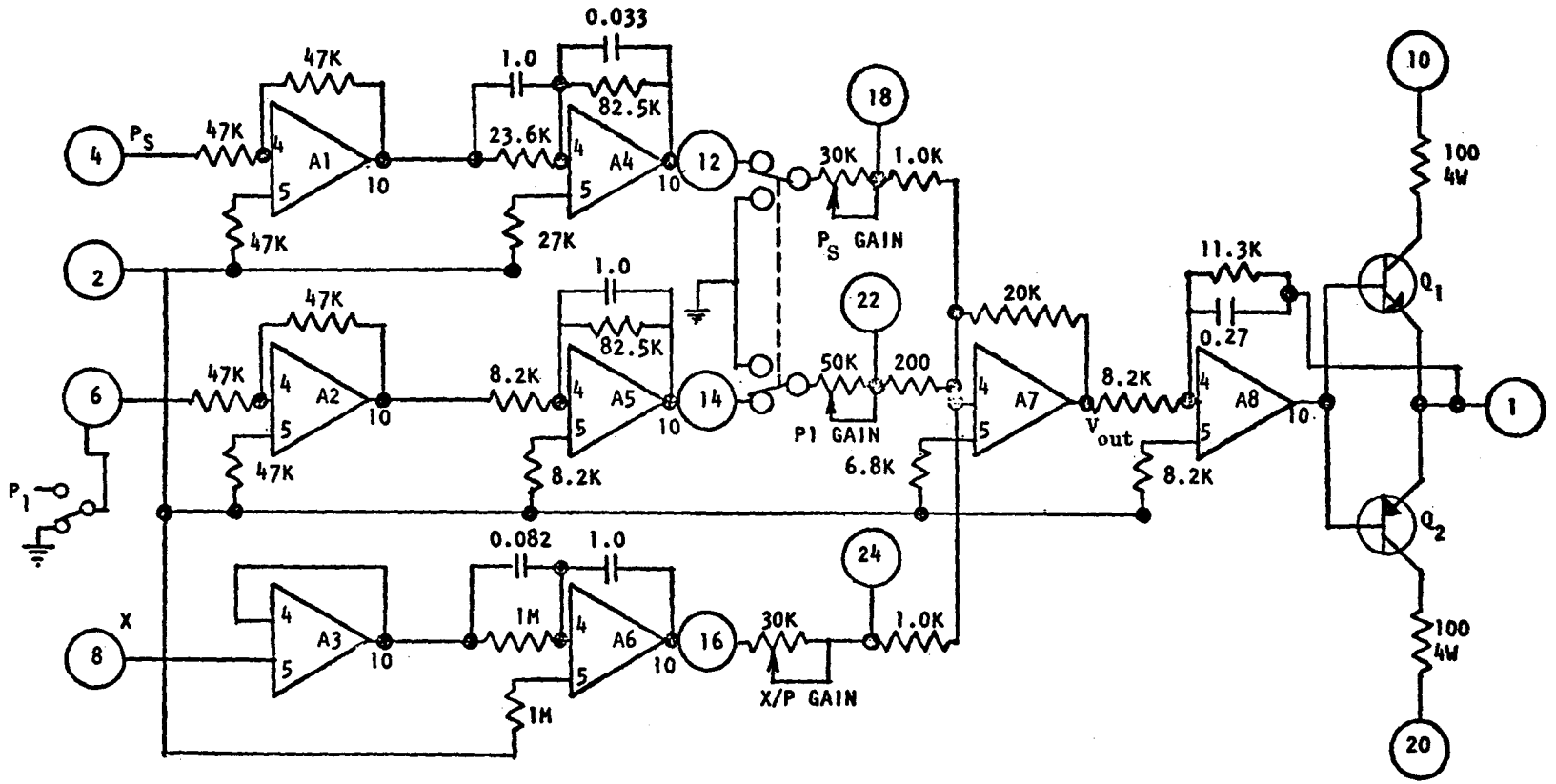

Figure 45. Schematic of Controller Electronics

Page intentionally left blank

APPENDIX C

TEST PROGRAM

A test program was conducted in Cell 2A of Rocketdyne test facility CTL-I to experimentally determine the frequency response characteristics of a low-speed inducer high-speed pump system in liquid oxygen, and the effectiveness of the analyzed and designed pressure oscillation suppression system. The test hardware consisted of a J-2S liquid oxygen pump modified with a J-2 pump inducer, a low-speed hydraulic-turbine driven inducer, a hydraulic driven flow disturbance pulser, and a hydraulic driven pressure oscillation controller with associated electronics. The low-speed inducer was designed, built, and tested in water under Contract NAS3-10280 and reported in Ref. 2. Cut-away drawings are shown in Fig. 46 and 47.

Tests were run for two different configurations. These configurations had the low-speed inducer close-coupled and remote-coupled to the main pump. In the close-coupled configuration, the flow disturbance pulser was the first component in the test section followed by a reducer section, an expander section, the controller manifold and piston, a bellows for absorbing thermal displacements, the low-speed inducer, and the main pump. The remote-coupled configuration interchanged the low-speed inducer and the reducer section. The turbine drive for the low-speed inducer was liquid oxygen tapped from the main pump discharge.

INSTRUMENTATION

Instrumentation consisted of measurements of pressures, structural acceleration, temperatures, pump and inducer speeds, flowrate disturbance pulser and controller piston positions, and electronic pulser and controller signals.

Table IV is a complete list of the instrumentation giving the required frequency response, range, recorder type, and location code. The instrumentation location in the test section is shown in Fig. 48 and locations outside the test section are shown in Fig. 49 .

Two types of pressure measurements were taken, one for steady-state performance, the other for determining frequency response characteristics. The steady-state transducers were remote-coupled Tabor strain gage type, while the dynamic measurements were made with flush mounted, data sensor transducers.

For recording dynamic data, two 14-channel tape recorders were used. The tape channel assignments are shown in Table V . The pulser command sine signal is common to both tapes and provides a data reference. Data not recorded on tape and intended for determination of steady-state data was recorded by the digital Astrodata system.

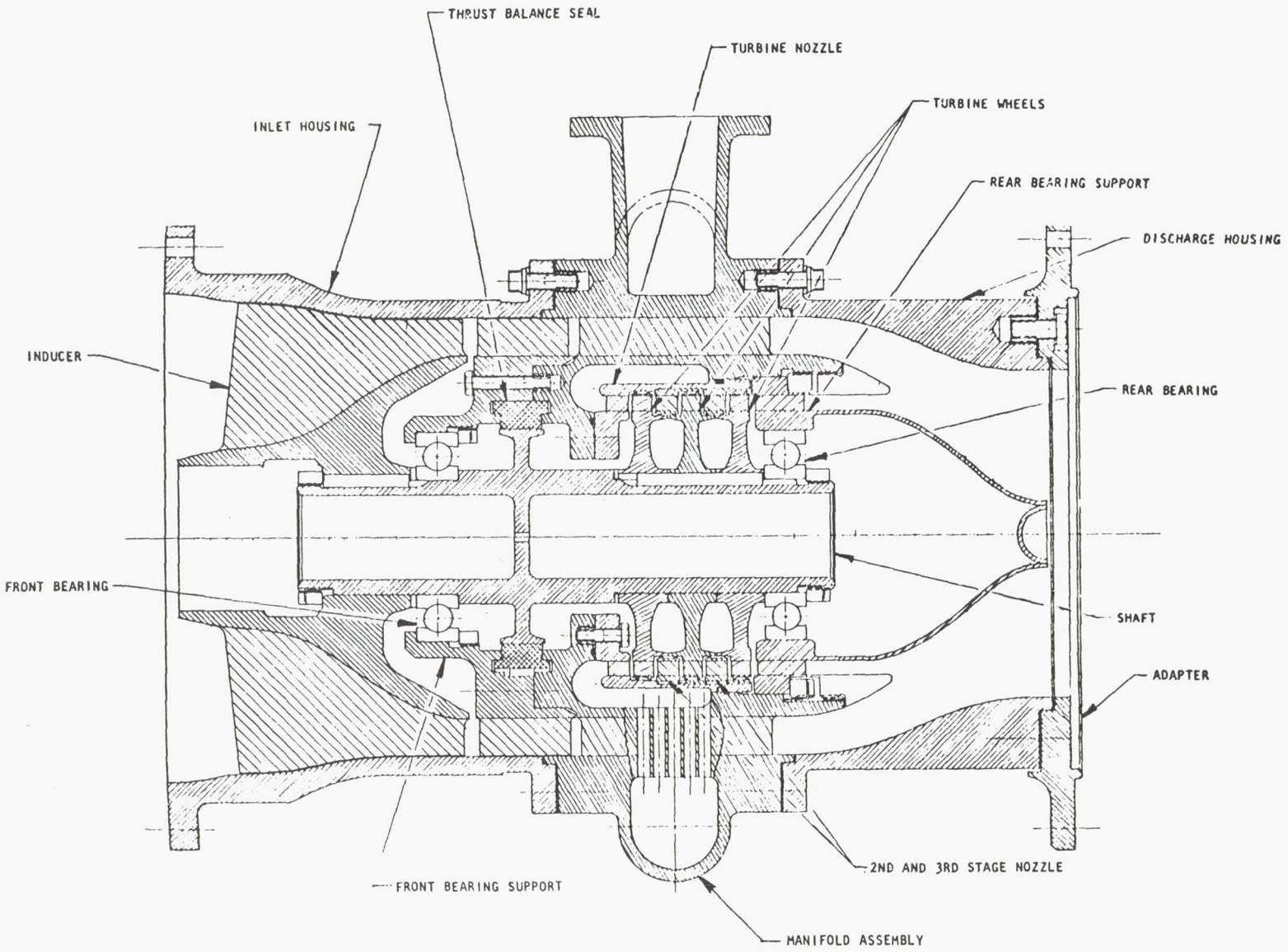

Figure 46. Inducer Cross Section

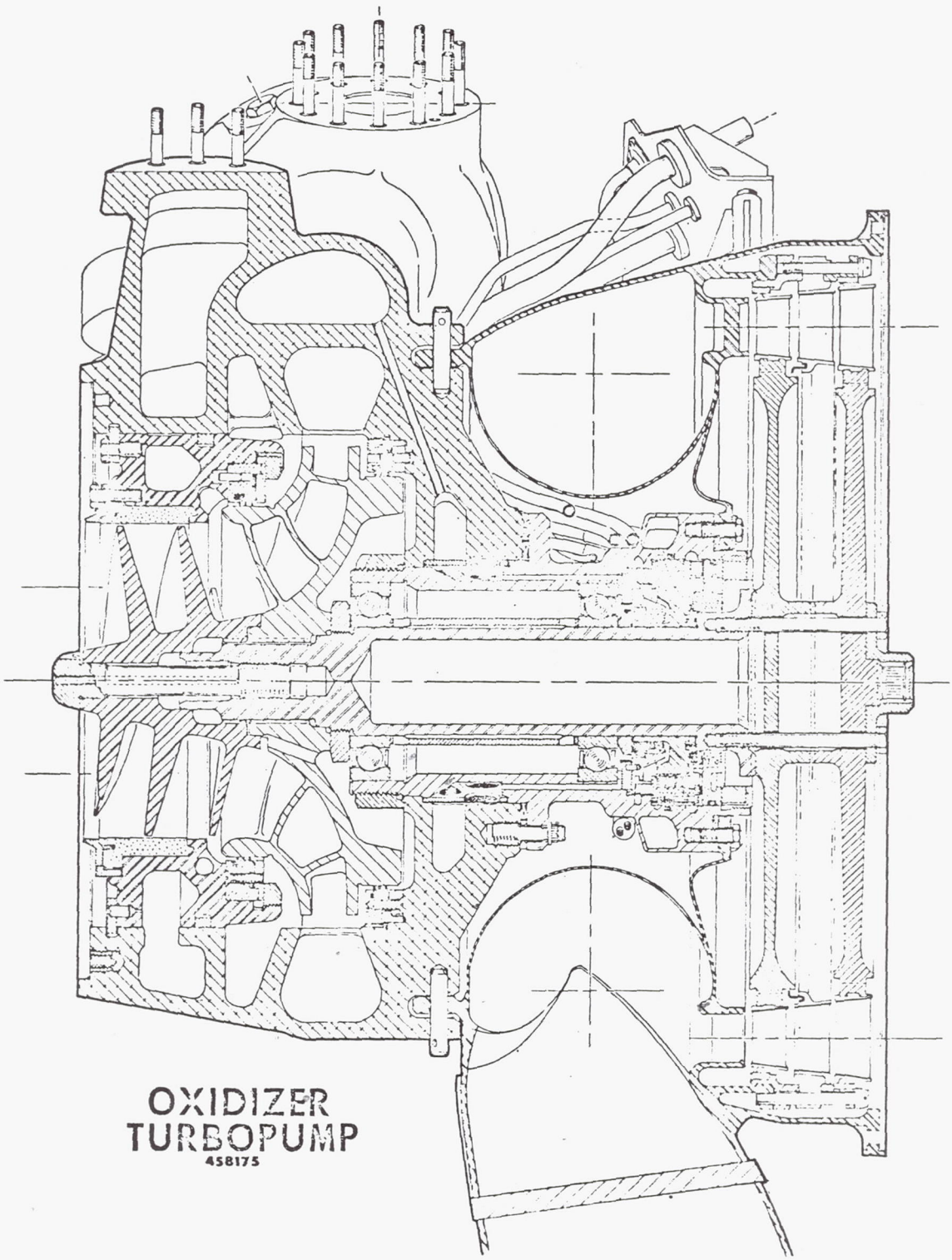

Figure 47. J-2 Oxidizer Pump Cutaway

TABLE IV

INSTRUMENTATION LIST FOR POGO SUPPRESSION PROGRAM

Parameter	Response	Range	Recorder	Code
Pressures (newtons/m^2)				
1. Inlet to position "A" (Facility duct discharge)	0-200 Hz	$0\text{-}14\times10^5$ (0-200)*	Tape	P-1
		$0\text{-}7\times10^5$	DIGR	PS-1
2. Reducer discharge	0-200 Hz	$0\text{-}14\times10^5$	Tape	P-2
	-	$0\text{-}14\times10^5$	Astrodata	PS-2
3. Anti-POGO pulser inlet	0-200 Hz	$0\text{-}14\times10^5$	Tape	P-3
4. Inducer inlet	0-200 Hz	$0\text{-}14\times10^5$	Tape	P-4
5. Inducer discharge	0-200 Hz	$0\text{-}14\times10^5$	Tape	P-5
6. Main pump discharge	0-200 Hz	$0\text{-}140\times10^5$	Tape	P-6
	-	$0\text{-}140\times10^5$	DIGR	PS-6
7. Inducer hydraulic turbine inlet	0-200 Hz	$0\text{-}140\times10^5$	Tape	P-7
	-	$0\text{-}140\times10^5$	Astrodata	PS-7
8. System P (P7-P1)	-	$0\text{-}140\times10^5$	Astrodata	DP-1
9. Hydraulic supply	0-200 Hz	$0\text{-}280\times10^5$	Astrodata	PS-8
10. Pulser control pressure	0-200 Hz	$0\text{-}280\times10^5$	Astrodata	PS-9
11. Anti-POGO control pressure	0-200 Hz	$0\text{-}280\times10^5$	Astrodata	PS-10
Accelerometers				
12. Pump flange - Axial	100 Hz (LP)	10 grms	Tape	A-1
- Radial	800 Hz (LP)	20 grms	Scope	A-2
13. Preinducer flange				
- Axial	100 Hz (LP)	10 grms	Tape	A-3
- Radial	800 Hz (LP)	20 grms	Scope Brush	A-4
14. Vertical duct run No. 1 - Axial	100 Hz (LP)	10 grms	Tape	A-5

*(psi)

TABLE IV. (CONTINUED)

INSTRUMENTATION LIST FOR POGO SUPPRESSION PROGRAM

Parameter	Response	Range	Recorder	Code
15. Horizontal duct run No. 1 - Axial	100 Hz (LP)	10 grms	Tape	A-6
16. Vertical duct run No. 2 - Axial	100 Hz (LP) (LP = Low pass)	10 grms	Tape	A-7
17. Horizontal duct run No. 2 - Axial	100 Hz (LP)	10 grms	Tape	A-8
18. Tank bottom - Axial	100 Hz (LP)	10 grms	Tape	A-9
19. Pump discharge line throttle valve - Axial	100 Hz (LP)	10 grms	Tape	A-10
Temperatures (deg C)				
20. Inlet to position "A"	-	-184/-156 (-300/250F)	Astrodata DIGR	T-1
21. Reducer discharge	-	-184/-156	Astrodata	T-2
22. Inlet of inducer hydraulic turbine	-	-184/-156	Astrodata	T-3
23. Main pump flowmeter	-	-184/-156	Astrodata	T-4
24. Pulser bleed line	-	-184/-156	DIGR	T-5
25. Anti-POGO pulser bleed line	-	-184/-156	Astrodata	T-6
Positions (Volts-d.c.)				
26. Pulser actuator	100 Hz	0-5	Tape Brush	X-1
27. Anti-POGO pulser actuator	100 Hz	0-5	Tape	X-2
Speeds (rpm)				
28. Main pump	-	0-10000	Astrodata	S-1
29. LeBow torque mater	-	0-10000	Astrodata	S-2

TABLE IV. (CONCLUDED)

INSTRUMENTATION LIST FOR POGO SUPPRESSION PROGRAM

Parameter	Response	Range	Recorder	Code
Flowrate (kgm/su)				
30. Main pump discharge	-	0-225 (0-500#/s)	Tape Astrodata DIGR	F-1
Electrical (Volts)				
31. Pulser command (sine)	100 Hz	0-10	Tape Brush	E-1
32. Pulse command (cosine)	100 Hz	0-10	Tape	E-2
33. Anti-POGO control command	100 Hz	0-10	Tape	E-3
34. Pulser servovalve command	100 Hz	0-5	Astrodata	E-4
35. Anti-POGO control servovalve command	100 Hz	0-5	Tape Astrodata	E-5
36. Anti-POGO control compensation	100 Hz	0-5	Tape	E-6

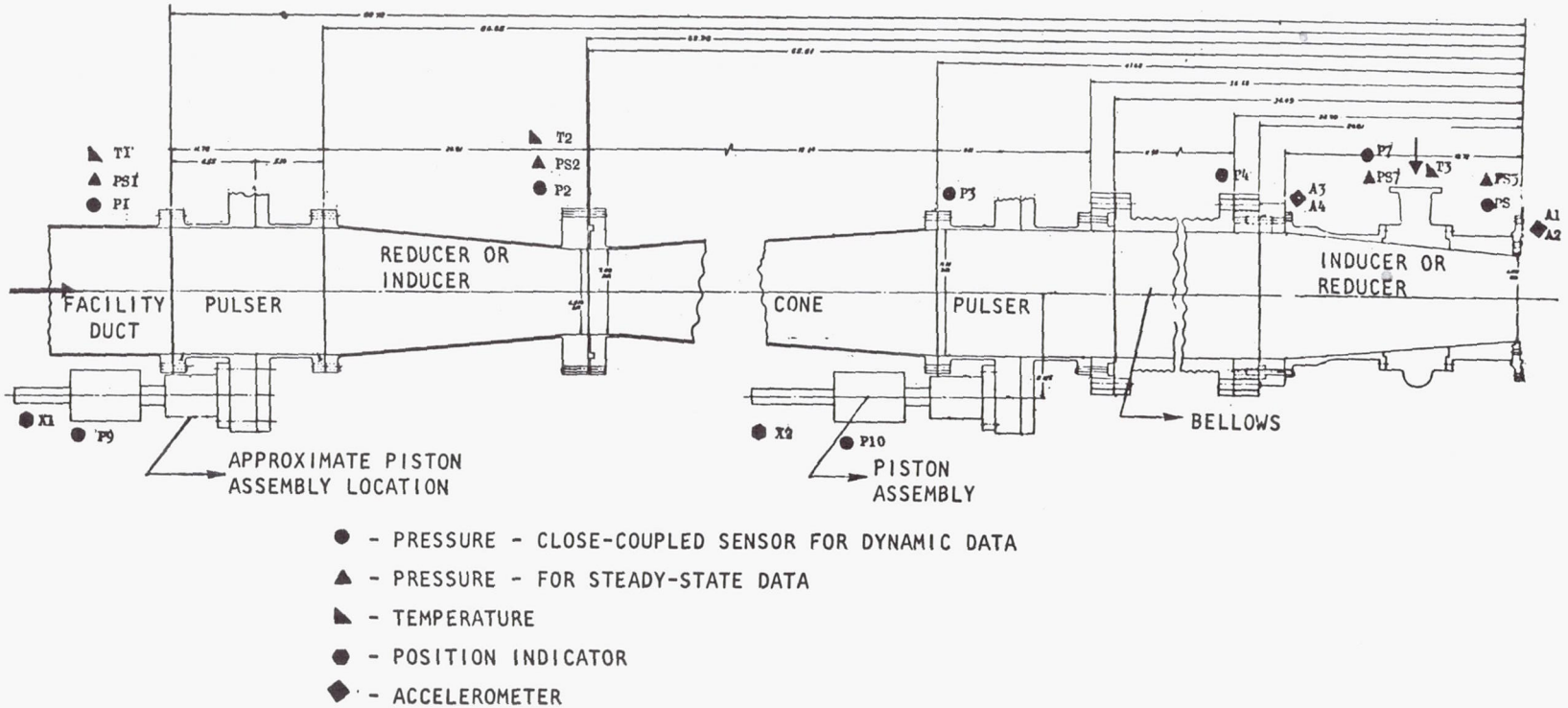

Figure 48. Test Section Layout and Instrumentation Locations

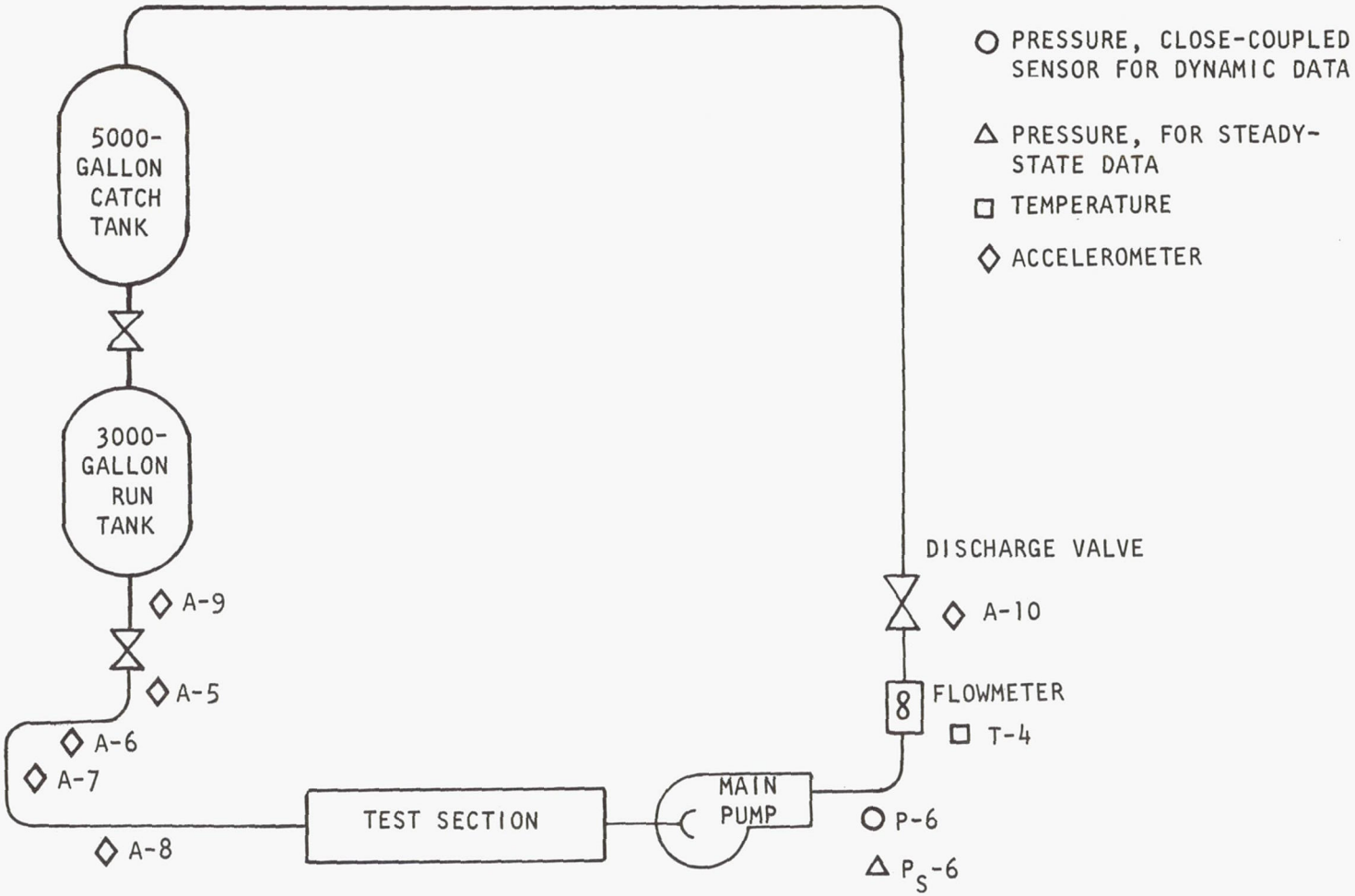

Figure 49. Facility Instrumentation

TABLE V

MAGNETIC TAPE CHANNEL ASSIGNMENT

Channel	Parameter	Code	Remarks
Tape Recorder No. 1			
1	Command sine	E-1	All tests
2	Command sine	E-2	All tests
3	Inlet pressure	P-1	All tests
4	Reducer discharge pressure	P-2	All tests
5	Anti-POGO inlet pressure	P-3	All tests
6	Inducer inlet pressure	P-4	
7	Inducer discharge pressure	P-5	All tests
8	Shorted input	-	All tests
9	Main pump discharge pressure	P-6	
10	Hydraulic turbine inlet	P-7	
11	Main pump flange axial	A-1	(Repeat)
12	Horizontal duct No. 2 axial	A-8	(Repeat)
13	Pulser position	X-1	All tests
14	Timer	-	All tests
Tape Recorder No. 2			
1	Command sine	E-1	All tests
2	Pulser SV current	E-4	
3	Pulser position	X-1	(Repeat)
4	Main pump flange axial	A-1	All tests
5	Inducer flange axial	A-3	All tests
6	Vertical duct No. 1	A-5	All tests
7	Horizontal duct No. 1	A-6	All tests
8	Shorted input	-	All tests
9	Vertical duct No. 2	A-7	All tests
10	Horizontal duct No. 2	A-8	All tests
11	Tank bottom axial	A-9	All tests
12	Throttle valve axial	A-10	All tests
13	Flowrate	F-1	All tests
14	Timer	-	All tests

HYDRAULIC SYSTEM

The hydraulic requirement for operating the disturbance pulser and control pistons was provided by a hydraulic mule with the capability of delivering fluid at 3000 psi. An analysis of the hydraulic system, to ensure that the system did not become limiting in the 2- to 50-Hz range, resulted in the accumulator system shown in Fig. 50. Three 10-gallon accumulators were added to the supply pressure side and one 10-gallon accumulator was added to the return line.

DISTURBANCE PULSER

The flow disturbances were generated by a hydraulically driven piston whose position was controlled by a servovalve and associated control electronics. The flow disturbance was injected into the main flow stream through a vaned manifold, designed to provide symmetrical flow distribution. The manifold, piston, and electronics were designed and built under Contract NAS9-19 and reported in Ref. 3. It should be noted that an identical piston and manifold were used for the oscillation suppression system.

The input command signal was a variable amplitude sine wave with a frequency sweep from 2 to 50 Hz. The variable amplitude versus frequency requirement for the pulser command signal was determined using the analog computer model and the criteria that:

1. The maximum pulser stroke will not exceed ±25 mm (±31.5 mm is stop-to-stop).

2. The maximum peak-to-peak generated pressure oscillation at the inducer inlet should not exceed 6.9×10^4 newtons/m^2 gage.

The reason for the first criteria was to assure that the pulser did not bottom out while the second criteria was established to minimize structural vibration. In addition, a recording of random noise, with a frequency content to 40 Hz was made. The response of the disturbance pulser derived from test data is shown in Fig. 51.

SYSTEM TESTS

A total of 41 tests were run, 20 tests with the inducer remote-coupled and 21 tests with the inducer close-coupled. The remote coupled tests, listed in Table VI , consisted of calibration runs, pulsing runs at two inducer Q/N values and two inlet pressures, and controller runs at two inducer Q/N values and two inlet pressures. The calibration runs were made to check out the system and to determine the regions of self-driven oscillations. To determine the region, the tank pressure was set for 2.76×10^5 newtons/m^2 gage. The tank pressure was then vented off until pump cavitation occurred. A review of the pressure data showed self-driven oscillation between 6.2×10^4 and 7.58×10^4 newtons/m^2 gage. The high NPSP tests were run with the test section inlet pressure at about 31×10^4 newtons/m^2 gage, while the low NPSP tests were made with the pressure at about 8.27×10^4 newtons/m^2 gage.

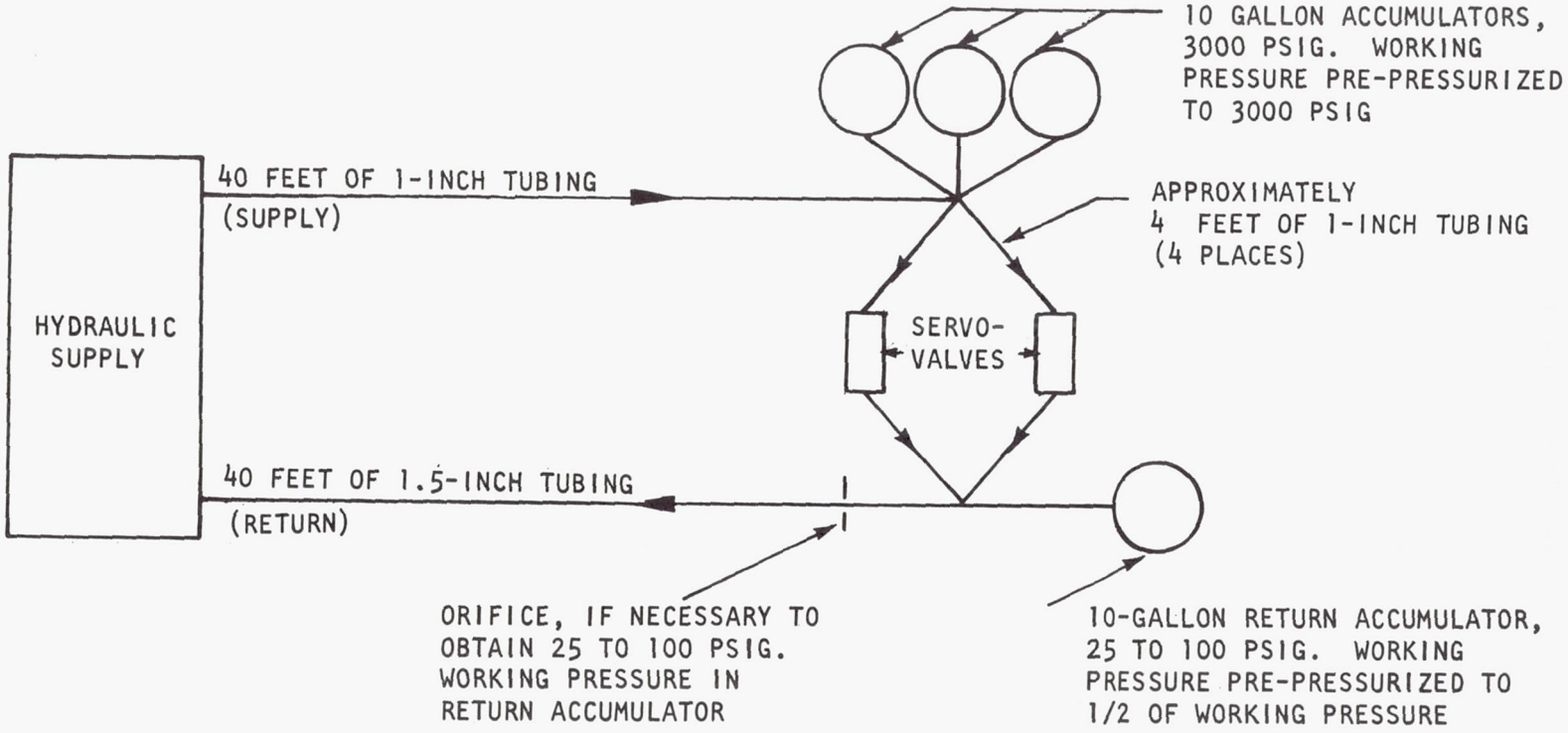

Figure 50. Test Hydraulic System

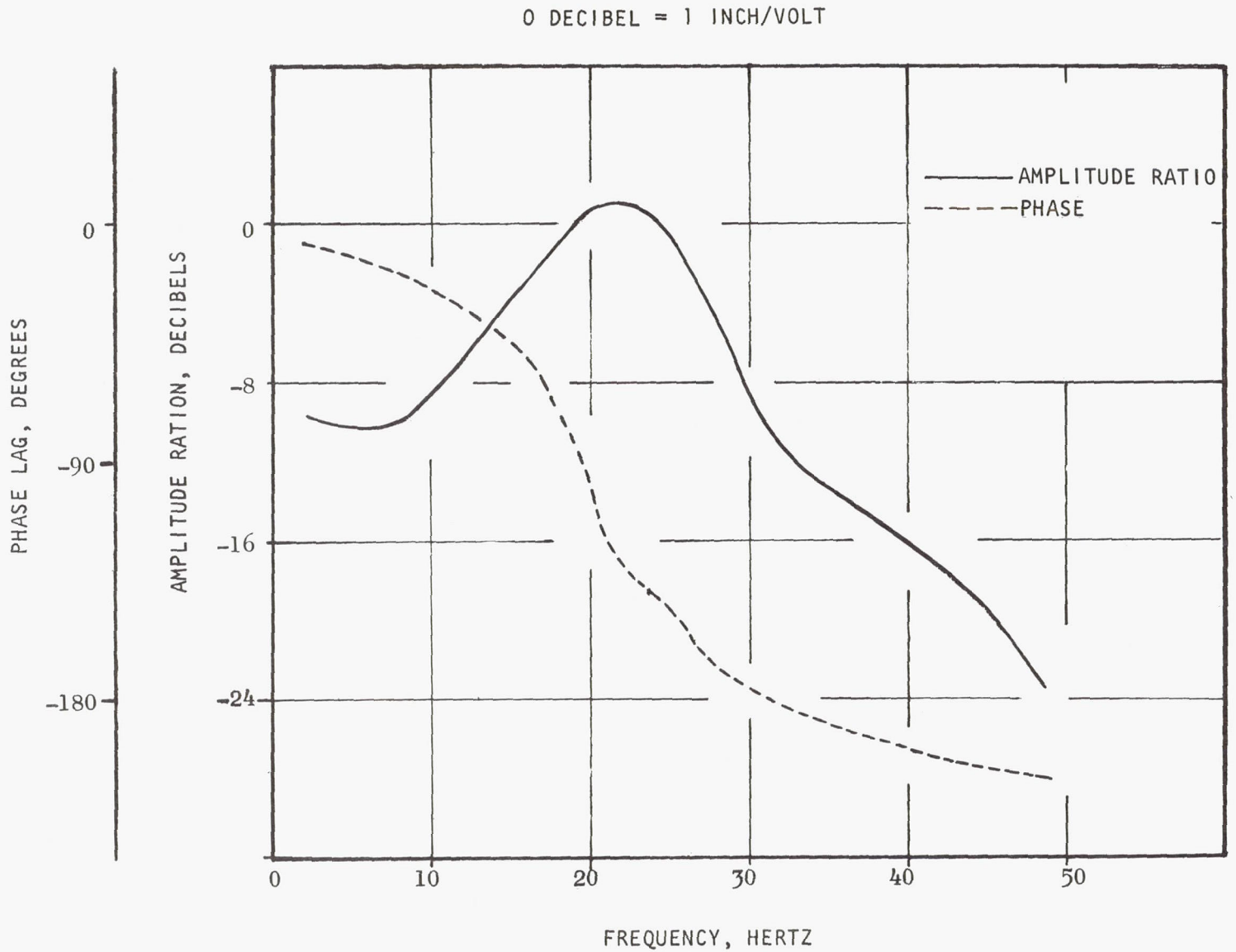

Figure 51. Response of Disturbance Pulser Position/Input Voltage

TABLE VI. REMOTE-COUPLED TESTS

Test Number	Test Conditions				Comments
	Q/N[1]	NPSP[2]	Pulser	Controller	
713-048	0.6	High	No	No	Calibration run
-049	0.6	High	↓	↓	Calibration run
-050	0.6	High			Cavitation run
-051	0.48	High			Cavitation run
-052	0.6	High	Yes		Pulser Frozen (Abort)
-053	0.6	High			Good run
-054	0.48	High			Good run
-055	0.6	Low			Cut due to cavitating pump
-056	0.6	Low			Pressure did not settle out
-057	0.48	Low			Good run
-058	0.6	Low			No time to run pulser
-059	0.6	Low			Pump cavitated on start - Cut
-060	0.6	Low			Good run
-061	0.48	High		Yes	Good run } Controller position as
-062	0.48	Low			Good run } recorded no good
-063	0.48	Low			Good run
-064	0.48	Low			Good run
-065	0.6	Low			Good run
-066	0.6	High			Good run
-067	0.48	Low	No		Good run - Inlet pressure decreased in 0.5 psi steps

Notes: (1) Q/N value is for the inducer
(2) Net positive suction pressure of the inducer - High = 30×10^4 newtons/m^2 (43.5 psi)
Low = 5.7×10^4 newtons/m^2 (8.3 psi)

The close-coupled configuration tests are listed in Table VII . They consisted of pulsing tests at two inducer Q/N values and two inlet pressure levels, controller runs at two inducer Q/N values and two inlet pressures, and a set of tests without the inducer or main pump operating. The high NPSP tests were run with a test section inlet pressure of about 31×10^4 newtons/m^2 gage, while the low NPSP tests were run with the pressure at about 6.98×10^4 newtons/m^2 gage. The tests run without the inducer or main pump operating were to evaluate various controller gains and lead pressure inputs. Reduction of the data indicated results for the test section were comparable to those obtained when the inducer and pump were operating.

TABLE VII. CLOSE-COUPLED TESTS

Test Number	Test Conditions				Comments
	Q/N[1]	NPSP[2]	Pulser	Controller	
713-068	0.48	High	Yes	No	Pulser did not work
-069	0.48	High			Good run
-070	0.48	Low			Good run
-071	0.48	Low			Good run
-072	0.48	Low			Good run
-073	0.6	High			Good run
-074a	-	High			All good runs. Data taken without pump or inducer running for various controller gains and lead pressure input
-074b	-	High		Yes	
-074c	-	High			
-074d	-	High			
-074e	-	High			
-074f	-	High		No	
-075	0.6	Low		No	Good run
-076	0.48	High		Yes	Good run
-077	0.48	Low			Good run
-078	0.6	High			Good run
-079	0.6	Low			Good run
-080	0.48	Low			Run includes control only, random input pulsing with control
-081	0.48	Low			Good run - Varied input and feedback gain
-082	0.48	Low			Good run - Includes pressure lead
-083	0.48	Low			Good run - Varied input gain

Notes: (1) Q/N value is for the inducer
(2) Net positive suction pressure of the inducer - High = 30×10^4 newtons/m^2 (43.5 psi)
Low = 5.7×10^4 newtons/m^2 (8.3 psi)

Page intentionally left blank

APPENDIX D

TEST RESULTS

Reduction of the tape recorded data was obtained by A-C coupled, 50-Hz low pass Brush recorded playback, statistical reduction using a Time Data T/D1923 Real-Time Data Analyzer, and a limited amount of tracking filter reductions. The output of the time data equipment provided transfer function phase and gain data, auto spectral and cross spectral density data, as well as coherance information. The tracking filter technique provided additional early data for transfer function determination.

Data analysis to support the conclusions concerning analytical model inducer performance correlation to test data and controller performance is presented in the body of the report. Additional reduction and analysis was performed to:

1. Evaluate the effect of mechanical vibrations on the suppressors operation.

2. Determine the frequency response of the flowmeter used in the pump discharge system.

3. Determine the spectral density content of the pressures with and without control.

4. Determine if cavitation of the liquid oxygen could have existed in the suppressor manifold or piston.

EFFECT OF FEEDLINE STRUCTURAL VIBRATION ON PULSING DATA

Previous fluid system pulsing tests have shown that structural motion of the ducting modifies the dynamic response of system pressure measurements. The test cell used in this program was previously used to conduct dynamic tests on the J-2 engine oxidizer pump (Ref. 4) and during that testing a number of structural supports were added to minimize ducting deflection and to raise significant structural frequencies as high as practical (30 to 40 Hz). A structural schematic of the flow system shown in Fig. 52 also displays the type of vibration that is considered to be the most likely made in the 30- to 40-Hz range.

By assuming only one fluid and one structural mode are significant, the equations for the system are as follows:

Structure:

$$A(P_2 - P_1) = K\,\ddot{x}\,(1 + 2\zeta s/\omega + S^2/\omega^2)/S^2$$

where the direction of x is indicated in Fig. 5.

K = effective spring rate - lb/in.

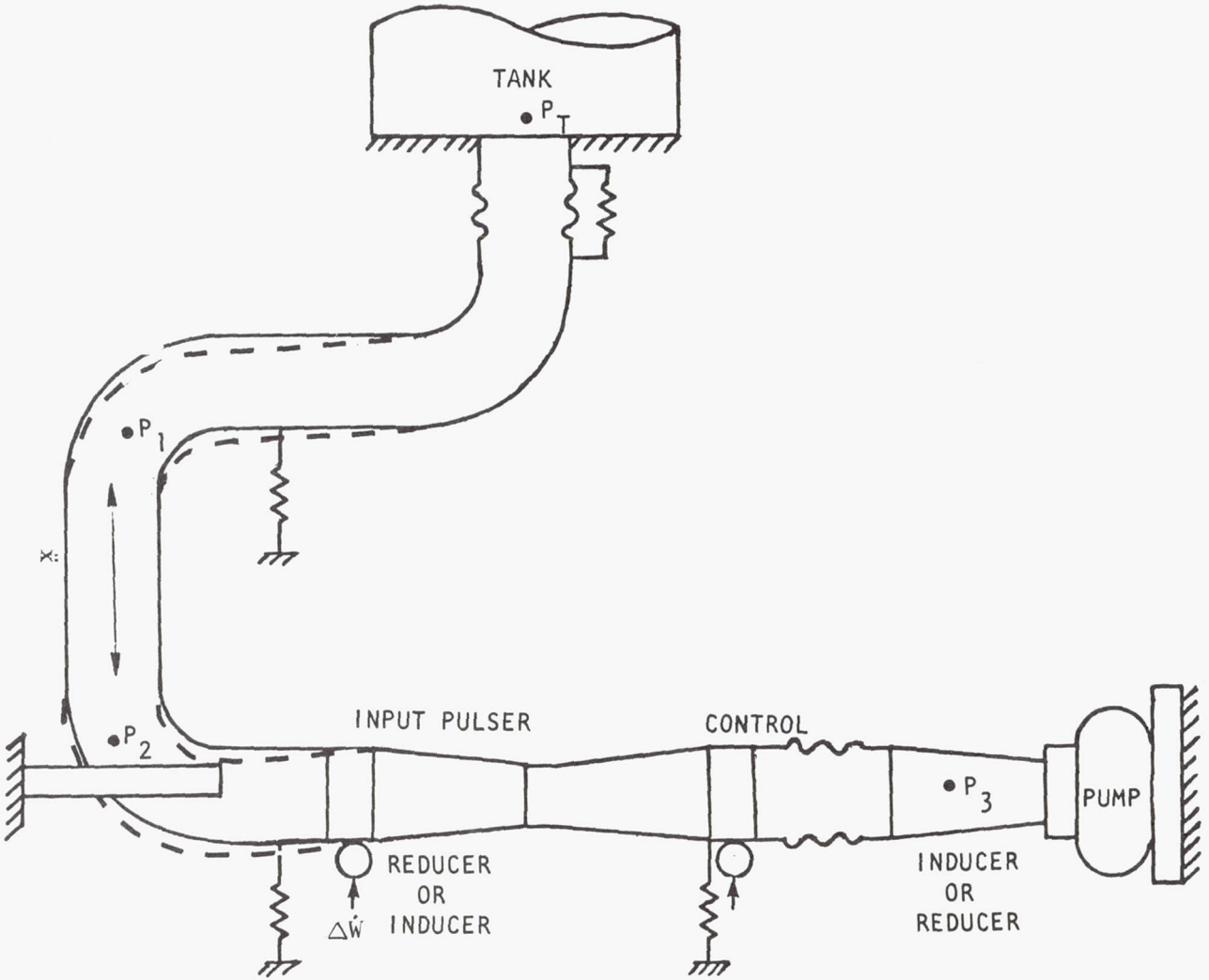

Figure 52. Test System Structural Schematic

Fluids:

$$P_T - P_1 = L_1 S\dot{W}_1$$

$$P_1 - P_2 = L_2 S (\dot{W}_1 + \rho A\ddot{x}/S)$$

$$P_2 - P_3 = L_3 S (\dot{W}_1 + \Delta\dot{W})$$

$$(\frac{1}{R} + CS) P_3 = (\dot{W}_1 + \Delta\dot{W})$$

$$\Delta\dot{W} = \rho A_p YS$$

where

Y = disturbance pulser stroke

The response of the pump inlet pressure (P_3) and duct acceleration ($\ddot{x}$) to input pulser stroke (Y) is then:

$$\frac{P_S}{Y} = \frac{A_p (L_1+L_2)S^2 \left\{1 + 2\zeta S/\omega = S^2 \left[1/\omega^2 + \rho A^2 L_1 L_2/K(L_1+L_2)\right]\right\}}{1 + S(L_1+L_2+L_3)\frac{1}{R} + CS\left(1 + 2\zeta S/\omega + S^2 \frac{1}{\omega^2} + \frac{\rho A^2 L_2}{K} - \frac{L_2^2 \rho A^2 S^3}{K}\left(\frac{1}{R}+CS\right)\right)}$$

$$\frac{\ddot{x}}{Y} = \frac{\frac{\rho A_p A L_2 S^4}{K}\left[1 + L_3 S/R + L_3 CS^2\right]}{\left[1+S(L_1+L_2+L_3)\left(\frac{1}{R}+CS\right)\right]\left[1+2\zeta S/\omega + S^2\left(1/\omega^2+\rho A^2 L_2/K\right)\right] - \frac{L_2^2 \rho A^2 S^3}{K}\left(\frac{1}{R}+CS\right)}$$

The affect of the structural resonance can be seen by letting K equal some value less than ω. Resonances due to the fluid and the structural frequencies will be seen in the data but the damping factors of each will be increased. The pressure data on antiresonances will be seen at a frequency lower than the structural natural frequency. In the structural data an antiresonance will be seen that is associated with fluid column downstream of the pulser and upstream of the pump compliance. Data reduced from high NPSP pulsing test 073 with the close-coupled pump configuration is shown in Fig. 53 through 56.

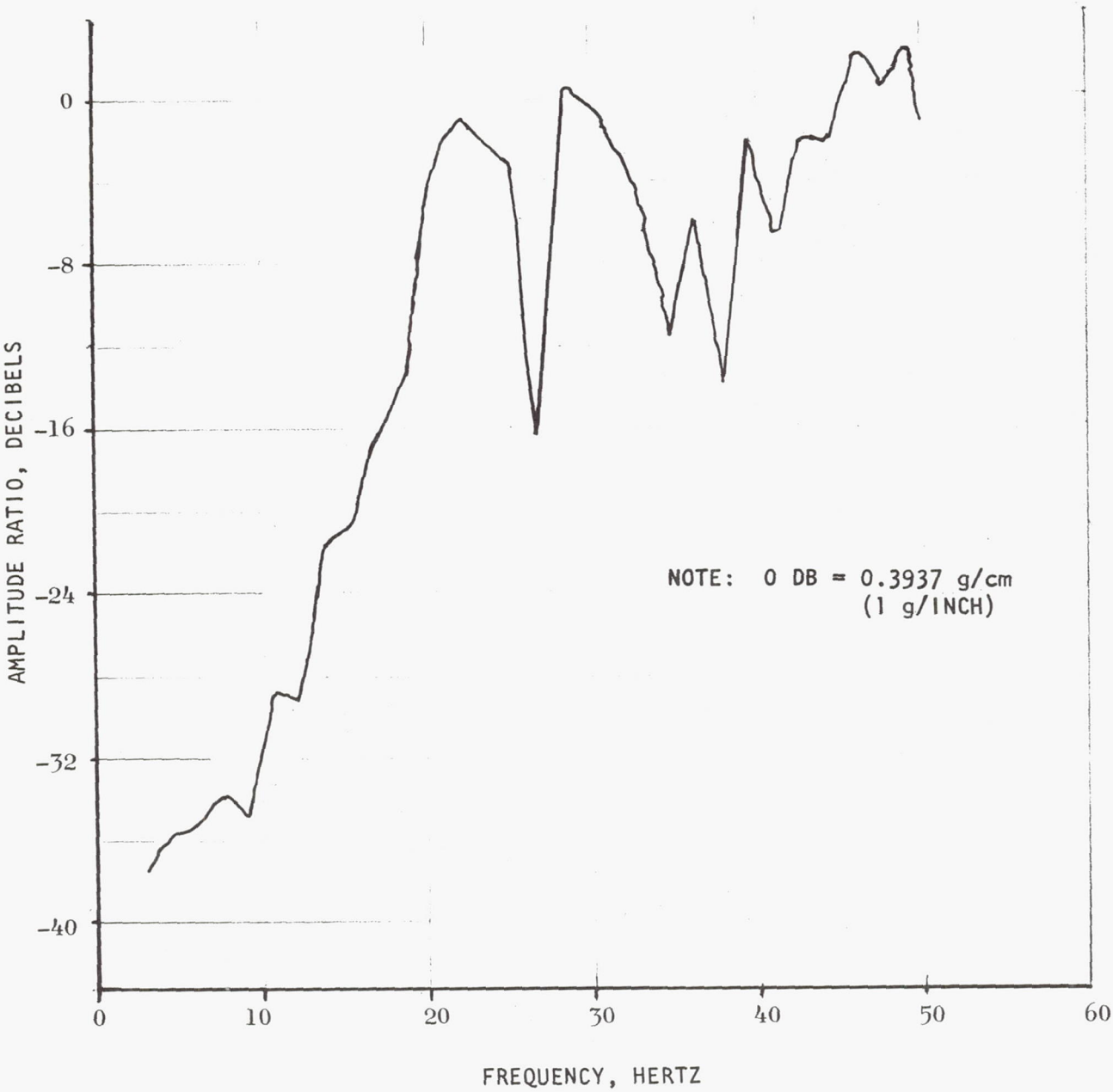

Figure 53. Amplitude Ratio Vertical Section 2 Acceleration/Disturbance Pulser Position, Close-Coupled Run 073

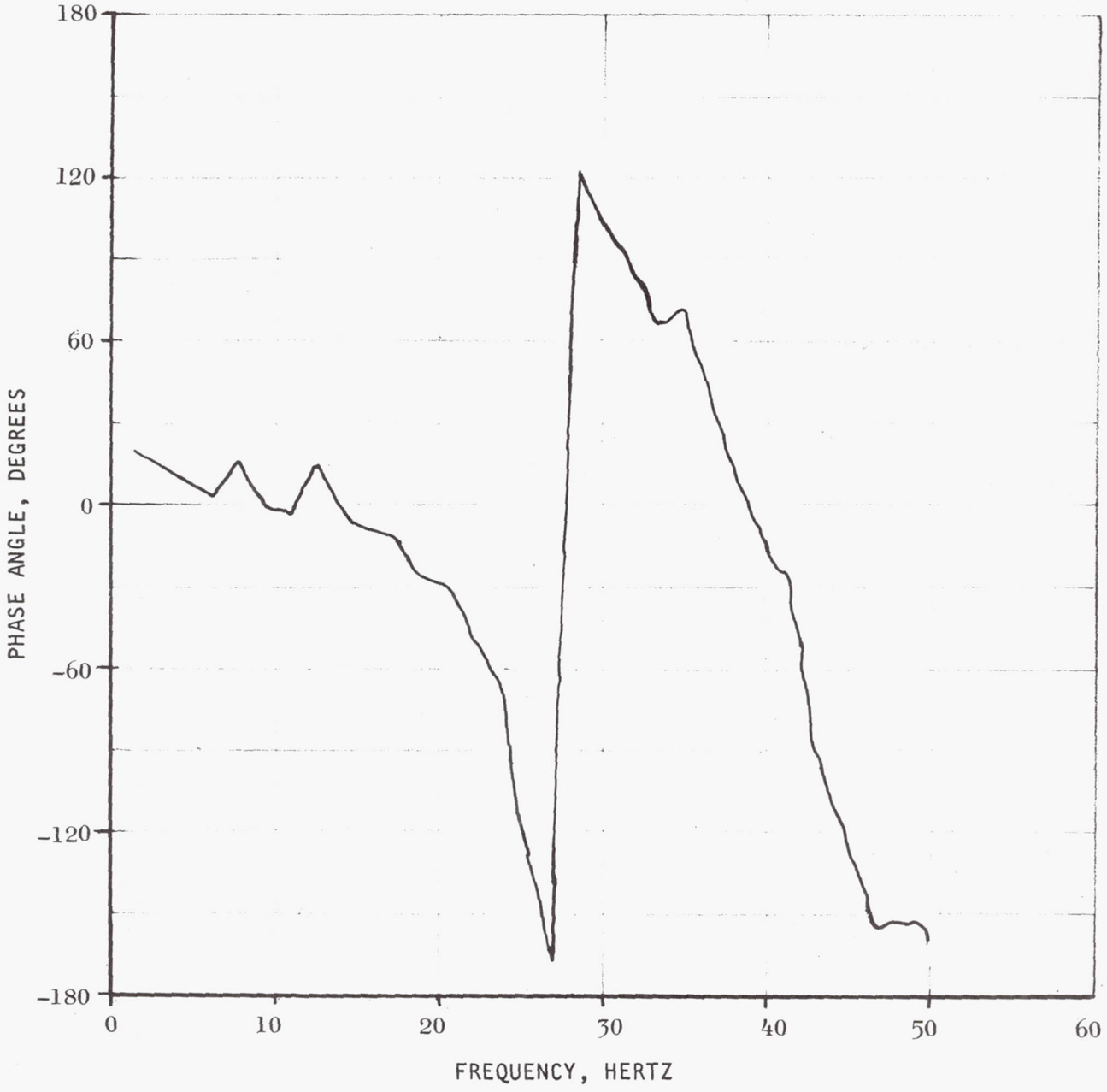

Figure 54. Phase of Vertical Section Acceleration/Disturbance Pulser Position, Close-Coupled

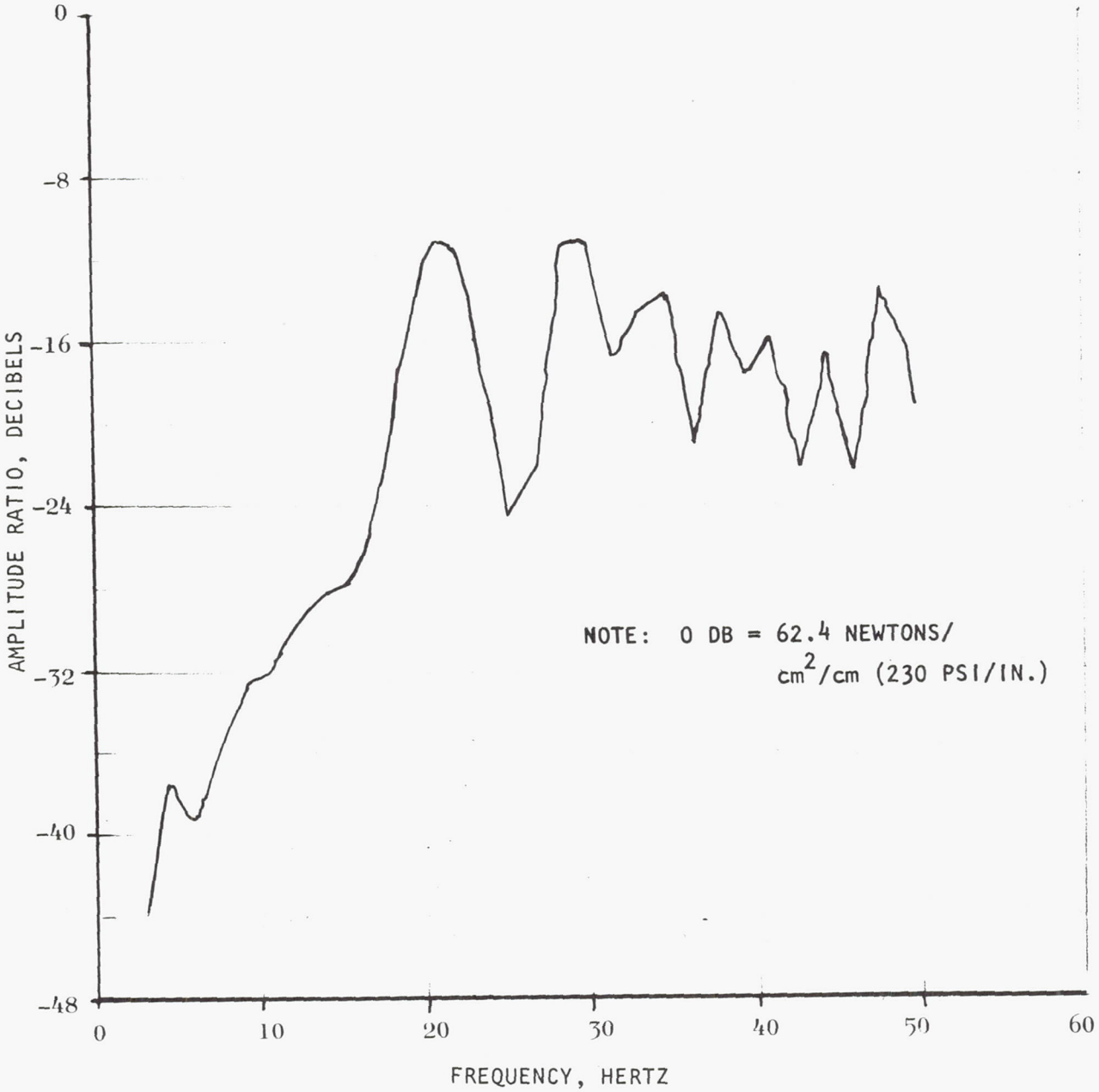

Figure 55. Amplitude Ratio of Pump Inlet Pressure/Disturbance Position, Close-Coupled

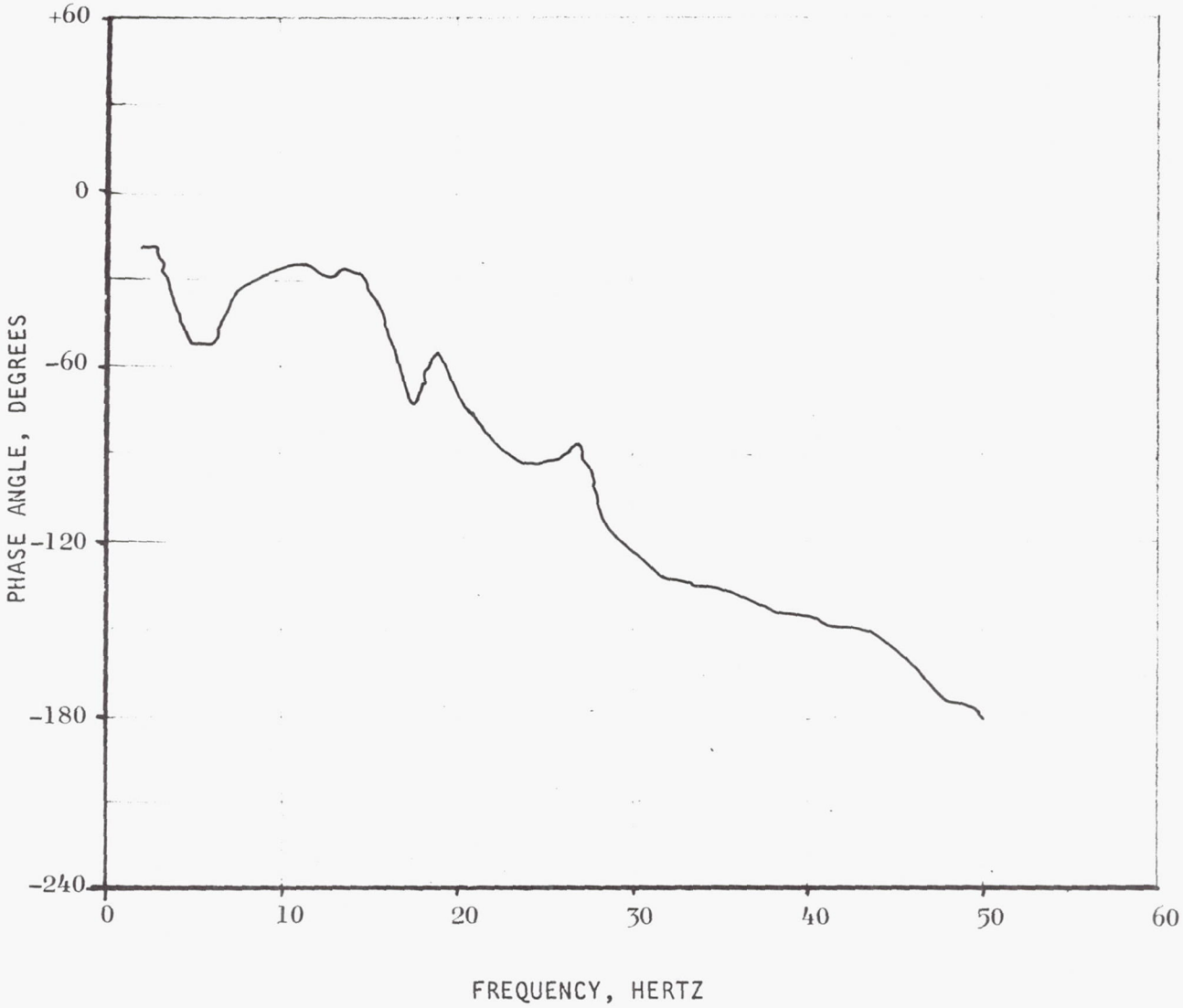

Figure 56. Phase of Pump Inlet Pressure/Disturbance Pulser Position, Close-Coupled

Looking at the amplitude ratio data, Fig. 53 and 55, it appears that three resonances occur in both the structural and pressure data below 50 Hz, one at about 22 Hz, a second at about 29 Hz, and a third at about 49 Hz. The first two of these are predicted by the assumed model and derived equations. The third resonance is probably due to a more complex structural system. Looking at the phase data, the structural data, Fig. 54, indicates three resonances without an anti-resonance (540-degree phase shift) while the pressure phase data, Fig. 56, indicates three resonances and three anti-resonances (180-degree shift). This also is consistant with the derived equations if the L_3C frequency is above 50 Hz.

So far as the controller is concerned, the source of the resonances have little affect on its operation as long as the controller phase error does not result in negative system damping. Pressure oscillations due to either structural or fluid resonances will be damped by the control if they are sensed by the pressure transducer.

FLOWMETER FREQUENCY RESPONSE

In 1964, an analytical estimate of turbine flowmeter response was made. The calculation indicated a first order break frequency of approximately 75 Hz for a 6 blade, 4-inch diameter flowmeter with 100 lb/sec of liquid oxygen flowrate. Flowmeter reduction from Saturn flight AS-508, during the period of POGO oscillation showed large amplitude flow variations at about 20 Hz.

In an effort to experimentally verify the frequency response characteristics, the flowmeter signal was converted to a voltage proportional to flow rate and the transfer function of the variation in voltage level to disturbance pulser position signal was obtained. The results in terms of gain and phase are shown in Fig. 57 and 58, respectively. The plots indicate at least 30-Hz response. At the fluid system resonant frequency of about 19 Hz, a phase shift of 90 degrees is indicated, a value to be expected for a second order system.

To obtain the flowmeter voltage signal, the recorded cycle signal was fed through a Hewlett-Packard Model 500 BR frequency meter that converts the cycle signal to a variable frequency, constant area pulse. The frequency meter output was then passed through a 50-Hz low pass filter and the transfer function obtained by processing with the Real-Time Data Analyzer.

To verify the flowmeter signal conclusion, the filtered frequency meter and pulser position signals were recorded on a Brush Recorder. The flowmeter oscillations, at the disturbance pulser frequency could be clearly seen. The maximum flow oscillation was about 2 percent of full flow.

The data from the one test reduced indicates that the flowmeter has sufficient frequency response to follow flow variations to at least 30 Hz. The signal processing required to extract the data, however, does not make this seem like a good control input signal.

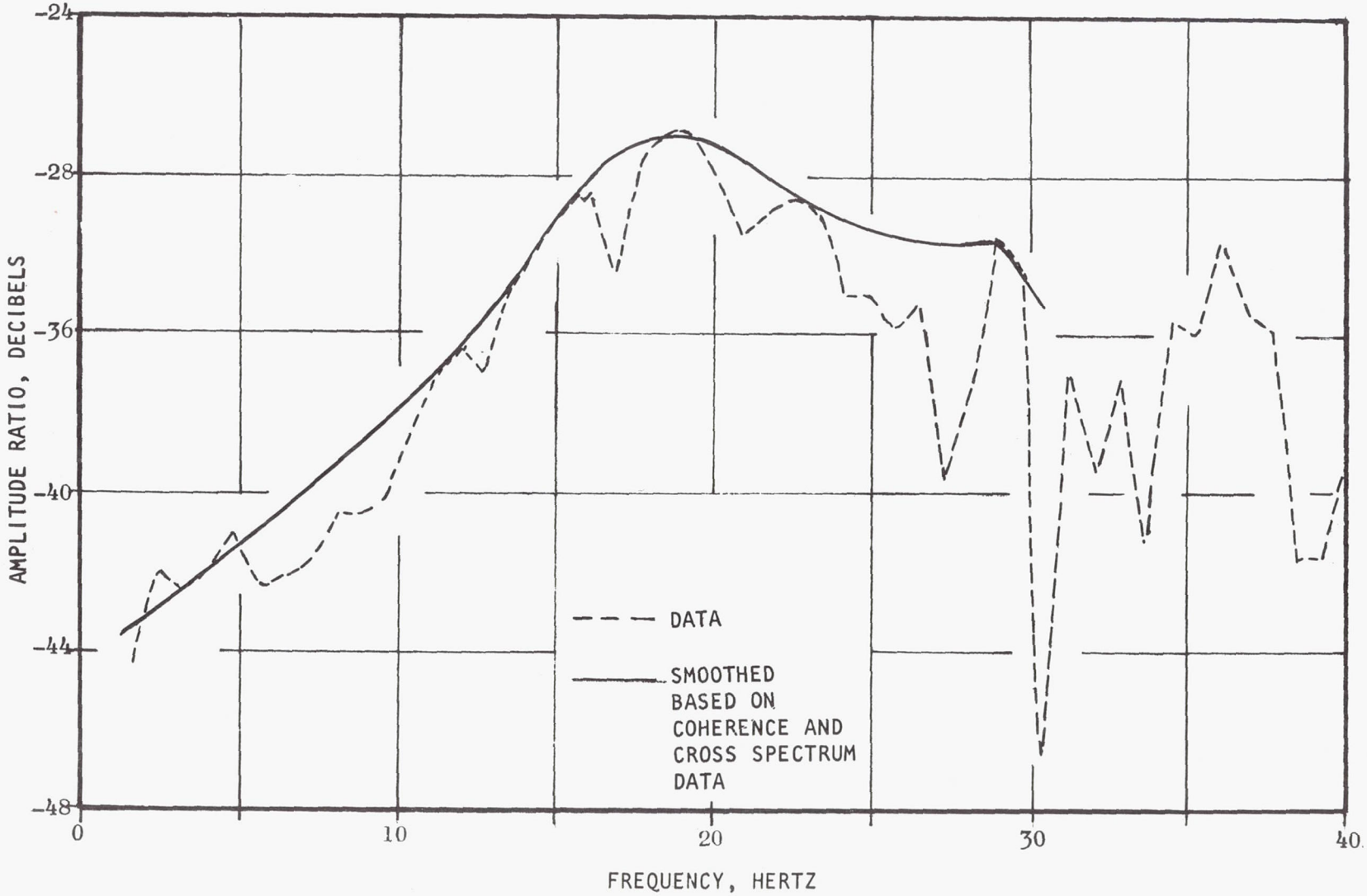

Figure 57. Amplitude Ratio of Flowmeter Response/Disturbance Pulse Position - Test 069

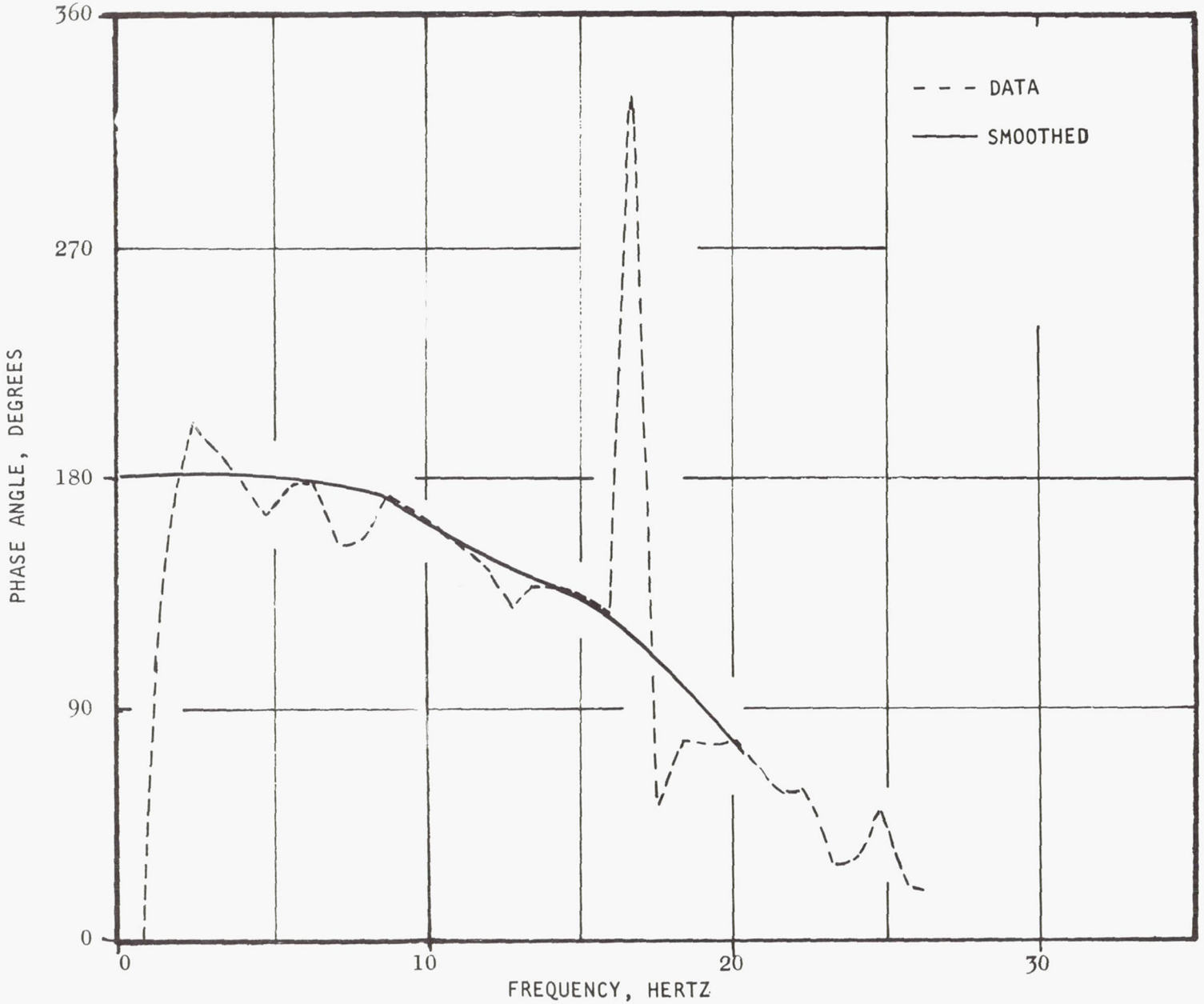

Figure 58. Phase of Flowmeter Response/Disturbance Pulser Position - Test 069

SPECTRAL DENSITY

Power spectral density processing, using the Real-Time Data Analyzer, was done for some of the remote coupled configuration tests. Pressure data was processed for high and low NPSP tests with and without the control active. The test numbers and test conditions are:

-053	High NPSP, No Control	
-066	High NPSP, With Control	
-060	Low NPSP, No Control	Disturbance pulser input on all tests
-065	Low NPSP, With Control	

Summarized plots for each test is shown in Fig. 59 through 62. Looking at Fig. 59 and 60, the data for the high NPSP condition, it can be seen that approximately constant power is present in the range of 7 to 15 Hz.

The controlled run, for pressures at and downstream of the controller, shows an attenuation of at least 6 db in this frequency range. It should be noted that the decibel (db) for the power data is defined as 10 x log (A^2), which is comparable to the transfer function decibel of 20 x log (A). For the location A pressure, upstream of the inducer, the attenuation due to the controller is approximately 3 db.

Above 15 Hz, the uncontrolled test shows a peak at about 21 Hz, while the controlled test shows an attenuation of at least 12 db at the controller and 7 db at the location A pressure. Above 25 Hz, the power content on the controlled test increases due to the phase shift of the controller. On the uncontrolled test, the disturbance pulser input frequency program was cut short, reaching only 25 Hz, because of test termination resulting from low liquid oxygen level in the run tank.

Results from the low inducer NPSP tests, Fig. 61 and 62, showed relatively high power levels below 10 Hz with a valley between about 12 and 15 Hz followed by a relatively low peak in power at 21 Hz. This pattern follows the pulser input amplitude program and is attributed to this. The transfer function reduction of the remote coupled low NPSP data is felt to better represent the system, a summary of gain being shown in Fig. 63. From the gain plot, the attenuation with control is about 8 db from 8 to 30 Hz. Compared to the low NPSP data for the close-coupled tests, which showed no effect with the controller, these results indicate that a control located between the inducer and main pump provides good control over a wide range of inducer inlet pressure.

Test 065 was run with the inlet pressure about 1.72×10^4 newtons/m^2 (2.5 psi) lower than the other pulsing tests and exhibited rather unique characteristics. There was no indication of pressure response at the input

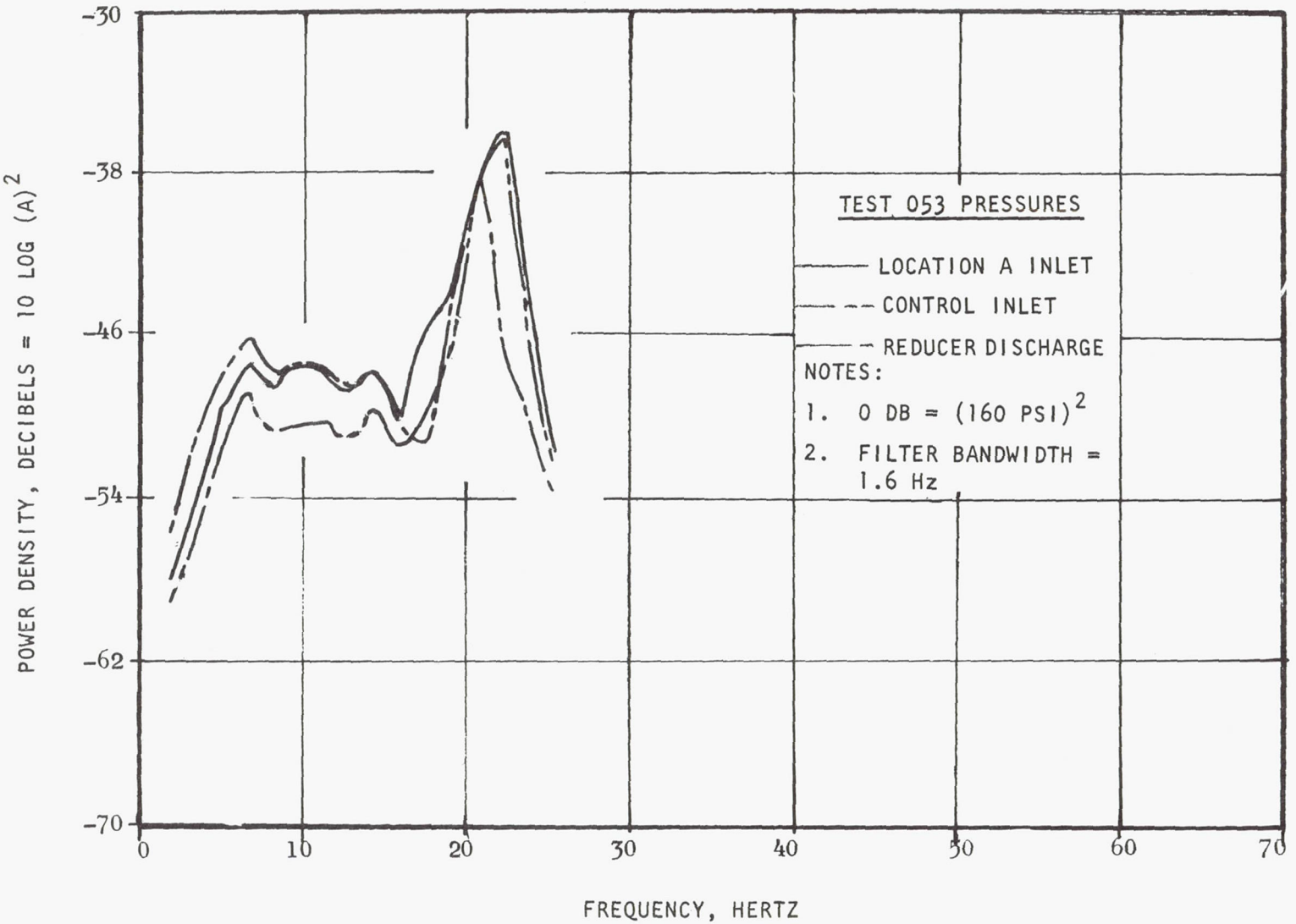

Figure 59. Spectral Densities of High NPSP, Uncontrolled, Remote-Coupled Test 053

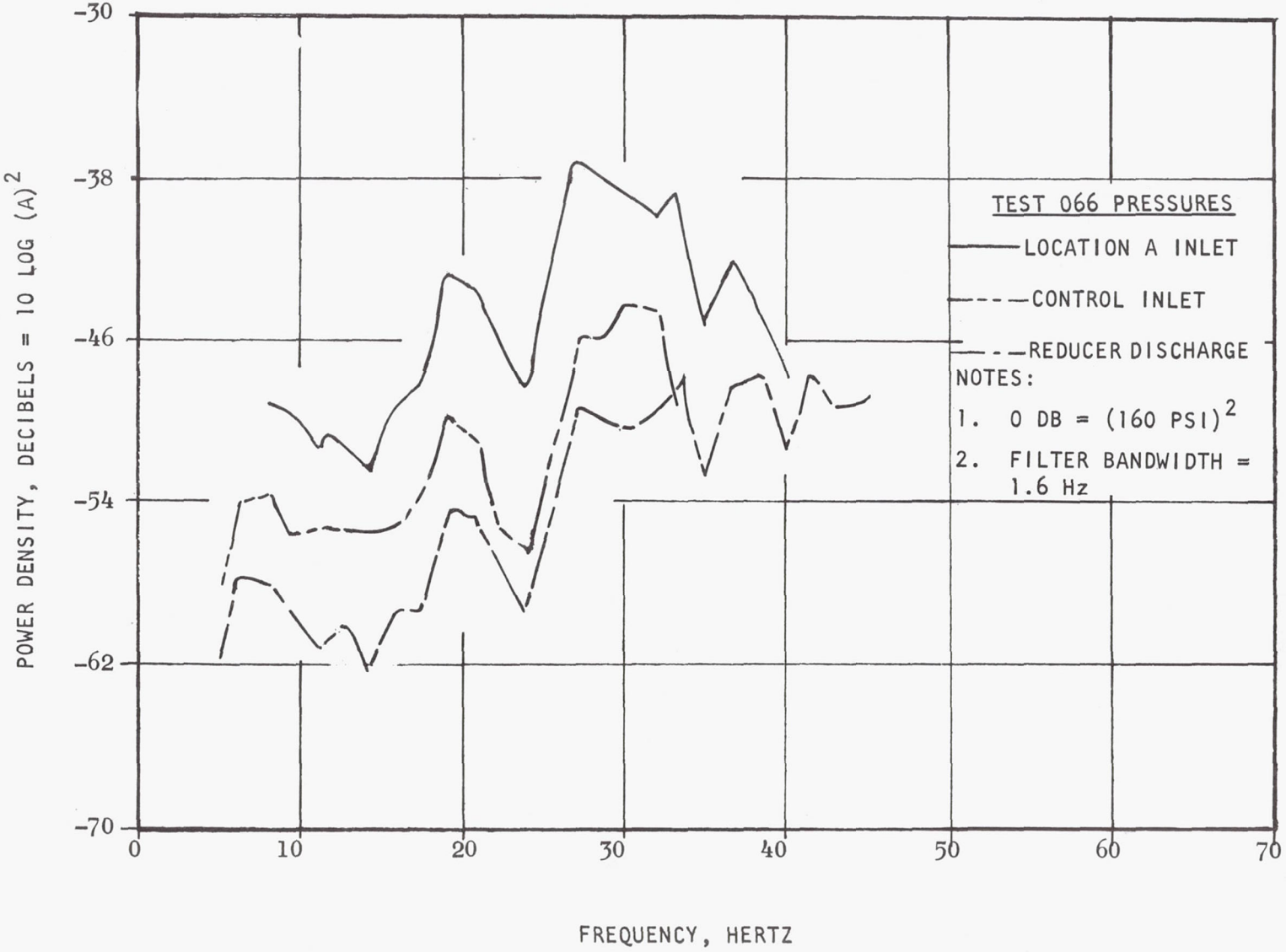

Figure 60. Spectral Densities of High NPSP, Controlled, Remote-Coupled Test 066

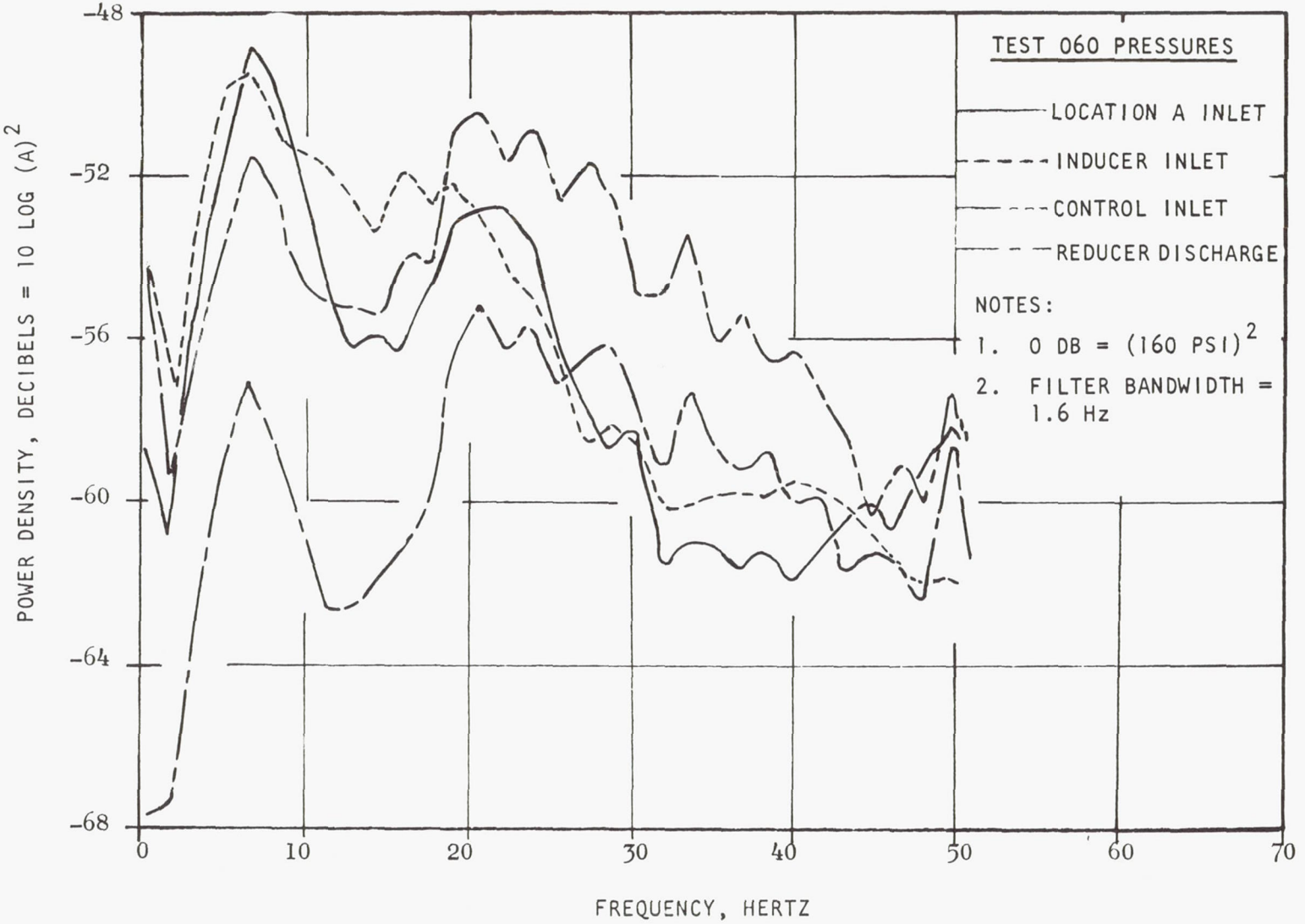

Figure 61. Spectral Densities of Low NPSP, Uncontrolled, Remote-Coupled Test 060

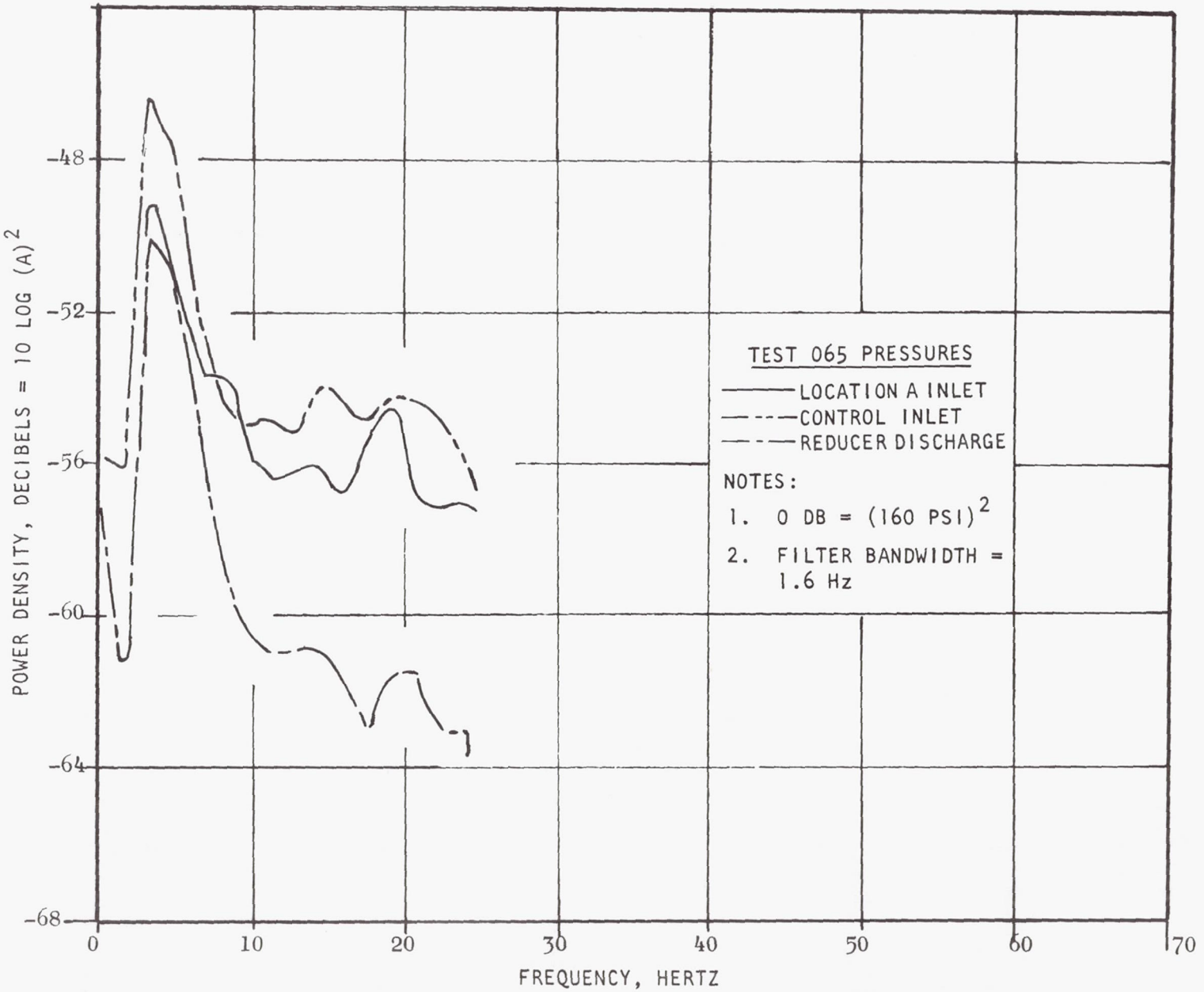

Figure 62. Spectral Densities of Low NPSP, Controlled, Remote-Coupled Test 065

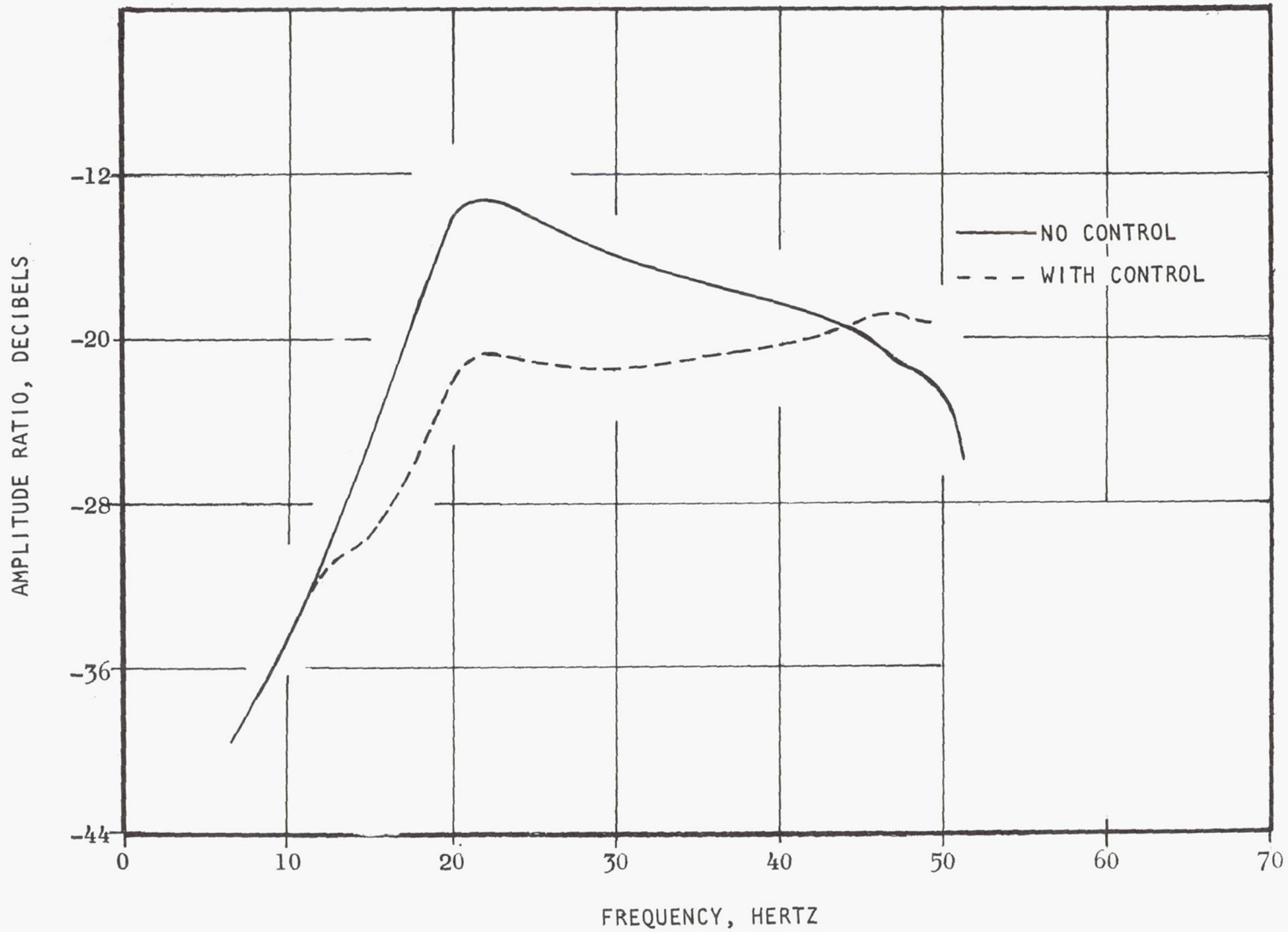

Figure 63. Averaged Amplitude Ratio of Control Inlet Pressure/Disturbance Pulser Position, Low NPSP, Remote-Coupled Tests

pulser frequency; however, there was a fairly constant 2.4 x 10^4 newton/m^2 (3.5 psi) peak-to-peak 3.5- to 4-Hz oscillation, to which the controller position responded, present for most of the run. This same type of oscillation was observed on non-pulsed cavitation Run 051 where a 4 Hz, 2.1 x 10^4 newton/m^2 (3 psi) oscillation was observed when the inducer inlet pressure reached approximately 9 psig. These are the inducer self-induced oscillations. A comparison of the control inlet pressure spectral density for Runs 051 and 065 is shown in Fig. 64. From the comparable spectral density of the two runs, it is concluded that the control neither reinforced nor attenuated the oscillation.

EFFECT OF CAVITATION ON SUPPRESSOR PERFORMANCE

The pulser manifold and piston were designed so that the flow velocities would be nearly uniform from the piston face to actual entrance into the main duct flow stream. The tendency for cavitation at low working pressures in the duct are thereby minimized. The possibility for local cavitation always exists, however, and its effect was calculated by assuming that it could be simulated by a compliant volume near the control piston face. The equations for the simulation are as follows:

Pump impedance with control and disturbance located near the pump inlet:

$$P_S \left(\frac{1}{R_P} + C_P S\right) = \dot{W}_L + \dot{W}_C + \Delta\dot{W}$$

Feed line flow:

$$-P_S = L_\ell S \dot{W}_L$$

Equivalent flow because of ideal controller motion:

$$\dot{W}_P = P_S \times D S^2/(\omega_o^2 + \omega_o S + S^2)$$

Compliance at piston face:

$$CSP_C = \dot{W}_P - \dot{W}_C$$

where

1. D is the controller admittance
2. C is the control cavitation capacitance

Flow into duct from control:

$$P_C - P_S + (R + LS)\dot{W}_C$$

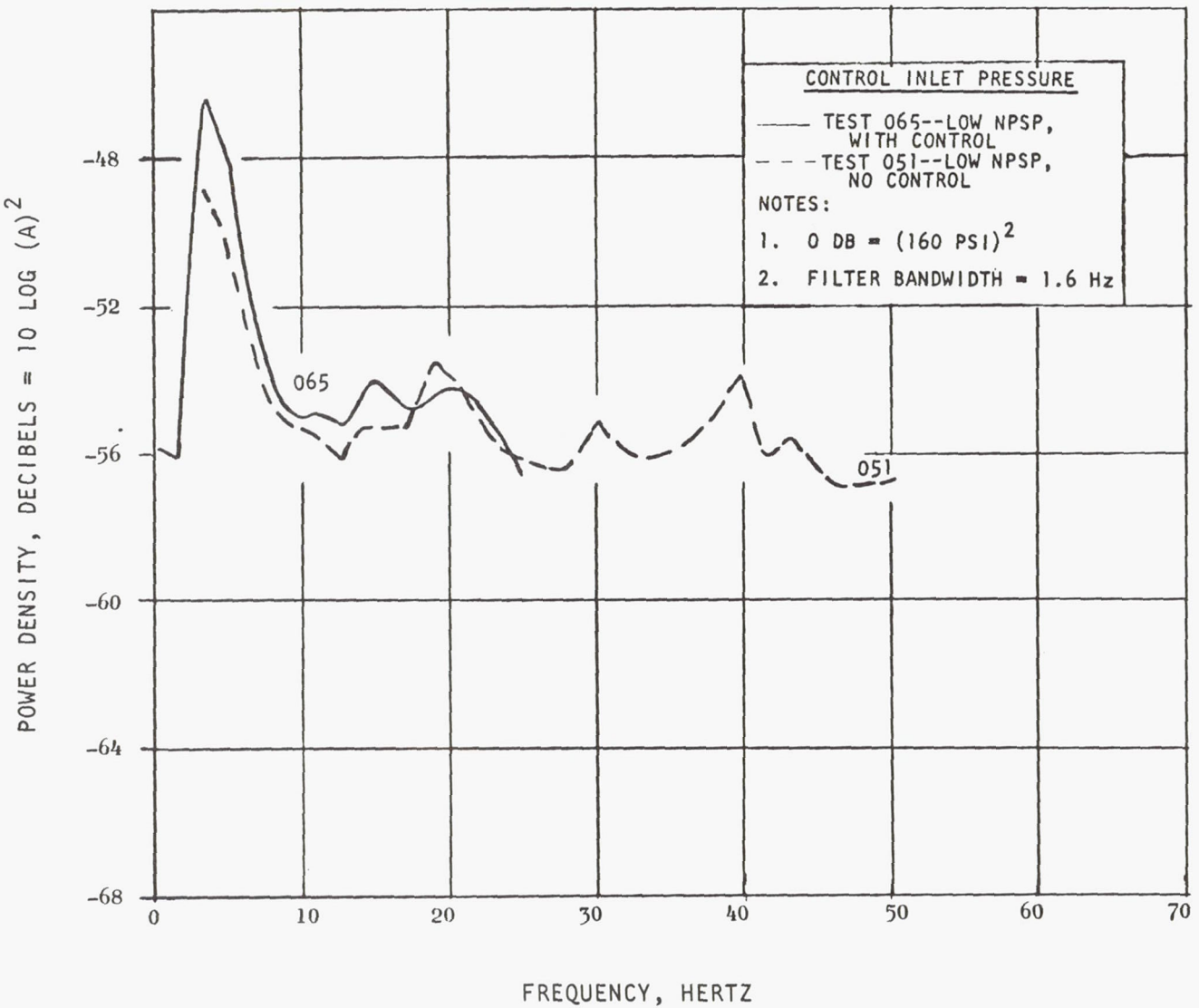

Figure 64. Power Spectral Densities of Cavitation Run 051 and Low NPSP, Controlled, Remote-Coupled Test 065

The transfer function relating pump suction pressure variations to input flow disturbance is:

$$\frac{P_S}{\Delta\dot{W}} = \frac{L_\ell S\left[1 + RCS + LCS^2\right]\left[\omega_o{}^2 + \omega_o S + S^2\right]}{\left[1 + \frac{L_\ell}{R_P} S + L_\ell C_P S^2\right]\left[1 + RCS + LCS^2\right]\left[\omega_o{}^2+\omega_o S+S^2\right] + L_\ell S^2\left[DS+C\left(\omega_o{}^2+S\omega_o+S^2\right)\right]}$$

Typically ω_o is small (as in our design where $\omega_o = 4\pi$). This sets the bandwidth and should be smaller than any other expected frequencies. For our purposes then:

$$P_S/\Delta\dot{W}\ \underset{S>\omega_o}{\doteq} = \frac{L_\ell S\left[1 + RCS + LCS^2\right]}{\left[1 + \frac{L_\ell}{R_P} S + L_\ell C_P S\right]\left[1 + RCS + LCS^2\right] + L_\ell S\ (D + CS)}$$

The denominator contains pertinent dynamic information (the characteristic equation) so we set it equal to zero to evaluate its roots.

$$0 = \left[1 + L_\ell\left(\frac{1}{R_P} + D\right)S + L_\ell C_P S^2\right] + CS\left[L_\ell S + (R+LS)\left(1 + \frac{L_\ell}{R_P} S + L_\ell C_P S^2\right)\right]$$

Typical values of the coefficients are:

L_ℓ = 8×10^{-3}, Feed Line Inertia

L = 5×10^{-3}, Control Manifold Fluid Inertia

R = 0 for most severe condition, Control Manifold Resistance

C_P = $\left\{3 \times 10^{-3}\right\}$ for high NPSP, $\left\{10^{-2}\right\}$ for low NPSP, Pump Capacitance

R_P = $\left\{3\right\}$ $\left\{1\right\}$ Pump Resistance

$C \doteq \overline{V}/P\gamma$ = 0 for high NPSP, 0.2 for a cavity piston D ~ 2.0, Cavitation Capacitance

Using high NPSP coefficients the characteristic equation is:

$$0.05C\ S^2(S^2 + 2 \times 0.17 \times 330S + 330S + 330^2)+(S^2 + 2 \times 1.9 \times 2045 + 204^2)=0$$

Using low NPSP coefficients the characteristic equation is:

$$0.005C\ S^2(S^2 + 2 \times 0.28 \times 180S + 180^2)+(S^2 + 2 \times 1.34 \times 112S + 112^2) = 0$$

The equations indicate the possibility for oscillatory instability for a range of values of cavitation compliance. The neutral stability frequency should be somewhat higher than the basic frequency of the feedline (330+ or 180+ rad/sec). Using Routh's criterion the critical values of C for neutral stability are as follows:

$$C \text{ (High NPSP)} = 3.525 \times 10^{-7} \text{ sec}^2\text{m (0.00535 lbs/psi)}$$

$$C \text{ (Low NPSP)} = 1.02 \times 10^{-6} \text{ sec}^2\text{m (0.0155 lbs/psi)}$$

The potential for this instability can be reduced by sensing the pressure in the manifold near the piston face. The equations for the system are similar to those previously written except that the control equation should be written as:

$$\dot{W}_P = -P_C DS^2/(\omega_o^2 + \omega_o S + S^2)$$

The resultant transfer function is then:

$$\frac{P_S}{\Delta\dot{W}} = \frac{L_\ell S\left[\left(\omega_o^2+S\omega_o+S^2\right)\left(1+RCS+LCS^2\right) + DS^2(R+CS)\right]}{\left(\omega_o^2+S\omega_o+S^2\right)\left[L_\ell CS^2+\left(1+RCS+LCS^2\right)\left(1+\frac{L_\ell}{R_P}S+C_P L_\ell S^2\right)\right]+DS^2\left[L_\ell S+(R+LS)\left(1+\frac{L_\ell}{R_P}S+L_\ell C_P S^2\right)\right]}$$

in the range of frequencies where $S>\omega_o$:

$$\frac{P_S}{\Delta\dot{W}} = \frac{L_\ell S\left[(1+RD) + (RC+DL)\ S + LCS^2\right]}{L_\ell S\ (D+CS) + \left(1 + \frac{L_\ell}{R_P}\ S + L_\ell C_P S^2\right)\left[(1+RD) +(RC+DL)\ S + LCS^2\right]}$$

Again, taking the most severe condition when the flow resistance into the pulser cavity (R) is zero, we have the characteristic equation:

$$DL_\ell S + \left(1 + \frac{L_\ell}{R_P}\ S + L_\ell C_P S^2\right)(1 + DLS) + CS\left[L_\ell S + LS\left(1 + \frac{L_\ell}{R_P} + L_\ell C_P S^2\right)\right] = 0$$

Using typical values as before for high NPSP conditions we have:

$$(S^3+S^2\ 1.694x10^2+S\ 1.194x10^5+4.167x10^6)+0.5CS^2(S^2+1.111x10^2S+1.083x10^5)=0$$

or $(S+36.3)\ (S^2+0.34S\ 340+340^2) + 0.5CS^2\ (S^2+0.34S\ 330+330^2) = 0$

While for low NPSP we have:

$$(S^3+2 \times 10^2S+4.25 \times 10^4S+1.25 \times 10^6) = 0.5CS^2(S^2+10^2S+3.25 \times 10^4) = 0$$

or $(S+33.9)\ (S^2+0.86S\ 190+190^2) + 0.5CS^2\ (S^2+0.56S\ 180+180^2) = 0$

Applying Routh's criterion we find that no real value of compliance will result in an instability.

Further consideration of the location of the pressure sensing point indicates that the critical situation occurs when the pressure against the piston face is more than 90 degrees out of phase with the sensed pressure and the control actually reinforces pressure oscillations at the piston face and hence in the system.

In a system designed for vehicle application the pressure sensing point should be in the liquid volume associated with the piston bore to eliminate possible control instability because of local cavitation.

Comparison of data from close coupled and remote tests indicate similar trends in system performance at high NPSP.

The controller manifold pressure is nearly 100-psi higher in the remote installation than in the close coupled installation. This implies no control cavitation in either installation. When the close-coupled configuration was run at low NPSP, no obvious tendency for an instability was observed in the data. In the discussion of system performance it is pointed out that the inlet admittance of the pump, running near cavitation is considerably greater than that of the control and, together with the low level of pressure oscillation, resulted in very little effect from the control. No additional resonance because of control cavitation is found in the data.

REFERENCES

1. RSS-8313-3, Final Report, Phase B POGO Suppression System, Rocketdyne, A Division of North American Rockwell, Canoga Park, California, 21 April 1971

2. King, J. A. and Farrel, E. C.: Final Report, The Transient Performance of a Hydraulic Turbine-Driven Inducer: Computer Predictions and Test Verification, NASA CR-72518, R-7747, Rocketdyne, A Division of North American Rockwell, Canoga Park, California, February 1969

3. R-6428, Final Report, J-2 Special Studies, Vehicle Longitudinal Stability Analysis (POGO Signal Generations), Rocketdyne, A Division of North American Rockwell, Canoga Park, California, 31 December 1965

4. R-6283, J-2 Vehicle Longitudinal Stability (POGO) Analysis Program, Rocketdyne, A Division of North American Rockwell, Canoga Park, California, 31 August 1965